The University of Southern Mississippi

The Aquila Digital Community

Fall 12-2016

Electrogenerated Chemiluminescence Study of Semiconductor Nanoparticles Towards Sensitive Detection of Biomolecules

Yiliyasi Wusimanjiang
University of Southern Mississippi

Recommended Citation

ELECTROGENERATED CHEMILUMINESCENCE STUDY OF SEMICONDUCTOR

NANOPARTICLES TOWARDS SENSITIVE DETECTION OF BIOMOLECULES

by

Yiliyasi Wusimanjiang

A Dissertation
Submitted to the Graduate School
and the Department of Chemistry and Biochemistry
at The University of Southern Mississippi
in Partial Fulfillment of the Requirements
for the Degree of Doctor of Philosophy

Approved:

_____
Dr. Wujian Miao, Committee Chair
Associate Professor, Chemistry and Biochemistry

_____
Dr. Douglas Masterson, Committee Member
Associate Professor, Chemistry and Biochemistry

_____
Dr. Karl Wallace, Committee Member
Associate Professor, Chemistry and Biochemistry

_____
Dr. Song Guo, Committee Member
Assistant Professor, Chemistry and Biochemistry

_____
Dr. Vijay Rangachari, Committee Member
Associate Professor, Chemistry and Biochemistry

_____
Dr. Karen S. Coats
Dean of the Graduate School

December 2016

ABSTRACT

ELECTROGENERATED CHEMILUMINESCENCE STUDY OF SEMICONDUCTOR

NANOPARTICLES TOWARDS SENSITIVE DETECTION OF BIOMOLECULES

by Yiliyasi Wusimanjiang

December 2016

The main focus of this dissertation is to unfold the fundamental aspects of electrogenerated chemiluminescence (ECL) generation from semiconductor nanoparticles (also known as quantum dots or QDs) within different ECL systems. The ECL and photo-physical interactions between the CdTe QDs ($\lambda_{emission}$= ~760 nm) and the CdSe QDs ($\lambda_{emission}$= ~550 nm), as well as the effects of carbon nanotubes on ECL of QDs were separately investigated. Optimum experimental conditions for peptide bond formation on an electrode surface through EDC (1-ethyl-3-(-3-dimethylaminopropyl) carbodiimide hydrochloride)/NHS (*N*-Hydroxysulfosuccinimide) coupling were also revealed using cyclic voltammetry technique. Based on the information obtained from these fundamental studies, a highly sensitive ECL immunoassay fabrication strategy was proposed with some preliminary results.

ECL mechanisms of water soluble CdTe QDs ($\lambda_{emission}$= ~760 nm) in the presence of tri-*n*-propylamine (TPrA) was first investigated, along with their strong interaction with CdSe QDs ($\lambda_{emission}$= ~550 nm), using electrochemical, fluorescence (FL), and UV-vis spectroscopic techniques. An anodic ECL signal with three distinctive peaks at ~1.0, ~1.2, and ~1.4 V vs. Ag/AgCl, respectively, was detected on a glassy carbon electrode (GCE) when the potential was scanned from 0.0 V to 1.55 V vs. Ag/AgCl. Direct oxidation of TPrA triggered the formation of the first ECL peak from the

ii

CdTe QDs/TPrA system, and the production of dipropylamine (DPrA) and propylamine (PrA) through successive dealkylation of TPrA played the crucial role for generation of the second and the third ECL peaks, respectively. Addition of the CdSe QDs enhanced the ECL signal intensity of the CdTe QDs/TPrA system up to ~16 times. An electron transfer process between CdSe QDs$^{\bullet-}$ and CdTe QDs was proven to be responsible for the above signal enhancement phenomenon. FL titration experiments revealed that the energy transfer from the excited state CdSe*QDs to CdTe QDs is feasible; however, contribution of this process to ECL signal enhancement of CdTe QDs by CdSe QDs was excluded by respective experimental results.

Immobilization of small molecules or bio-molecules on an electrode surface through amide bond formation using EDC as a coupling reagent is one of the most commonly used strategies during various surface-confined electrochemical or ECL biosensor fabrication. The optimum reaction conditions, reaction time, reagent concentration, pH, buffer composition, for this immobilization method were systematically studied for two different strategies. A pH 4.50 was proven to be the optimum pH value for activation of carboxylic acid groups on a GCE surface and a pH around 7.5 was favorable to the coupling reaction between the EDC-activated intermediate and the primary amine groups. Addition of NHS was found to be beneficial for increasing the stability of the active intermediate during EDC coupling reaction, which could react with primary amine groups to form amide bond. When carboxylic group activation and the coupling steps were taken place in the same media without separation, a compromised pH value of 5.0 was suggested to be the optimum pH condition for amid bond formation on a GCE surface. The components of a buffer

solution were also found to affect the EDC coupling efficiency. MES (2-ethanesulfonic acid) buffer was recommended to be the most suitable buffer among five frequently used buffers (phosphate, $NaHCO_3$, 1-methylimidazole, Tris, and MES) for EDC coupling.

The effects of multi-wall carbon nanotubes (CNTs) that were immobilized on a GCE surface on the ECL signal of CdTe QDs in the presence of different coreactants (TPrA and 2-(dibutylamino) ethanol (DBAE)) were investigated, respectively. Depending on the types of coreactant, concentration of coreactant and CdTe QDs in the test solution, CNTs on GCE surface were observed to perform as both quencher (~ 80% quench) and the enhancer (~7-fold enhancement) of the ECL signal from CdTe QDs. The quenching effect of CNTs on ECL of CdTe QDs was caused by the dynamic quenching mechanism and the Stern Volmer constant (11.7 g/L) as well as an estimated quenching constant (1.2×10^9 L/g•s) for this mechanism were calculated based on a set of FL titration experiments. The excellent electronic and physical properties of CNTs were discussed as the reason for ECL enhancement from CdTe QDs. Which one of these two different effects of CNTs on ECL of CdTe QDs played the dominant role was strongly depended on factors, such as the types of coreactant, concentrations of coreactants and CdTe QDs. The quenching effect of CNTs on ECL of CdTe QDs was increased with increasing concentration of CdTe QDs. When compared with TPrA, the enhancing effect of CNTs on ECL of CdTe QDs was more significant than when DBAE was used as coreactant.

A layer-by-layer deposition technique was successfully used to load CdTe QDs on the surface of polystyrene beads (~ 4.6×10^5 CdTe QDs/PSB). These CdTe QDs loaded PSB was shown a promising potential as a candidate for ECL label of anti-$A\beta_{1-42}$ (anti-Amyloid β 42) to detect $A\beta_{1-42}$ at low concentrations with high selectivity. A potentially

highly sensitive ECL immunoassay was proposed with some preliminary results to detect

$A\beta_{1-42}$ in biological media.

ACKNOWLEDGMENTS

TABLE OF CONTENTS

ix

LIST OF TABLES

LIST OF ILLUSTRATIONS

LIST OF SCHEMES

CHAPTER I - INTRODUCTION

The main focus of this dissertation is to study the fundamental electrogenerated

chemiluminescence (ECL) properties of semiconductor nanoparticles (quantum dots or

QDs) which could be directly applied to the fabrication of ultrasensitive ECL

immunoassays. In this chapter, basic principles of electrochemistry, electrochemical

techniques (e.g. cyclic voltammetry), and ECL which were used frequently throughout

this dissertation are discussed with illustration of some classic examples. Fundamentals

of QDs and their applications in ECL based bioanalysis are also introduced in this

chapter. Brief introduction of other spectroscopic techniques, e.g., fluorescence

spectroscopy and UV-vis spectroscopy, that were used in this dissertation will be

provided in the respective chapters.

1.1 Fundamentals of Electrochemistry and Electrochemical Techniques

Electrochemistry is a branch of chemistry which studies the correlation between

chemical and electrical processes. A major part of this field deals with the interchange

between chemical energy and electrical energy. Techniques that are developed based on

the principles of electrochemistry are called electrochemical techniques. Electrochemical

techniques could be used for a variety of purposes. For instance, they could be used to

obtain thermodynamic data about a chemical reaction; Unstable intermediates such as

radical ions could be generated through electrochemical processes; Electrochemical

techniques also could be used to detect a trace amount of different species in a solution of

interest. In the following section, a commonly used electrochemical technique, cyclic

voltammetry, will be discussed in detail to illustrate how electrochemical principles are

applied in this technique to study a system of interest, such as the $Fe(CN)_6^{3-}/Fe(CN)_6^{4-}$

redox couple.[1-4]

1.1.1 Cyclic Voltammetry

Cyclic voltammetry (CV) is an electrochemical technique in which the electro-

current generated from a given system is measured when the potential that is applied to

the system is changing linearly at a constant rate between two values in a cycling fashion

(Figure 1.1). Because in CV the potential is linearly proportional to the time of potential

scanning, the current could also be plotted against the time. Due to its efficiency and

ability to provide a wide range of information about the system under study, CV is the

most heavily used electrochemical technique to explore the redox behavior of a chemical

system. To illustrate the basic concepts of this powerful electrochemical technique, the

classic redox couple, $Fe(CN)_6^{3-}/Fe(CN)_6^{4-}$ (Equation 1.1), will be used as an example

during the rest of this section.[5-15]

$$Fe(CN)_6^{3-} + e^- \rightleftharpoons Fe(CN)_6^{4-} \qquad\qquad 1.1$$

Redox behavior of this reversible system is govern by the Nernst equation

(Equation 1.2):

$$E = E^0_{Fe(CN)_6^{3-}/Fe(CN)_6^{4-}} + \frac{RT}{nF} \ln \frac{[Fe(CN)_6^{3-}]}{[Fe(CN)_6^{4-}]} \qquad\qquad 1.2$$

where E^0 is the standard reduction potential of the $Fe(CN)_6^{3-}/Fe(CN)_6^{4-}$ redox couple (V),

R is the gas constant (8.314472 J K^{-1} mol^{-1}), T is temperature (K), F is the Faraday

constant (96485.34 C mol^{-1}), and n is the number of electron transfer during the process.

At 25 °C, for this one electron transfer system, the Nernst equation can be rewritten as:

$$E = E^0_{Fe(CN)_6^{3-}/Fe(CN)_6^{4-}} + 0.059 \log \frac{[Fe(CN)_6^{3-}]}{[Fe(CN)_6^{4-}]} \ (at\ 25\ °C) \qquad\qquad 1.3$$

in which the redox potential of the system (E) is proportional to logarithm of $[Fe(CN)_6^{3-}]/[Fe(CN)_6^{4-}]$. Therefore, when the potential that is applied to this system changes, $[Fe(CN)_6^{3-}]/[Fe(CN)_6^{4-}]$ will also change through electron transfer to fulfill the Nernst Equation (Equation 1.3). This process causes transferring of electrons between the test solution and the working electrode which generates a current flow through this system. When this current is plotted against the applied potential, i.e; a current vs. potential diagram (Figure 1.2), which is called the cyclic voltammogram, can be recorded by a potentiostat. Cyclic voltammogram in Figure 1.2 was obtained from 6.0 mM $K_3Fe(CN)_6$ aqueous solution with 1.0 M KNO_3 (supporting electrolyte) on a Pt electrode when the cyclic potential was scanned between 0.80 and 0 V vs.Ag/AgCl (3.0 M KCl) for one cycle at 50.0 mV/s scan rate. At initially phase of the potential scan (a → b in Figure 1.2), there is no detectable current flow through the system because the applied potential is too positive than E^0 to cause distinguishable $[Fe(CN)_6^{3-}]/[Fe(CN)_6^{4-}]$ change. When the potential scans to further cathodic direction, a positive current starts to form (b in Figure 1.2.) because $Fe(CN)_6^{3-}$ begin to be reduced to $Fe(CN)_6^{4-}$ in order to decrease the value of $[Fe(CN)_6^{3-}]/[Fe(CN)_6^{4-}]$. This positive current keeps increasing with the decreasing potential and reaches to a maximum value (b → c in Figure 1.2) before decreasing back with further potential scanning towards cathodic direction (c → d in Figure 1.2). This peak-shaped current (b → c → d in Figure 1.2) is generated because, with the decreasing applied potential, more $Fe(CN)_6^{3-}$ ions are reduced which produces more electron flow from the test solution to the working electrode. However, the current starts to decrease from point c to point d in Figure 1.2 when $[Fe(CN)_6^{3-}]$ is approaching zero on the electrode surface. When the potential is scanned back from 0 V to 0.80 V,

3

similar process takes place on the working electrode surface in which the reaction in

Equation 1.1 is driven to the formation of $Fe(CN)_6^{3-}$ ions (d → e → a in Figure 1.2).
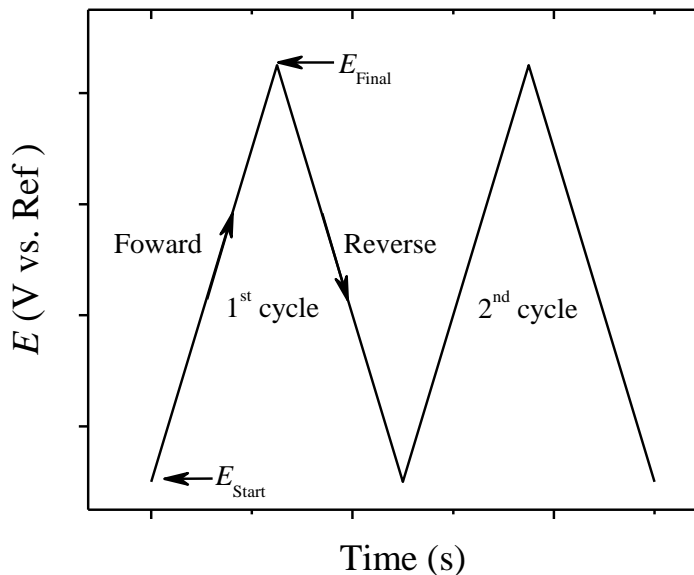
Figure 1.1 The potential wave form of cyclic voltammetry.

In cyclic voltammetry, the value of the peak current (i_p) from a reversible system

is governed by the Randles-Sevcik equation (Equation 1.4):[1]

$$i_p = (2.69 \times 10^5)n^{3/2}AD^{1/2}Cv^{1/2} \qquad 1.4$$

in which n is number of electron transferred, A is electrode surface area (cm^2), D is

diffusion coefficient (cm^2/s), C is concentration of electroactive species (mol/cm^3), v is

scan rate (V/s) at which the potential was applied to the system through a working

electrode. Therefore, peak current of a reversible system (i_p) is linearly proportional to

the concentration of the electroactive species and the square root of the scan rate at which

the potential that is applied on the system is changed.

4
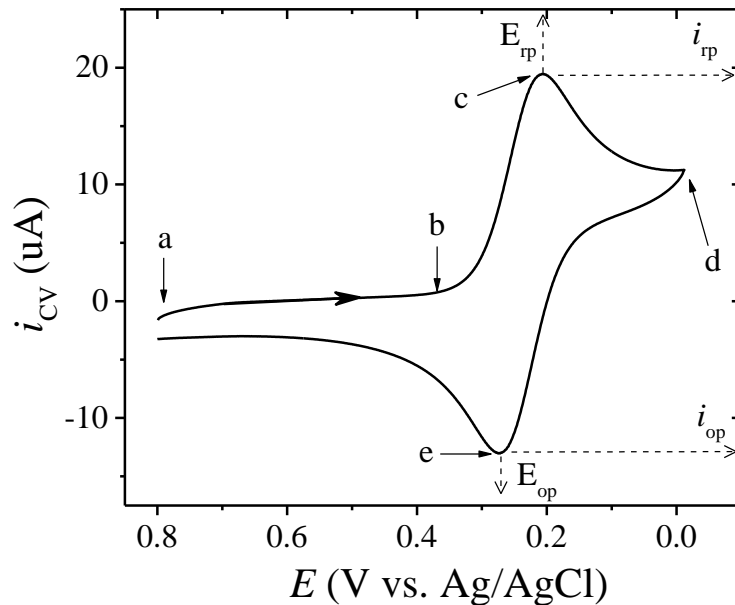
Figure 1.2 Cyclic voltammogram of the $Fe(CN)_6^{3-}/Fe(CN)_6^{4-}$ redox couple.

Note: CV signal was obtained from 6.0 mM $K_3Fe(CN)_6$ in 1.0 M KNO_3 on a 2.0 mm-diameter Pt electrode with a scan rate of 50.0 mV/s.

1.1.1.2 Electrode Surface Charge

The electrolyte double layer and heterogeneous electron transfer rate on an electrode surface can be affected by the presence of an ionic compound on the electrode surface. In addition, if the electroactive species in the test solution is also an ionic compound, the electrostatic (or repulsion) interaction can change the concentration of electroactive species on the electrode surface (pre-concentration effect). As a result, when an electrode surface modified with an ionic compound, compare with the bare electrode, different CV behavior will be observed the same ionic electroactive species on this electrode.[16-19]

The effect of electrode surface charges, which is introduced through electrode modification, on CV current are illustrated in scheme 1.1. When a positively charged

5

species A^+ is studied on a neutral electrode surface (bare electrode), a current i will generate from this system. If the surface of this electrode is modified with a positively charged ion and other conditions remain constant, compared with the case in Scheme 1.1c, the concentration of A^+ on this electrode surface will be decreased through electrostatic repulsion. As a result, a lower CV current will be generated from Scheme 1.1a (i_a) compared with that from Scheme 1.1c (i). On the other hand, the CV current will be increased by the electrostatic interaction between the electrode surface and A^+ if the electrode surface is negatively charged as compared with the neutral electrode surface (Scheme 1.1b vs. Scheme 1.1c).

This concept is successfully applied in a study of EDC coupling reaction on a glassy carbon electrode surface which will be discussed in Chapter III

(a)   (b)   (c)

$i_a > i$ $i_b < i$ i
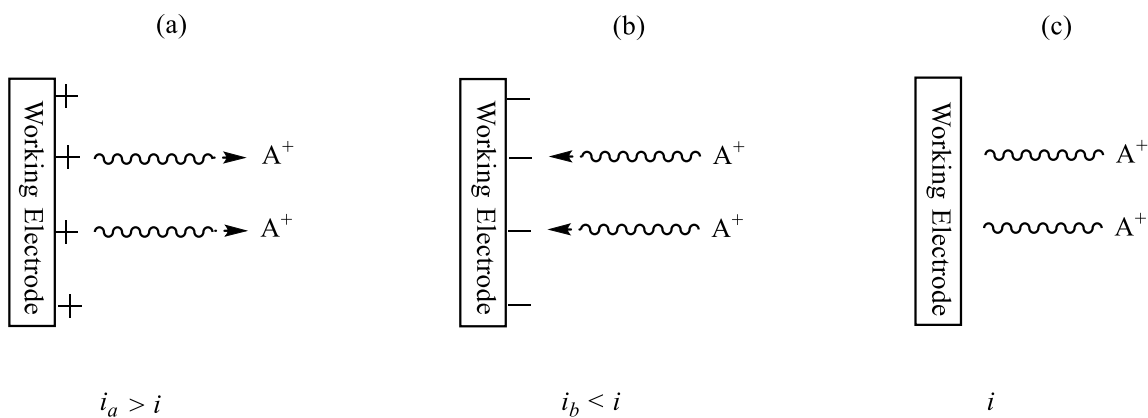
Scheme 1.1 Effect of electrode surface charge on CV current.

1.2 Fundamentals of Electrogenerated Chemiluminescence

Luminescence is generation of light from light producible species called luminophores without releasing heat.[20] There are many different ways to generate luminescence from luminophores and the general mechanisms of three most common luminesence processes are illustrated in Scheme 1.2.[21] These three luminesence processes

6

are different in the way that how the final exited state of the luminophore is produced.

For instance, the ground state of the luminophore is exited through absorption of light in

fluorescence (FL).[22-24] In chemiluminescence (CL), on the other hand, two highly

reactive species go through an electron transfer process to form the exited state

luminiphore.[25,26] Electrogenerated chemiluminescence (ECL) can be considered as a

special type of chemiluminescence, because the exited state luminophore is also formed

through chemical reaction of highly energetic species which are generated specifically

through electrochemical reactions on an electrode surface.[27]

FL	CL	ECL
		$A - e^- \longrightarrow A^+$
$A + h\nu_1 \longrightarrow A^*$	$A + B \longrightarrow C^* + D$	$B + e^- \longrightarrow B^-$
$A^* \longrightarrow A + h\nu_2$	$C^* \longrightarrow C + h\nu$	$A^+ + B^- \longrightarrow A^* + B$
		$A^* \longrightarrow A + h\nu$
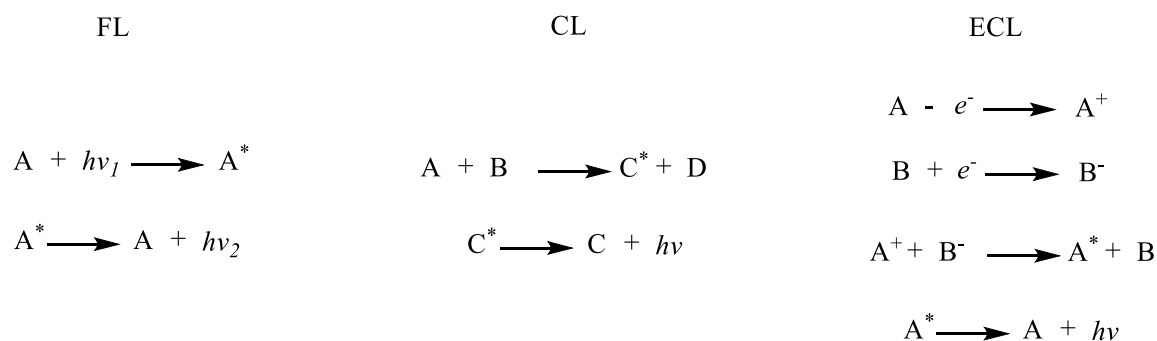
Scheme 1.2 Different types of luminescences generation mechanisms

Note: FL - fluorescence, CL - chemiluminescence, ECL - electrogenerated chemiluminescence

By definition, ECL is a type of luminescence which involves the generation of

light-generable species after electron-transfer reactions on an electrode surface.[27-31] For

instance, when an anodic potential is applied an ECL luminophore

(e.g., CdTe quantum dots), ECL can be generated on an electrode surface if an ECL

coreactant (e.g., tri-*n*-propylamine, TPrA) is present. Since the first detailed ECL study

was reported. in the mid-1960s by Hercules and Bard et al,[31-33] ECL has become a very

powerful analytical technique. ECL has been successfully used in the areas such as

immunoassay, food and water testing, and biowarfare agent detection.[27,34-51]

ECL is used in so many different fields as an analytical technique because it possesses some distinct advantages over other luminescence based techniques.[21] Due to the requirement of an extra light source to generate excited state luminophores, FL technique always encounters problems, such as light scattering, impure luminescence et al. These problems can be completely avoided in ECL since the extra light source is not needed for this technique. ECL can be generated only on an electrode surface when a potential is applied which is controlled by a potentiostat. CL lacks the similar controllability over the position and the time of the light emitting reaction. Therefore, ECL usually has a much high sensitivity relative to CL, because the electrode, on which ECL is produced, can be aligned directly with the detector. In addition, the crucial chemicals are normally regenerable in ECL, whilst the same claim cannot be made for CL.[21,27]

ECL can be produced through different pathways, such as anihilation, coreactant, hot-electron injection, and electrostatic chemiluminescence.[27,40,52-54] In the following two sections, the basic mechanisms of two pathways (annihilation and coreactant) that are used in this dissertation will be elaborated.

1.2.1 Annihilation Pathway

In annihilation pathway, ECL luminophore is oxidized and reduced to form different ion radicals which then can annihilate with each other to generate the exited state of ECL luminiphore. Possible mechanisms for annihilation ECL pathway are demonstrated in Equations 1.5-1.10. After the ion radicals ($A^{\bullet+}$, $A^{\bullet-}$) of the ECL luminophore (A) are formed electrochemically, if the energy of the ion radicals is sufficiently high, they could generate singlet exited ECL luminophore ($^1A^*$) by direct

annihilation as shown in Equations 1.5 - 1.7. If less energetic ion radicals are formed in the first two steps (Equations 1.5-1.6), triplet excited state ECL luminophore ($^3A^*$) can be formed (Equations 1.5-1.6, 1.8). These triplet-excited state ECL luminophores then can go through a self-annihilation process to generate the final singlet excited state (Equation 1.9).[21]

$$A - e^- \rightarrow A^{\bullet+} \qquad\qquad 1.5$$

$$A + e^- \rightarrow A^{\bullet-} \qquad\qquad 1.6$$

$$A^{\bullet+} + A^{\bullet-} \rightarrow A + {}^1A^* \qquad\qquad 1.7$$

Or

$$A^{\bullet+} + A^{\bullet-} \rightarrow A + {}^3A^* \qquad\qquad 1.8$$

$$^3A^* + {}^3A^* \rightarrow A + {}^1A^* \qquad\qquad 1.9$$

$$^1A^* \rightarrow A + h\nu \qquad\qquad 1.10$$
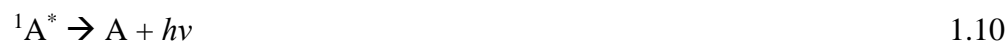
In order to generate ECL from an ECL luminophore through annihilation pathway, there are two requirements that need to be met:[27]

(1) Solvent of choice for ECL generation must possess relatively large potential window, since the ECL luminophore needs to be both oxidized and reduced electrochemically during the process.

(2) Ion radicals with relatively long lifetime need to be generated

electrochemically from the ECL luminophore, because ECL luminophore often cannot be

electrochemically oxidized and reduced simultaneously on the electrode surface.

Few ECL systems which could meet all requirements above have been found.

Therefore, annihilation pathway has not been the first choice for many ECL based bio-

analysis studies. However, annihilation ECL can be used to obtain some redox

information of a system where other conventional methods fail to do so. ECL generation

requires both electrochemical reduction and oxidation of the ECL luminophore during

annihilation pathway. Therefore, the potential at which the ECL signal starts to be

generated could be estimated as the reduction/oxidation potential of the ECL

luminophore. This concept will be applied and explained in more detail in Chapter II.

1.2.2 Coreactant Pathway

Compared with annihilation ECL, which requires both electrochemical oxidation

and reduction of ECL luminophores, coreactant ECL is generated only by one directional

potential scanning within a much shorter potential range.[55] In coreactant ECL pathway, a

strong oxidative or reductive intermediate forms after electrochemical reaction of a

deliberately-added species called coreactant. ECL luminophore could also be

electrochemically oxidized or reduced during the above step. Finally, the ECL

luminophore can go through a series of electron transfer reactions with the reactive

intermediate generated from the coreactant to produce the final excited state ECL

luminophore.

Although, there are four different ways to generate ECL as previously mentioned,

commercially available ECL devices are mainly designed based on the coreactant

pathway. This is because coreactant ECL owns the following advantages over other pathways.[21] First, ECL can be generated from the ECL luminophores with only one electrochemical state, either oxidation or reduction, in the presence of a suitable coreactent. Second, solvents with a narrow potential window can be used for coreactant ECL systems because only one directional potential scanning is needed. Third, coreactant ECL does not often require long lifetime radicals from ECL luminophore and coreactant redox reaction as they can be generated almost spontaneously on an electrode surface.[55]

The excited state of the ECL luminophore in coreactant ECL pathway is generated in a much complex way which varies for different coreactants as well.[55] In the following two sections two classic coreactant ECL systems, $Ru(bpy)_3^{2+}$/TPrA and $Ru(bpy)_3^{2+}$/$S_2O_8^{2-}$, will be used as examples to explain the basic mechanisms of coreactant ECL.[56-64]

1.2.2.1 $Ru(bpy)_3^{2+}$/TPrA System

Tris(bipyridine)ruthenium(II) ($Ru(bpy)_3^{2+}$) possess excellent chemical, electrochemical, and photophysical properties in aqueous media in the presence of oxygen. Therefore, $Ru(bpy)_3^{2+}$/TPrA system is the most heavily studied coreactant ECL system with a large number of applications.[65-70] It has been shown that the ECL emission of this system consists of two anodic ECL waves on a glassy carbon electrode when low concentration of $Ru(bpy)_3^{2+}$ was used as shown in Figures 1.3.[64]
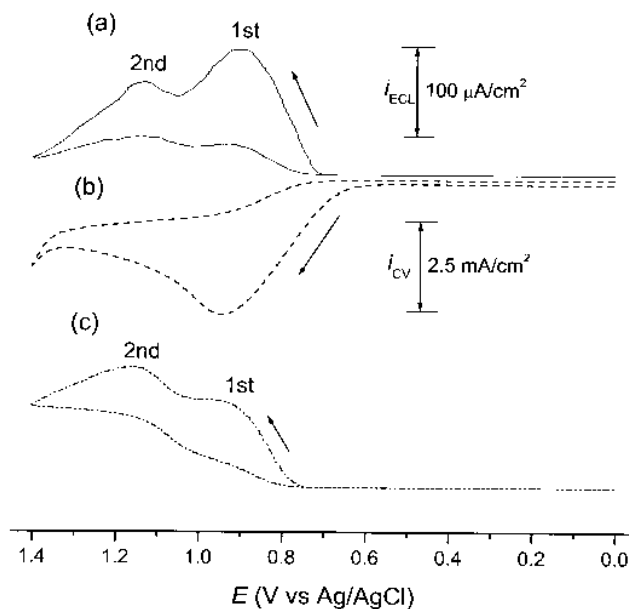
Figure 1.3 (a) ECL and (b) cyclic voltammogram of the Ru(bpy)$_3^{2+}$/TPrA system.

Note: Signals were obtained from1.0 nM Ru(bpy)$_3^{2+}$ in 0.10 M Tris/0.10 M LiClO$_4$ buffer (pH 8.0) with 0.10 M TPrA at a 3.0 mm

diameter glassy carbon electrode at a scan rate of 50.0 mV/s. Adapted with permission from Ref 64. Copyright (2002) American

Chemical Society. [64]
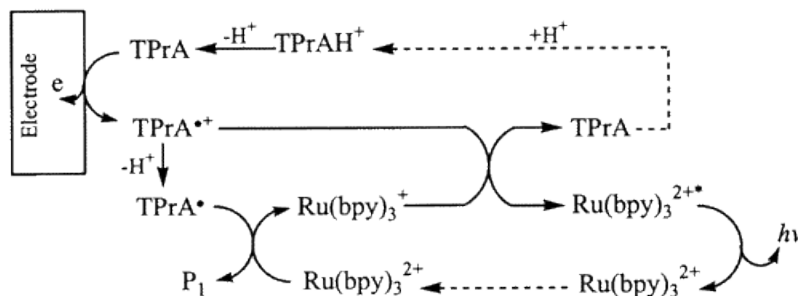
Scheme 1.3 Mechanism of the first ECL wave of the Ru(bpy)$_3^{2+}$/TPrA system

Note: where TPrA$^{•+}$ = (CH$_3$CH$_2$CH$_2$)$_3$N$^{•+}$, TPrAH$^+$ = Pr$_3$NH$^+$, TPrA$^•$ = Pr$_2$NC$^•$HCH$_2$CH$_3$, P$_1$=Pr$_2$N$^+$CH=CH$_2$CH$_3$. Adapted with

permission from Ref 64. Copyright (2002) American Chemical Society.[64]

Mechanism responsible for the first ECL wave was reported by Miao et al

(Scheme 1.3).[64] According to this mechanism, TPrA is, first, electrochemically oxidized

on the electrode surface to generate TPrA$^{•+}$ which then immediately deprotonates to

produce highly reductive TPrA$^•$. In the next step, Ru(bpy)$_3^{2+}$ is reduced to Ru(bpy)$_3^+$ by

12

TPrA$^{\bullet}$ and the final excited state of Ru(bpy)$_3^{2+}$ (Ru(bpy)$_3^{2+*}$) was generated by oxidation

of Ru(bpy)$_3^+$ with TPrA$^{\bullet+}$ in the following step.
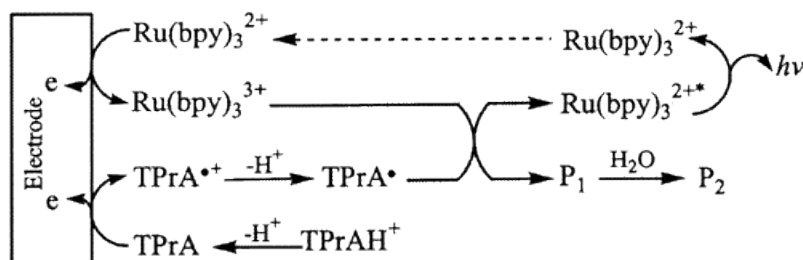
Scheme 1.4 First possible mechanism for the second ECL wave of the Ru(bpy)$_3^{2+}$/TPrA system.

Note: Adapted with permission from Ref 64. Copyright (2002) American Chemical Society.[64]
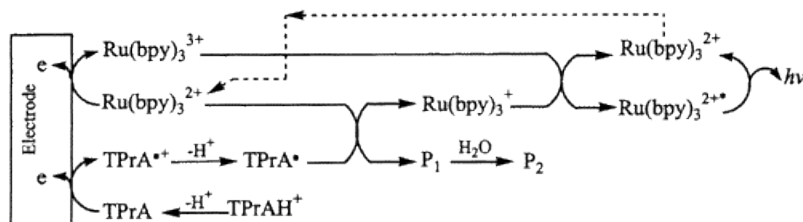
Scheme 1.5 Second possible mechanism for the second ECL wave from the Ru(bpy)$_3^{2+}$/TPrA system.

Note: Adapted with permission from Ref 64. Copyright (2002) American Chemical Society.[64]

Two different possible mechanisms could contribute to the formation of the

second ECL wave from the Ru(bpy)$_3^{2+}$/TPrA system.[64] In the potential range of second

ECL wave (1.10 V – 1.40 V), Ru(bpy)$_3^{2+}$ can be directly oxidized to Ru(bpy)$_3^{3+}$ on the

electrode surface. A strong reducing agent, TPrA$^{\bullet}$, is also generated after TPrA goes

through electrochemical oxidation and deprotonation process, respectively, similar to the

first peak mechanism mentioned above (Scheme 1.3). This strong reducing agent, then,

could directly reduce Ru(bpy)$_3^{3+}$ to Ru(bpy)$_3^{2+*}$ (Scheme 1.4). The other possible

mechanism for the second ECL wave is shown in Scheme 1.5. In this mechanism, besides

the formation of Ru(bpy)$_3^{3+}$ through electrochemical oxidation of Ru(bpy)$_3^{2+}$, Ru(bpy)$_3^+$

13

could also be generated via reduction of $Ru(bpy)_3^{2+}$ by $TPrA^\bullet$. $Ru(bpy)_3^{3+}$ and $Ru(bpy)_3^{+}$ then can transfer electron to generate $Ru(bpy)_3^{2+*}$.

ECL mechanisms of the CdTe QDs/TPrA system which is proposed based on these mechanisms will be discussed in Chapter II with relevant experimental results.

1.2.2.2 $Ru(bpy)_3^{2+}/S_2O_8^{2-}$ System

As previously discussed, formation of the strong reductant $TPrA^\bullet$ (E^0 = ~-1.70 V vs. SCE)[71] is crucial for ECL generation from the $Ru(bpy)_3^{2+}/TPrA$ system. A strong oxidizing agent, $SO_4^{\bullet-}$, (E^0 = ~3.15 V vs. SCE),[58] could be considered as the counterpart of $TPrA^\bullet$ in the $Ru(bpy)_3^{2+}/S_2O_8^{2-}$ system. However, unlike the $Ru(bpy)_3^{2+}/TPrA$ system, $Ru(bpy)_3^{2+}/S_2O_8^{2-}$ system only contains one ECL wave.[56] During the cathodic potential scanning, no ECL signal was generated even at ~-1.50 V (vs. SCE), a sufficiently negative potential to reduce $S_2O_8^{2-}$, but not negative enough to reduce $Ru(bpy)_3^{2+}$. This indicates that direct electrochemical reduction of $Ru(bpy)_3^{2+}$ was also necessary to generate $Ru(bpy)_3^{2+*}$ from the $Ru(bpy)_3^{2+}/S_2O_8^{2-}$ system.

Equations 1.11-1.18 summarize the possible mechanisms for generation of ECL from the $Ru(bpy)_3^{2+}/S_2O_8^{2-}$ system.[55] First, $S_2O_8^{2-}$ is electrochemically reduced to $S_2O_8^{3-\bullet}$ (Equation 1.11). Formation of $Ru(bpy)_3^{+}$ on the electrode surface in the next step (Equation 1.12) also helps the formation of $S_2O_8^{3-\bullet}$ through chemical reduction (Equation 1.13). Then, a strong oxidant, $SO_4^{\bullet-}$, is formed by decomposition of $S_2O_8^{3-\bullet}$ (Equation 1.14). $SO_4^{\bullet-}$ could either oxidize $Ru(bpy)_3^{+}$ (Equation 1.15) to final excited state of $Ru(bpy)_3^{2+*}$, or react with $Ru(bpy)_3^{2+}$ to generate $Ru(bpy)_3^{3+}$ (Equation 1.16) in the following step. Finally, $Ru(bpy)_3^{3+}$ and $Ru(bpy)_3^{+}$ can also generate $Ru(bpy)_3^{2+*}$ by ion annihilation (Equation 1.17).

$$S_2O_8{}^{2-} + e^- \rightarrow S_2O_8{}^{3-\bullet} \tag{1.11}$$

$$Ru(bpy)_3{}^{2+} + e^- \rightarrow Ru(bpy)_3{}^+ \tag{1.12}$$

$$Ru(bpy)_3{}^+ + S_2O_8{}^{2-} \rightarrow Ru(bpy)_3{}^{2+} + S_2O_8{}^{3-\bullet} \tag{1.13}$$

$$S_2O_8{}^{\bullet 3-} \rightarrow SO_4{}^{\bullet-} + SO_4{}^{2-} \tag{1.14}$$

$$Ru(bpy)_3{}^+ + SO_4{}^{\bullet-} \rightarrow Ru(bpy)_3{}^{2+*} + SO_4{}^{2-} \tag{1.15}$$

Or

$$Ru(bpy)_3{}^{2+} + SO_4{}^{\bullet-} \rightarrow Ru(bpy)_3{}^{3+} + SO_4{}^{2-} \tag{1.16}$$

$$Ru(bpy)_3{}^+ + Ru(bpy)_3{}^{3+} \rightarrow Ru(bpy)_3{}^{2+*} + Ru(bpy)_3{}^{2+} \tag{1.17}$$

$$Ru(bpy)_3{}^{2+*} \rightarrow Ru(bpy)_3{}^{2+} + h\nu \tag{1.18}$$
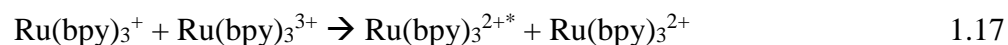
1.3 Fundamentals of Semiconductor Nanoparticles (Quantum Dots)

Semiconductor nanoparticles (also called quantum dots or QDs) are colloidal semiconductor with a size in several nanometer rang.[72-74] After the first report on QDs in 1980s, tremendous amount of research interests have been shown to this field.[74,75] As a result, increasingly more scientific aspects of QDs have begun to unfold and their applications have been explored in two major areas: bio-analysis/diagnosis and electro-optic devices.[76-82]

The most unique characteristic of QDs is their size dependent optical and electronic properties.[72,73,83,84] For instance, within their Bohr radius range, optical and

electronic properties of QDs are tunable via size modification. Furthermore, because of the extremely large surface to volume ratio of QDs, many of the optical and electrochemical properties of them are extremely sensitive to their surface properties. This, again, provides scientists with freedom of controlling different properties of QDs through surface modifications.[84]

1.3.1 Size Dependent Optical Properties of QDs

In bulk semiconductor materials, when an electron from the valance band is excited to the conduction band via absorption of a photon, a positively charged hole forms at the valance band at the same time (Figure 1.4). This electron and the hole are separated by an energy forbidden area called bandgap between conduction band and valance band. The energy state of these two oppositely charged carrier pair (also called exciton) is mainly governed by Columbus interaction due to the continuum nature of the both bands in bulk materials. However, when the size of the semiconductor particles become comparable to Bohr radius of their bulk materials, the continuum energy bands will turn into discrete energy levels (quantum confinement effect). As a result, energy state of the exciton in a QDs will become higher than that in its bulk material (Figure 1.4).[85]

The approximation of energy bandgap in a spherical QDs is reported by Brus as Equation 1.19.[75]

$$E_{g,effective}(R) = E_g(\infty) + \frac{h^2\pi^2}{2R^2}\left(\frac{1}{m_e} + \frac{1}{m_h}\right) - \frac{1.8e^2}{\varepsilon R} \qquad 1.19$$

In this equation, $E_g(\infty)$ is the energy bandgap of the bulk material, m_e and m_h are the effective masses of hole and electron respectively, and ε is the dielectric constant of the bulk material. According to Equation 1.19, the effective bandgap of a QDs is inversely

proportional to R^2 in the second term which is the representation of the particle in a box

model. The third term in this equation is the expression of the Columbus interaction. For

the QDs with a size in nanometer range, the second term becomes dominant in Equation

1.19. Consequently, energy bandgap in a QD increases with decreasing particle size.

Optical signature of quantum confinement effect in QDs is the blue shifted emission and

absorption spectrum of the QDs with decreasing particle size.[86] Figure 1.5 shows the

increasing PL emission peak wavelength from CdTe QDs with increasing particle size.[86]
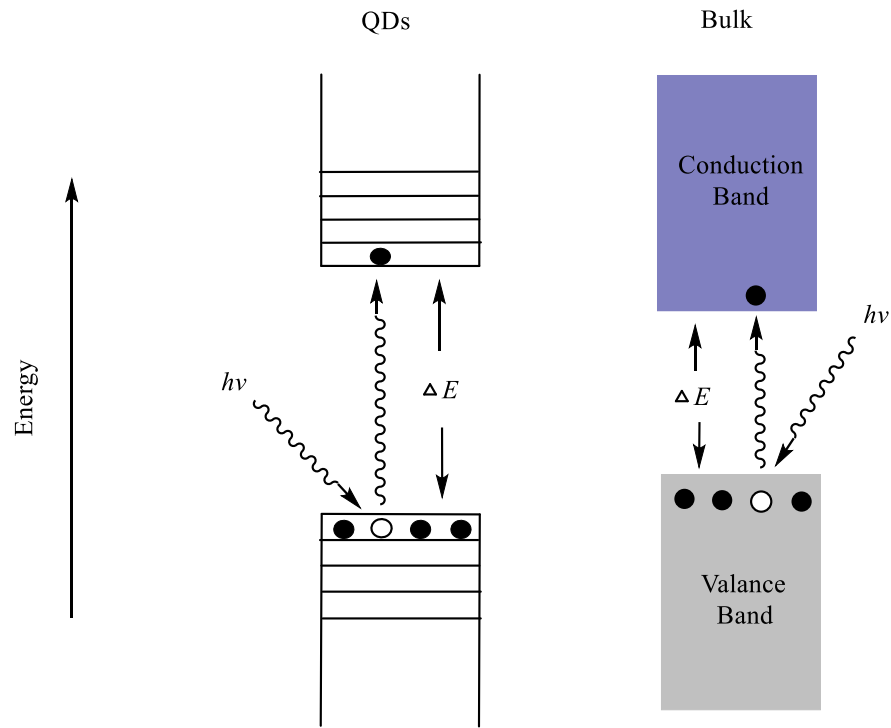
Figure 1.4 Schematic energy bandgap representation of QDs and their bulk materials.
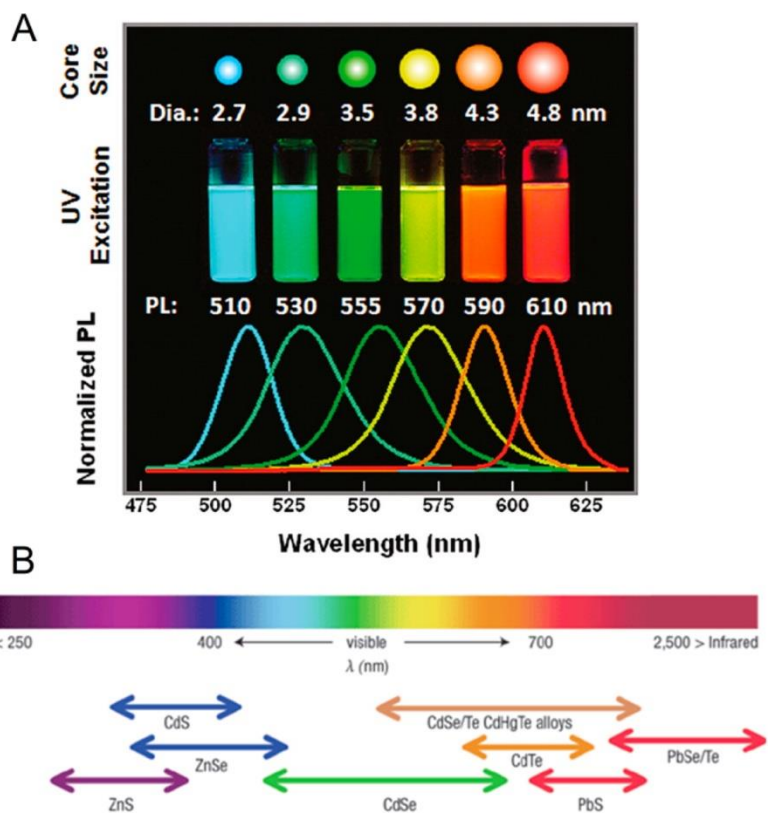
Figure 1.5 Fluorescence spectra of CdTe QDs with different particle sizes.

The size dependent properties of QDs (quantum confinement effect) becomes significant especially when the particle size is similar or smaller than the Bohr exciton radius,α_B, which is given by:[75]

$$\alpha_B = \frac{\varepsilon_0 \varepsilon h^2}{\pi \mu e^2}$$ 1.20

where ε_0 and ε are the permittivity of vacuum and relative permittivity of the semiconductor, μ is the reduced mass of the electron and hole, e is the electron charge, and h is the Planck constant.

1.3.2 Photoluminescence (PL) versus ECL of QDs

After showing tremendous potential in the field of bioanalyses as photoluminescence emitters,[46,87-92] QDs started to attract the attention of the scientific

community as a potential ECL luminophore. The first ECL signal generation from QDs using silicon nanoparticles[93] and several more follow up studies using CdSe QDs,[94] CdSe@ZnS QDs,[95] and CdTe QDs[96] as ECL luminophore were reported by Bard et. al in early 2000s. This breakthrough provided ECL related studies with a totally new and superior type of ECL emitters as compared with the previously existed organic emitters and inorganic emitters.[21]

Contrary to the common belief, emission spectra of the same QDs were discovered to be different through varies luminescence processes.[96,97] To explain these different emissions from the same QDs through various luminescence processes, one must understand the two different electronic energy state of QDs, namely the band gap states and the surface states (Figure 1.6).[96,97]

The band gap state is originated from confining free electrons in QDs in certain dimension as a result of QDs formation. This is the electronic state that is govern by the quantum confinement effect. Therefore, the energy of the band gap state is sensitive to the particle size of the QDs.[98]
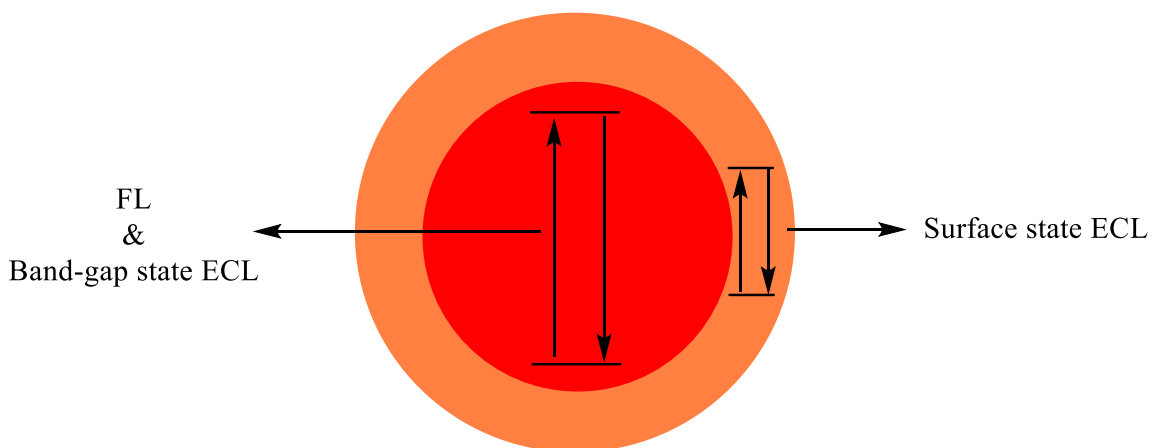
Figure 1.6 PL and ECL states of QDs.

The surface state, on the other hand, is not affected by size change of QDs. Due to the nano-scale size, QDs have a high surface to volume ratio and this ratio increases with decreasing particle size. For example, when around 33% of the atoms in a QDs with 5.0 nm diameter are located on the surface of the particle, it will increase up to 99% when the size of this quantum dot decreased to 1.0 nm.[99] This significant surface to volume ratio indicates that electronic and optical characteristics of QDs are very sensitive to their surface properties. Hence, surface defects, such as dangling bonds and unsaturated sites, of QDs could cause surface trapping of electrons and form a new and lower energetic (compared with band gap state) electronic state, the surface state.[94] When the surface defects on QDs are eliminated by application of proper capping agents, the surface state can be passivated. The experimental signature for this surface state passivation is overlapped ECL and PL spectra from the same QDs.[96,97]

However, PL, in many cases, is much less sensitive to the surface state of QDs than ECL.[97] This is because, during PL process, surface state acts more of a quenching center than a new emission band.[97] As a result, surface state PL emission intensity is significantly lower than pure band gap state PL emission which makes it less obvious than it is in ECL emission process.[97] Although, PL is much less sensitive to surface state, its existence still could be indicated by signs such as, unsymmetrical PL spectrum with elongated non-zero background tail et al.[94]

Photoluminescence and ECL emission peak wavelengths obtained from CdSe QDs,[94] CdSe@ZnSe QDs,[95] and CdTe QDs[96] are the perfect examples for demonstration of surface state and band gap state ECL. As summarized in Table 1.1, ECL emission peak of CdSe QDs is red shifted from its PL peak by ~160 nm.[94] Two ECL

peaks, at ~580 nm and ~740 nm respectively from CdSe@ZnSe QDs and a single PL

peak at ~580 nm were reported by Bard et al.[95] Although the first ECL peak was almost

at the same wavelength at the PL peak of CdSe@ZnSe, the second ECL peak was, again,

appeared at much higher wavelength (740 nm vs. 580 nm). A single ECL peak and a PL

peak at almost the same wavelength (~635 nm) were generated from CdTe QDs.[96] The

significant red-shifted ECL peak of CdSe QDs compared with its PL peak was generated

from surface state of this QDs. Two ECL peaks of CdSe@ZnSe QDs indicates that both

surface state and bandgap state were present in these QDs which was caused by

incomplete passivation of the surface state. The ECL peak of CdTe QDs was observed

almost at the same wavelength as its PL peak because the surface state of the QDs was

successfully passivated.

Table 1.1

PL and ECL emission peak wavelengths of CdSe QDs, CdSe@ZnS QDs, and

CdTe QDs

Spectrum	QDs		
	CdSe QDs[94]	CdSe@ZnS QDs[95]	CdTe QDs[96]
PL	~555 nm	~580 nm	~635 nm
ECL	~740 nm	1st peak ~580 nm 2nd peak~740 nm	~638 nm

1.4 QDs Based ECL Immunoassay

A large number of QDs based bio-analytical techniques have been developed

since the QDs were started to be used as ECL emitters.[97,98,100,101] Varies trace amount of

target biological molecules, such as DNAs,[101-106] and antigens[107-111] etc., were selectively detected using QDs base ECL.[111-120] Sandwich type ECL immunoassays with QDs as signal generator is the most frequently used strategy to detect a trace amount of antigen in an unknown sample.[101,121] QDs based ECL immunoassays possess selectivity of antigen-antibody interactions and the sensitivity of ECL signal generation from QDs.[21] Therefore, many promising ECL immunoassays have been fabricated towards different target antigens over the past decade.[97,98]

Basic principle of QDs based ECL immunoassays is to correlate the ECL signal generated from the QDs, which are labeled on the antibody, with the concentration of the target antigen.[21] The general scheme of QDs based ECL immunoassay is demonstrated in Figure 1.7. An antibody attached on the electrode surface is used to capture the target antigen. Then, a secondary antibody, which is labeled with QDs, is bonded to the antigen on the electrode surface through specific antigen-antibody interaction. The ECL signal intensity generated from the QDs on this electrode surface, usually in the presence of a coreactant, can be correlated to the concentration of antigen.
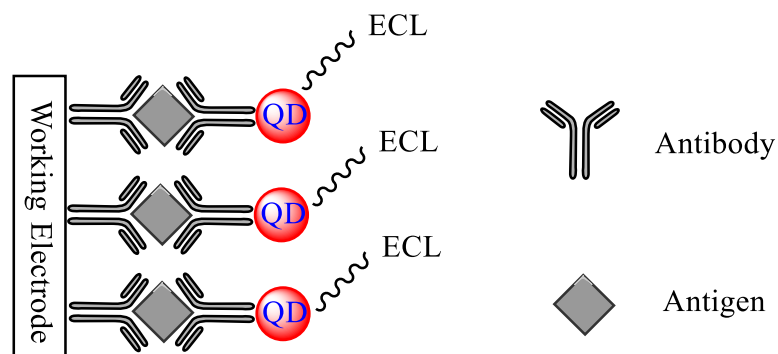
Figure 1.7 Basic QDs based ECL immunoassay.

The antibody does not have to be directly labeled by the ECL emitter QDs. In some ECL immunoassays, the secondary antibody was labeled with signal changing

reagent, quencher or enhancer, which could cause a detectable signal change from the ECL signal of constant amount of QDs in the system. For example, a signal-off ECL immunoassay towards α-fetoprotein was fabricated by labeling the antibody with Hemin loaded gold nanoparticles which could quench the ECL signal of CdS QDs that were immobilized on a GCE.[114,122]

1.4.1 Performance Improvement Strategies

An ideal QDs based ECL system for immunoassay fabrication is expected to be able to generate strong ECL signal at low potentials.[97,98] ECL efficiency from the QDs could directly determine the sensitivity of the immunoassay. Low operating potential could prevent electrochemical damaging of the biological components in the immunoassay. However, very few QDs based ECL systems meet these requirements. Therefore, materials with excellent electrochemical properties and good stabilities were introduced to the QDs based ECL immunoassays to improve their performance.

1.4.1.1 Carbon Nano-Materials

Carbon nano-materials, such as carbon nanotubes, graphite, graphene et al, are recognized as an excellent supporting materials for electrochemical studies.[98,123-125] Owning to their high conductivity and electro-catalytic properties, presence of carbon nanomaterials on an electrode surface could lower the potential necessary for an electrochemical process.[123-125] In addition, the effective surface area of the electrode could be increased by modification with carbon nano-materials which will result in generation of more electrochemically generated products on this electrode.[123-125] Therefore, carbon nano-materials have been commonly used in ECL immunoassay fabrications as supporting materials to improve their performance. For instance, a ~4

times enhanced ECL signal from CdS QDs on carbon nanospheres modified GCE than that on a bare GCE was reported by Ju et al.[116] The similar effect of graphene on ECL signal of CdS QDs was discovered.[126] Interestingly, however, quenching of ECL signal from CdS QDs and $Ru(bpy)_3^{2+}$ by carbon nanotubes was also reported.[122,127] These completely opposite effects of carbon nanotubes on ECL intensity of QDs will be discussed in detail with a series of experimental results in Chapter IV.

1.4.1.2 ECL Emitters Loaded Polystyrene Beads (PSBs)

Another strategy to improve the performance of ECL immunoassays is to use PSBs that are loaded with a large amount of ECL emitters, e.g. $Ru(bpy)_3^{2+}$, as ECL labels.[67,128,129] In this strategy, the number of ECL emitters that correspond to each antibody-antigen interaction are significantly larger than labeling the antibody with individual ECL emitters. Therefore, the ECL immunoassays fabricated by this strategy were reported to be highly sensitive towards their corresponding target antigens.[67,103,128]
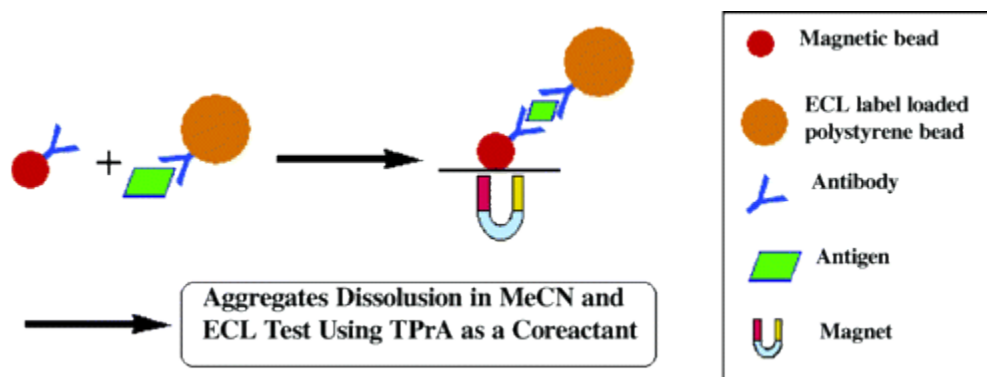
Figure 1.8 Schematic representation of ECL immunoassay using $Ru(bpy)_3^{2+}$ loaded PSBs as antibody labels.

Note: Adopted with permission from Ref. 128 Copyright (2004) American Chemical Society.[128]

Schematic of an ECL immunoassay using $Ru(bpy)_3^{2+}$ loaded PSBs as ECL labels fabricated by Miao et al is shown in Figure 1.8.[128] In this ECL immunoassay, $Ru(bpy)_3^{2+}$

loaded PSBs and magnetic beads labeled antibodies (anti-C-reactive protein or anti-CRP) were separately prepared. After the immunoreaction between labeled antibodies and the antigen (CRP), the final conjugate was separated from the reaction system and was dissolved in an ECL test solution (TPrA containing acetonitrile) to release the $Ru(bpy)_3^{2+}$ from PSBs. The final solution was used for ECL generation, intensity of which was linearly correlated to $\log C_{CRP}(\mu g.\,mL^{-1})$. Owning to loading of approximately ~10^9 $Ru(bpy)_3^{2+}$ molecule to each PSB, a detection limit of 0.010 µg.mL^{-1} was obtain by this immunoassay, which was much lower than other reported detection methods for the same target antigen.[128] Recently, an ECL immunoassay was fabricated using the similar strategy to detect Zika virus in biological fluids.[129]

1.5 References

(1)   Faulkner, L. R; Bard, A. J. *Electrochemical Methods–Fundamentals and Applications* 2nd ed.; John Wiley and Sons: New York, 2000.

(2)   Koryta, J. D., J. *Principles of Electrochemistry*; John Wiley and Sons: New York, 1987.

(3)   Sawyer, D. T. S., A.; Roberts, J. J. L.; *Electrochemistry for Chemists:*; Second Edition ed.; Wiley, 1995.

(4)   Scholz, F. *Electroanalytical Methods: Guide to Experiments and Applications*; 2nd printing; Springer, 2005.

(5)   Arrigan, D. W. M. *Analyst.* **1994**, *119*, 1953.

(6)   Dong, S.; Wang, Y. *Electroanalysis.* **1989**, *1*, 99.

(7)   Evans, D. H.; O'Connell, K. M.; Petersen, R. A.; Kelly, M. J. *J. Chem. Educ.* **1983**, *60*, 290.

(8)   Gosser, D. K. *Cyclic Voltammetry: Simulation and Analysis of Reaction Mechanisms;* ; VCH, 1993.

(9)   Holder, G. N.; Farrar, D. G.; McClure, L. L. *Chem. Educ.* **2001**, 343.

(10)   Kalcher, K. *Electroanalysis.* **1990**, *2*, 419.

(11)   Kalcher, K.; Kauffmann, J. M.; Wang, J.; Švancara, I.; Vytřas, K.; Neuhold, C.; Yang, Z. *Electroanalysis.* **1995**, *7*, 5.

(12)   Scott, K. F.; Phillips, C. S. G. *J. Chromatogr. Sci.* **1983**, *21*, 125.

(13)   Toma, H. E.; Araki, K.; Dovidauskas, S. *J. Chem. Educ.* **2000**, *77*, 1351.

(14)   Walcarius, A. *Electroanalysis.* **1996**, *8*, 971.

(15)   Walcarius, A.; Despas, C.; Trens, P.; Hudson, M. J.; Bessière, J. *J. Electroanal.*

Chem. **1998**, *453*, 249.

(16)   Eggers, P. K.; Hibbert, D. B.; Paddon-Row, M. N.; Gooding, J. J. *J. Phys. Chem. C.*
2009, *113*, 8964.

(17)   Campiña, J. M.; Martins, A.; Silva, F. *J. Phys. Chem. C.* **2009**, *113*, 2405

(18)   Calvente, J. J.; López-Pérez, G.; Ramírez, P.; Fernández, H.; Zón, M. A.; Mulder,
W. H.; Andreu, R. *J. Am. Chem. Soc.***2005**, *127*, 6476.

(19)   Campiña, J. M.; Martins, A.; Silva, F. *J. Phys. Chem. C.* **2007**, *111*, 5351.

(20)   Lakowicz, J. R. *Principles of Fluorescence Spectroscopy*; Springer: New Mexico,
2006.

(21)   Miao, W. *Chem. Rev.* **2008**, *108*, 2506.

(22)   Agbaria, R. A.; Oldham, P. B.; McCarroll, M.; McGown, L. B.; Warner, I. M. *Anal.
Chem.* **2002**, *74*, 3952.

(23)   Oldham, P. B.; McCarroll, M. E.; McGown, L. B.; Warner, I. M. *Anal. Chem.* **2000**,
72, 197.

(24)   Powe, A. M.; Fletcher, K. A.; St. Luce, N. N.; Lowry, M.; Neal, S.; McCarroll, M.
E.; Oldham, P. B.; McGown, L. B.; Warner, I. M. *Anal. Chem.* **2004**, *76*, 4614.

(25)   Roda, A.; Guardigli, M.; Michelini, E.; Mirasoli, M.; Pasini, P. *Anal. Chem.* **2003**,
75, 462 A.

(26)   Kuyper, C.; Milofsky, R. *TrAC, Trends Anal. Chem.* **2001**, *20*, 232.

(27)   Bard, A. J. Ed; *Electrogenerated Chemiluminescence*; Marcel Dekker, Inc.: New
York, 2004.

(28)   Richter, M. M. *Chem. Rev.* **2004**, *104*, 3003.

(29)   Knight, A. W. In *Chemiluminescence in Analytical Chemistry*; Grarcia-Campana,

A. M., Baeyens, W. R. G., Eds.; Marcel Dekker: New York, 2001, p 211.

(30) Knight, A. W. *TrAC, Trends Anal. Chem.* **1999**, *18*, 47.

(31) Hercules, D. M. *Science.* **1964**, *145*, 808.

(32) Visco, R.; Chandross, E. *J. Am. Chem. Soc.* **1964**, *86*, 5350.

(33) Santhanam, K. S. V.; Bard, A. J. *J. Am. Chem. Soc.* **1965**, *87*, 139.

(34) Yin, X.-B.; Dong, S.; Wang, E. *TrAC, Trends Anal. Chem.* **2004**, *23*, 432.

(35) Zou, G.; Ju, H. *Anal. Chem.* **2004**, *76*, 6871.

(36) Ding, S.-N.; Xu, J.-J.; Chen, H.-Y. *Electroanalysis.* **2005**, *17*, 1517.

(37) Kawahara, K.; Suzuki, K.; Ohko, Y.; Tatsuma, T. *PCCP.* **2005**, *7*, 3851.

(38) Kim, D.-J.; Lyu, Y.-K.; Choi, H. N.; Min, I.-H.; Lee, W.-Y. *Chem. Commun.* **2005**, 2966.

(39) Xu, Z.; Guo, Z.; Dong, S. *Biosensors & Bioelectronics.* **2005**, *21*, 455.

(40) Eskola, J.; Maekinen, P.; Oksa, L.; Loikas, K.; Nauma, M.; Jiang, Q.; Hakansson, M.; Suomi, J.; Kulmala, S. *J. Lumin.* **2006**, *118*, 238.

(41) Zhang, L.; Guo, Z.; Xu, Z.; Dong, S. *J. Electroanal. Chem.* **2006**, *592*, 63.

(42) Han, H.; Sheng, Z.; Liang, J. *Anal. Chim. Acta.* **2007**, *596*, 73.

(43) Jiang, H.; Ju, H. *Chem. Commun.* **2007**, 404.

(44) Jiang, H.; Ju, H. *Anal. Chem.* **2007**, *79*, 6690.

(45) Ju, H. J. a. H. *Anal. Chem.* **2007**, *79*, 6690.

(46) Somers, R. C.; Bawendi, M. G.; Nocera, D. G. *Chem. Soc. Rev.* **2007**, *36*, 579.

(47) Lin, Z.; Liu, Y.; Chen, G. *Electrochem. Commun.* **2008**, *10*, 1629.

(48) Wei, H.; Wang, E. *TrAC, Trends Anal. Chem.* **2008**, *27*, 447.

(49) Jie, G.; Li, L.; Chen, C.; Xuan, J.; Zhu, J.-J. *Biosens. Bioelectron.* **2009**, *24*, 3352.

(50)   Wang, X.-F.; Zhou, Y.; Xu, J.-J.; Chen, H.-Y. *Adv. Funct. Mater.* **2009**, *19*, 1444.

(51)   Ying Wang, J. L., Longhua Tang, Haixin Chang, and Jinghong Li *Anal. Chem.* **2009**, *81*, 9710.

(52)   Kulmala, S.; Ala-Kleme, T.; Heikkila, L.; Vare, L. *J. Chem. Soc., Faraday Trans.* **1997**, *93*, 3107.

(53)   Liu, C.; Bard, A. J. *Nat. Mater.* **2008**, *7*, 505.

(54)   Spehar-Deleze, A.-M.; Suomi, J.; Jiang, Q.; De Rooij, N.; Koudelka-Hep, M.; Kulmala, S. *Electrochim. Acta* **2006**, *51*, 5438.

(55)   Miao, W.; Choi, J.-P. In *Electrogenerated Chemiluminescence*; Bard, A. J., Ed.; Marcel Dekker, Inc.: New York, 2004, p 213.

(56)   White, H. S.; Bard, A. J. *J. Am. Chem. Soc.* **1982**, *104*, 6891.

(57)   Bolleta, F.; Ciano, M.; Balzani, V.; Serpone, N. *Inorg. Chim. Acta.* **1982**, *62*, 207.

(58)   Memming, R. *J. Electrochem. Soc.* **1969**, *116*, 785.

(59)   He, L.; Cox, K. A.; Danielson, N. D. *Anal. Lett.* **1990**, *23*, 195.

(60)   Leland, J. K.; Powell, M. J. *J. Electrochem. Soc.* **1990**, *137*, 3127.

(61)   Noffsinger, J. B.; Danielson, N. D. *Anal. Chem.* **1987**, *59*, 865.

(62)   Zu, Y.; Bard, A. J. *Anal. Chem.* **2000**, *72*, 3223.

(63)   Kanoufi, F.; Zu, Y.; Bard, A. J. *J. Phys. Chem. B.* **2001**, *105*, 210.

(64)   Miao, W.; Choi, J.-P.; Bard, A. J. *J. Am. Chem. Soc.* **2002**, *124*, 14478.

(65)   Zhang, L.; Dong, S. *Anal. Chem.* **2006**, *78*, 5119.

(66)   Yu, Y.; Lu, C.; Zhang, M. *Anal. Chem.* **2015**, *87*, 8026.

(67)   Miao, W.; Bard, A. J. *Anal. Chem.* **2004**, *76*, 5379.

(68)   Wang, X.; Yun, W.; Dong, P.; Zhou, J.; He, P.; Fang, Y. *Langmuir.* **2008**, *24*, 2200.

(69)　Zanarini, S.; Rampazzo, E.; Ciana, L. D.; Marcaccio, M.; Marzocchi, E.; Montalti, M.; Paolucci, F.; Prodi, L. *J. Am. Chem. Soc.* **2009**, *131*, 2260.

(70)　Feng, Q.-M.; Shen, Y.-Z.; Li, M.-X.; Zhang, Z.-L.; Zhao, W.; Xu, J.-J.; Chen, H.-Y. *Anal. Chem.* **2016**, *88*, 937.

(71)　Lai, R. Y.; Bard, A. J. *J. Phys. Chem. A.* **2003**, *107*, 3335.

(72)　Alivisatos, A. P. *Science.* **1996**, *271*, 933.

(73)　Alivisatos, A. P. *J. Phys. Chem.* **1996**, *100*, 13226.

(74)　Rossetti, R.; Nakahara, S.; Brus, L. E. *J. Chem. Phys.* **1983**, *79*, 1086.

(75)　Brus, L. E. *J. Chem. Phys.* **1984**, *80*, 4403.

(76)　Nozik, A. J.; Beard, M. C.; Luther, J. M.; Law, M.; Ellingson, R. J.; Johnson, J. C. *Chem. Rev.* **2010**, *110*, 6873.

(77)　Bhattacharya, P.; Ghosh, S.; Stiff-Roberts, A. D. *Annual Review of Materials Research* **2004**, *34*, 1.

(78)　Kamat, P. V.; Tvrdy, K.; Baker, D. R.; Radich, J. G. *Chem. Rev.* **2010**, *110*, 6664.

(79)　Talapin, D. V.; Lee, J.-S.; Kovalenko, M. V.; Shevchenko, E. V. *Chem. Rev.* **2010**, *110*, 389.

(80)　Kamat, P. V. *J. Phys. Chem. C.* **2008**, *112*, 18737.

(81)　Dai, Q.; Duty, C. E.; Hu, M. Z. *Small* **2010**, *6*, 1577.

(82)　Demir, H. V.; Nizamoglu, S.; Erdem, T.; Mutlugun, E.; Gaponik, N.; Eychmüller, A. *Nano Today* **2011**, *6*, 632.

(83)　Weller, H. *Angew. Chem. Int. Ed. Engl.* **1993**, *32*, 41.

(84)　Guozhong Cao, C. J. B. *Annual Review of Nano Research*; World Scientific Publishing Co. Pte. Ltd, 2008; Vol. 2.

(85)   Rogach, A. L.; Talapin, D. V.; Weller, H. In *Colloids and Colloid Assemblies*;
         Wiley-VCH Verlag GmbH & Co. KGaA: 2004, p 52.

(86)   Medintz, I. L.; Uyeda, H. T.; Goldman, E. R.; Mattoussi, H. *Nat Mater.* **2005**, *4*,
         435.

(87)   Bruchez, M.; Moronne, M.; Gin, P.; Weiss, S.; Alivisatos, A. P. *Science.* **1998**, *281*,
         2013.

(88)   Chan, W. C. W.; Nie, S. *Science.* **1998**, *281*, 2016.

(89)   Gill, R.; Zayats, M.; Willner, I. *Angew. Chem. Int. Ed.* **2008**, *47*, 7602.

(90)   Freeman, R.; Willner, I. *Chem. Soc. Rev.* **2012**, *41*, 4067.

(91)   Delehanty, J. B.; Susumu, K.; Manthe, R. L.; Algar, W. R.; Medintz, I. L. *Anal.
         Chim. Acta.* **2012**, *750*, 63.

(92)   Algar, W. R.; Susumu, K.; Delehanty, J. B.; Medintz, I. L. *Anal. Chem.* **2011**, *83*,
         8826.

(94)   Ding, Z.; Quinn, B.; Haram, S.; Pell, L.; Korgel, B.; Bard, A. J. *Science.* **2002**, *296*,
         1293.

(94)   Myung, N.; Ding, Z.; Bard, A. J. *Nano Lett.* **2002**, *2*, 1315.

(95)   Myung, N.; Bae, Y.; Bard, A. J. *Nano Lett.* **2003**, *3*, 1053.

(96)   Bae, Y.; Myung, N.; Bard, A. J. *Nano Lett.* **2004**, *4*, 1153.

(97)   Wu, P.; Hou, X.; Xu, J.-J.; Chen, H.-Y. *Chem. Rev.* **2014**, *114*, 11027.

(98)   Deng, S.; Ju, H. *The Analyst.* **2013**, *138*, 43.

(99)   Nalwa, H. S., Ed *In Handbook of Nanostructured Materials and Nanotechnology*;
         Academic Press 2000; Vol. 4.

(100)   Zhao, W.-W.; Wang, J.; Zhu, Y.-C.; Xu, J.-J.; Chen, H.-Y. *Anal. Chem.* **2015**, *87*,

9520.

(101)   Zhou, H.; Han, T.; Wei, Q.; Zhang, S. *Anal. Chem.* **2016**, *88*, 2976.

(102)   Bist, I.; Song, B.; Mosa, I. M.; Keyes, T. E.; Martin, A.; Forster, R. J.; Rusling, J. F. *ACS Sens* **2016**, *1*, 272.

(103)   Graybill, R. M.; Bailey, R. C. *Anal. Chem.* **2016**, *88*, 431.

(104)   Zhang, P.; Zhuo, Y.; Chang, Y.; Yuan, R.; Chai, Y. *Anal. Chem.* **2015**, *87*, 10385.

(105)   Zhang, Y.-Y.; Feng, Q.-M.; Xu, J.-J.; Chen, H.-Y. *ACS Appl. Mater. Interfaces.* **2015**, *7*, 26307.

(106)   Lei, Y.-M.; Huang, W.-X.; Zhao, M.; Chai, Y.-Q.; Yuan, R.; Zhuo, Y. *Anal. Chem.* **2015**, *87*, 7787.

(107)   Zhang, X.; Ding, S.-N. *ACS Sens.* **2016**, *1*, 358.

(108)   Liu, X.; Jiang, H.; Fang, Y.; Zhao, W.; Wang, N.; Zang, G. *Anal. Chem.* **2015**, *87*, 9163.

(109)   Cai, F.; Zhu, Q.; Zhao, K.; Deng, A.; Li, J. *Environ. Sci. Technol.* **2015**, *49*, 5013.

(110)   Ji, J.; He, L.; Shen, Y.; Hu, P.; Li, X.; Jiang, L.-P.; Zhang, J.-R.; Li, L.; Zhu, J.-J. *Anal. Chem.* **2014**, *86*, 3284.

(111)   Wu, M.-S.; Shi, H.-W.; He, L.-J.; Xu, J.-J.; Chen, H.-Y. *Anal. Chem.* **2012**, *84*, 4207.

(112)   Wang, G.; Jin, F.; Dai, N.; Zhong, Z.; Qing, Y.; Li, M.; Yuan, R.; Wang, D. *Anal. Biochem.* **2012**, *422*, 7.

(113)   Venkatanarayanan, A.; Crowley, K.; Lestini, E.; Keyes, T. E.; Rusling, J. F.; Forster, R. J. *Biosens. Bioelectron.* **2012**, *31*, 233.

(114)   Guo, Z.; Hao, T.; Wang, S.; Gan, N.; Li, X.; Wei, D. *Electrochem. Commun.* **2012**, *14*, 13.

(115)   Zhou, H.; Liu, J.; Xu, J.-J.; Chen, H.-Y. *Anal. Chem.* **2011**, *83*, 8320.

(116)   Zhang, Y.; Deng, S.; Lei, J.; Xu, Q.; Ju, H. *Talanta.* **2011**, *85*, 2154.

(117)   Shen, W.; Tian, D.; Cui, H.; Yang, D.; Bian, Z. *Biosens. Bioelectron.* **2011**, *27*, 18.

(118)   Shen, L.; Li, J.; Li, L.; Zou, G.; Zhang, X.; Jin, W. *Electrochem. Commun.* **2011**, *13*, 1499.

(119)   Mao, L.; Yuan, R.; Chai, Y.; Zhuo, Y.; Xiang, Y. *Biosens. Bioelectron.* **2011**, *26*, 4204.

(120)   Guo, Y.; Jia, X.; Zhang, S. *Chem. Commun.* **2011**, *47*, 725.

(121)   Zhang, X.; Zhang, B.; Miao, W.; Zou, G. *Anal. Chem.* **2016**, *88*, 5482.

(122)   Lin, D.; Wu, J.; Yan, F.; Deng, S.; Ju, H. *Anal. Chem.* **2011**, *83*, 5214.

(123)   Ambrosi, A.; Chua, C. K.; Bonanni, A.; Pumera, M. *Chem. Rev.* **2014**, *114*, 7150.

(124)   Luo, X.-L.; Xu, J.-J.; Wang, J.-L.; Chen, H.-Y. *Chem. Commun.* **2005**, 2169.

(125)   Zhao, Q.; Gan, Z.; Zhuang, Q. *Electroanalysis.* **2002**, *14*, 1609.

(126)   Wang, K.; Liu, Q.; Wu, X.-Y.; Guan, Q.-M.; Li, H.-N. *Talanta.* **2010**, *82*, 372.

(127)   Tang, X.; Zhao, D.; He, J.; Li, F.; Peng, J.; Zhang, M. *Anal. Chem.* **2013**, *85*, 1711.

(128)   Miao, W.; Bard, A. J. *Anal. Chem.* **2004**, *76*, 7109.

(129)   Acharya, D.; Bastola, P.; Le, L.; Paul, A. M.; Fernandez, E.; Diamond, M. S.; Miao, W.; Bai, F. *Sci. Rep.* **2016**, *6*, 32227.

CHAPTER II -ELECTROGENERATED CHEMILUMINESCENCE AND

FLOURESCENCE STUDY OF CdTe QUANTUM DOTS AND THEIR

INTERACTION WITH CdSe QUANTUM DOTS

2.1 Introduction

Electrogenerated chemiluminescence (also known as electrochemiluminescence or ECL) is a light generation process from species on an electrode surface after their electrochemical and chemical reactions.[1,2] Because of ECL's ability to detect trace amounts of target molecules with high sensitivity, it has been used in a variety of areas such as immunoassays and biowarfare agents detection.[2]

Many species have been used as ECL luminophores since the first systematic ECL study was reported in the 1960s.[3-5] $Ru(bpy)_3^{2+}$ (bpy = 2,2-bipyridine) and its derivatives have been the most frequently used ECL luminophores,[6,7] and ECL mechanisms of $Ru(bpy)_3^{2+}$ were studied with different coreactants, such as tri-*n*-propylamine (TPrA),[8,9] oxalate,[10] and peroxodisulfate $(S_2O_8^{2-})$[11]. For instance, a two-wave ECL signal was detected from the $Ru(bpy)_3^{2+}$/TPrA system in aqueous media on glassy carbon electrode. The direct oxidation of TPrA and classic "oxidative reduction" routes were proven to be the mechanisms of the two ECL waves of the $Ru(bpy)_3^{2+}$/TPrA system, respectively.[2]

Semiconductor nanoparticles (also called quantum dots or QDs) have become a superior alternatives to $Ru(bpy)_3^{2+}$ as ECL luminophores in different areas, especially in bioanalysis,[12-15] after successful ECL generation from silicon nanoparticles for the first time in 2002.[16] Size dependent optical properties and excellent bio-compatibilities have given QDs the edge over the traditional $Ru(bpy)_3^{2+}$ based ECL systems.[12,13] Especially, feasibility of obtaining light emissions from QDs at different wavelengths merely by

changing their particle sizes, overcomes the problem of fixed emission wavelength with

$Ru(bpy)_3^{2+}$ ($\lambda_{Emission}$ = ~620 nm) based ECL luminophores.[17] This has made the

simultaneous detection of multiple target molecules theoretically possible.

Although, tremendous amount of studies have been reported about QDs based

ECL,[14,15,18-22] these studies were almost exclusively focused on their analytical

applications for detection of different target molecules. On the other hand, the basic ECL

mechanisms of QDs systems were rarely investigated comprehensively while the

understanding of them play an important role on the development of more sensitive ECL

systems and on discovering better coreactants.[9] This could be due to the belief that

different ECL luminophores might share the ECL mechanisms of the well-studied

$Ru(bpy)_3^{2+}$/coreactant system while the same coreactant was used in similar conditions.

However, according to the results discussed in this chapter, QDs do not completely share

the ECL generation mechanisms with $Ru(bpy)_3^{2+}$ when TPrA is used as the coreactant.

In this chapter, the basic ECL mechanisms of the CdTe QDs/TPrA system were

investigated. A strong ECL interaction between water soluble CdTe QDs

($\lambda_{emission}$= 760 nm) and CdSe QDs ($\lambda_{emission}$= 550 nm) was discovered and the possible

mechanisms responsible for this phenomenon were also examined with fluorescence,

UV-vis, ECL spectroscopies, and electrochemical techniques.

2.2 Experimental Section

2.2.1 Materials

Cadmium chloride ($CdCl_2$, ≥ 95%), sodium hexametaphosphate (HMP, 96%),

sodium tellurite (Na_2TiO_3, 99%), 3-mercaptopropionic acid (MPA, ≥ 99%), potassium

chloride (KCl, ≥ 99%), hydrazine hydrate solution (N_2H_4•H_2O, 80%), tri-*n*-propylamine

(TPrA, $\geq$ 98%), dipropylamine (DPrA, $\geq$ 99%), propylamine (PrA, $\geq$ 99%), ammonium

peroxodisulfate ($(NH_4)_2S_2O_8$, 98%) were purchased from Sigma-Aldrich (Milwaukee,

WI). Sodium phosphate monobasic monohydrate ($NaH_2PO_4 \cdot H_2O$, 99.9%) was purchased

from Fisher Scientific (Waltham, MA). CdSe/ZnS core-shell quantum dots

($\lambda_{Emission}$ = ~550 nm, will be referred as CdSe QDs in this chapter) were purchased from

Mesolight (Little Rock, AR). Unless otherwise stated, all reagents were used as received.

2.2.2 Apparatus and Methods

ECL, cyclic voltammetry (CV), and chronoamperometry signals were obtained

with a CHI 660A electrochemical workstation (CH Instruments, Austin, TX) along with a

photomultiplier tube (PMT, Hamamatsu R928, Japan) installed in a light-tight box

covered with a black blanket.[2,23] A model 472A Brandenburg PMT power supply

(England) was used to supply a voltage of -700 V to the PMT. A highly sensitive

Keithley 6514 electrometer (Keithley, Cleveland, OH) was used to measure the ECL

current from the sample and converted it to a voltage (in $\pm$ 2.0 V) which was collected

with the electrochemical workstation.

ECL spectra were acquired using a workstation from Princeton Instrument

(Acton, MA) that consisted of a Spec-10:400B/LN-eXcelon digital charge-coupled

device (CCD) camera spectroscopy system that was cooled to -120 °C with liquid

nitrogen, a ST-133B controller, and an Acton SP-2156 imaging spectrograph.

WinSpec/32 software from the same company was used to collect the spectra. The light

generated on GCE was directed through a 1.0 m optical fiber placed under the ECL cell

to the detector through a 1.5 mm size slit. Cyclic sweep or pulse potentials were applied

to the electrochemical cell by a model 173 potentiostat/galvanostat compiled with a

model 175 Universal Programmer from Princeton Applied Research (Oak Ridge, TN). A traditional three-electrode electrochemical cell was used for all electrochemical and ECL experiments. These three electrodes were a platinum mesh as the counter electrode, a Ag/AgCl (3.0 M KCl) as the reference electrode, and a glassy carbon electrode (GCE, 3.0 mm diameter) as the working electrode. Before each electrochemical or ECL experiment, the working electrode was polished with 0.3 µm alumina slurry and repeatedly washed with large amounts of distilled water as well as ethanol and dried with Kimwipes tissue. The Vycor tip of the reference electrode was regularly replaced with a new one to eliminate possible contamination.

A QuantaMaster^{TM} 40 Intensity Based spectrofluorometer from PTI Technologies (Oxnard, CA) was used to collect FL spectra of CdTe QDs and CdSe QDs at a slit width of 0.50 mm with 450 nm excitation wavelength from 470 nm to 850 nm. UV-vis absorption spectra of CdTe QDs were obtained by using Evolution 300 UV-vis spectrometer from Thermo Fishier Scientific (Waltham, MA). For both FL and UV-vis studies, a quartz crystal cuvette with 1.0 cm light path length was used as the sample container.

2.2.3 Synthesis of Dual-Capped CdTe QDs

Dual capping agents stabilized CdTe QDs were synthesized by following a one-pot strategy reported by Zou et al after minor modifications.[24] Briefly, 1.60 mL of 0.20 M CdCl$_2$ solution was added to a three-necked flask containing 100.0 mL of distilled water. 84.0 µL of MPA and 587.0 mg of HMP were then added to the above solution successively under magnetic stirring. After the pH of the above reaction mixture was adjusted to 8.0 with 450.0 µL of 6.0 M NaOH, 10.30 mg of Na$_2$TiO$_3$ was added.

37

Resultant mixture was refluxed for 10 min, then 4.8 mL of $N_2H_4 \cdot H_2O$ was injected into the above solution and the final mixture was refluxed under open-air condition. Samples were taken after the final mixture was refluxed for a different amount of time to obtain CdTe QDs with various particle sizes. The final products were cleaned by 1/1 and 1/10 of water/acetone (v/v) mixture using centrifugation at 12,000 rpm for one hour, respectively, and the final precipitates were redissolved in distilled water and kept at 4 °C for further use. The empirical equations reported by Yu et al and the Beer's Law were used to estimate the concentration of CdTe QDs stock solutions.[25,26]

2.2.4 Preparation of TPrA Coreactant Solutions

0.10 M phosphate buffer (PB) solution was first prepared by adjusting the pH of 0.10 M NaH_2PO_4 solution with 6.0 M NaOH and 1.0 M H_3PO_3 solutions under a pH meter. TPrA solutions in 0.10 M phosphate buffer (PB) were prepared by adding a certain amount of TPrA in 0.10 M PB solution. 6.0 M NaOH and 1.0 M H_3PO_4 were used to adjust the pH of the TPrA solutions back to the targeted pH values under constant stirring until clear, homogeneous solutions were obtained.

2.3 Results and Discussion

2.3.1 Characterization of CdTe QDs

Fluorescence and UV-vis spectra of as-prepared CdTe QDs were obtained in aqueous media. As shown in Figure 2.1, a single absorption peak (Figure 2.1B) and a single emission peak (Figure 2.1A-a), respectively, at ~710 nm and ~760 nm wavelength, are generated from CdTe QDs. These data indicate that the size of the as-prepared CdTe QDs are nearly monodispersed and a 6.4 nm diameter is estimated for these QDs based on their peak absorption wavelength using an empirical equation.[25]

ECL spectra of the same QDs, which were collected while TPrA were used as coreactant

on GCE, is shown in Figure 2.1A-b. The nearly overlap between the ECL and the FL

spectra (Figure 2.1A-a vs. Figure 2.1A-b) suggests that the surface state of as-prepared

CdTe QDs is effectively passivated by capping agents, MPA and HMP.[27]
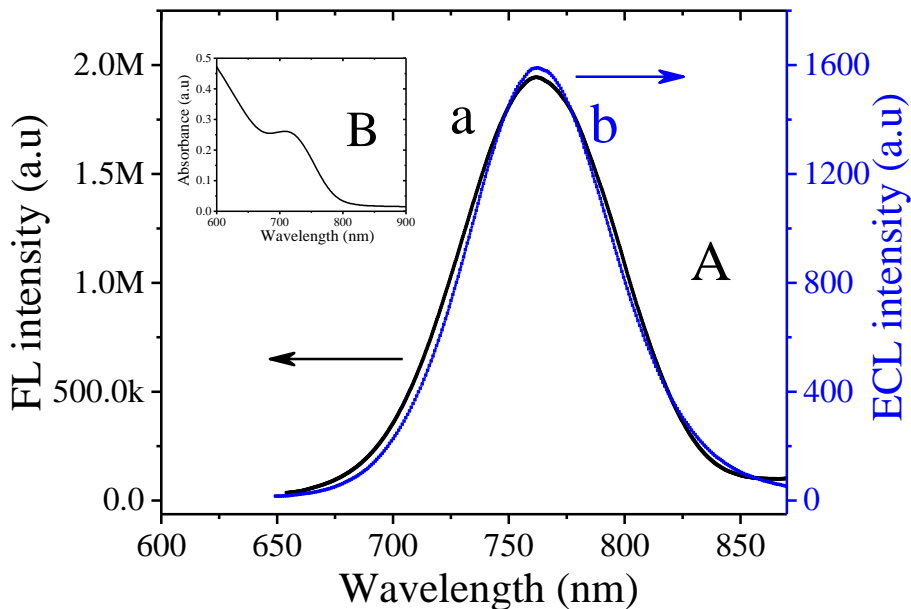
Figure 2.1 (A) (a) FL (b) ECL and (B) UV-vis spectra of CdTe QDs.

Note: CdTe QDs were obtained by cleaning the samples collected at 24 hrs. of synthesis reaction. (CdTe QDs obtained at

24 hrs. of synthesis reaction will be referred to as CdTe QDs for the rest of the chapter unless otherwise stated.) 1.0 μM

CdTe QDs and 20.0 nM CdTe QDs aqueous solutions were used for UV-vis and FL measurements, respectively. ECL

spectrum was obtained on a GCE from 40.0 nM CdTe QDs with 70.0 mM TPrA in 0.10 M PB (pH 8.5) by cyclic potential

scanning at 50 mV/s between 0 V and 1.55 V for one cycle.

2.3.2 pH Dependence Study

ECL intensity of TPrA coreactant based system is highly sensitive to the pH of

the solution, because deprotonation of some crucial intermediates, like HTPrA$^+$ and

TPrA$^{\bullet+}$, are involved in their ECL mechanisms.[8,9,28] Hence, effect of pH on ECL intensity

from the CdTe QDs/TPrA system was examined while other experimental conditions

remained constant and the results of this set of experiments are shown in Figure 2.2.
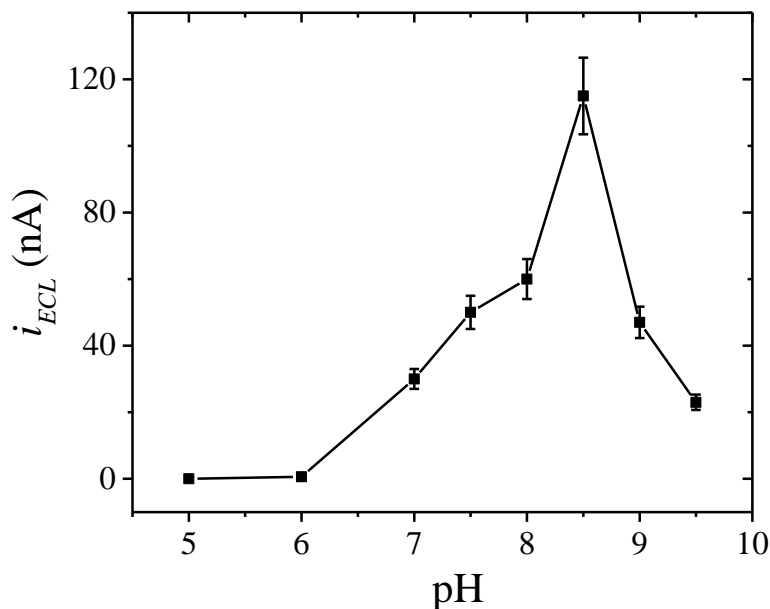
Figure 2.2 Effect of pH on ECL intensity of the CdTe QDs/TPrA system.

Note: ECL signals were obtained from 50.0 nM CdTe QDs with 50.0 mM TPrA in 0.10 M PB by cyclic scanning the potential

at 50.0 mv/s between 0.0 V and 1.55 V for one cycle at different pH values on GCE.

With the increasing pH value of the test solution, ECL intensity of the CdTe

QDs/TPrA system increases drastically starting from pH 7.0 and reaches a maximum

value at pH 8.5 before decreasing back at higher pH values. The trend in Figure 2.2 is

generated because deprotoation of $HTPrA^+$ (pK_a 3.3)[9] rather than $TPrA^{\bullet+}$ (pKa 10.4)[29]

played the dominant role during this ECL generation process.[28] This profile is consistent

with the reported result for the $Ru(bpy)_3^{2+}$/TPrA system.[28] The mismatch in the optimum

pH value of the CdTe QDs/TPrA system (pH 8.5) and that of the $Ru(bpy)_3^{2+}$/TPrA

system (pH 7.5)[28] could be resulted from different electrochemical and physical

characteristics of the two ECL luminophores.

2.3.3 ECL Mechanism of CdTe QDs/TPrA System

CV and ECL responses of 50.0 nM CdTe QDs in 0.10 M PB (pH 8.5) with 70.0 mM TPrA on a GCE are shown in Figure 2.3. In an anodic potential range from 0 to 1.50 V, a broad ECL peak at ~0.92 V (Figure 2.3_blue curve) is observed along with an oxidation current of TPrA which starts from ~0.6 V and reaches the maximum current at ~1.13 V (Figure 2.3_black curve).
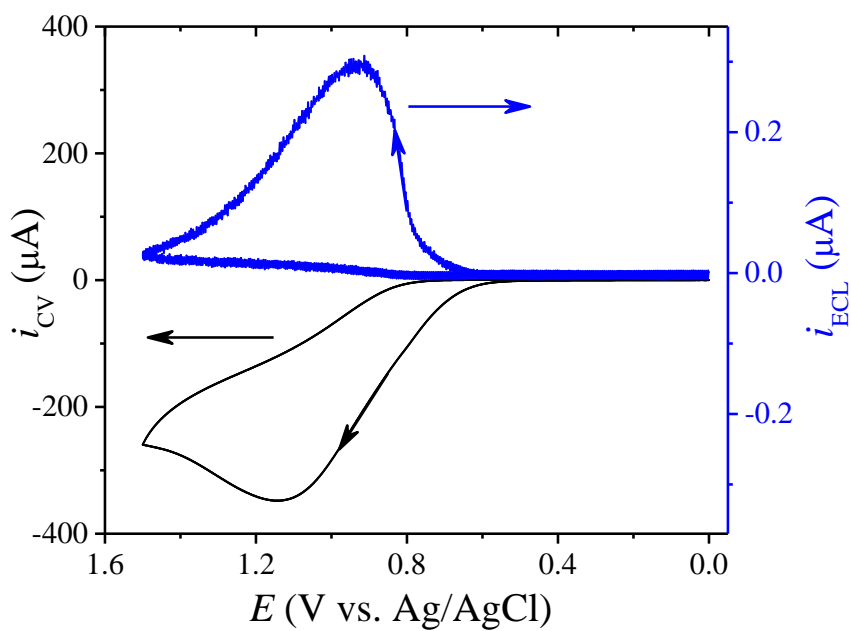
Figure 2.3 ECL (blue curve) and CV (black curve) response of CdTe QDs/TPrA system

Note: ECL and CV signals were generated from 50.0 nM CdTe QDs with 70.0 mM TPrA in 0.10 M PB (pH 8.5) by cyclic potential scanning at 50 mV/s between 0 and 1.50 V for one cycle on GCE.
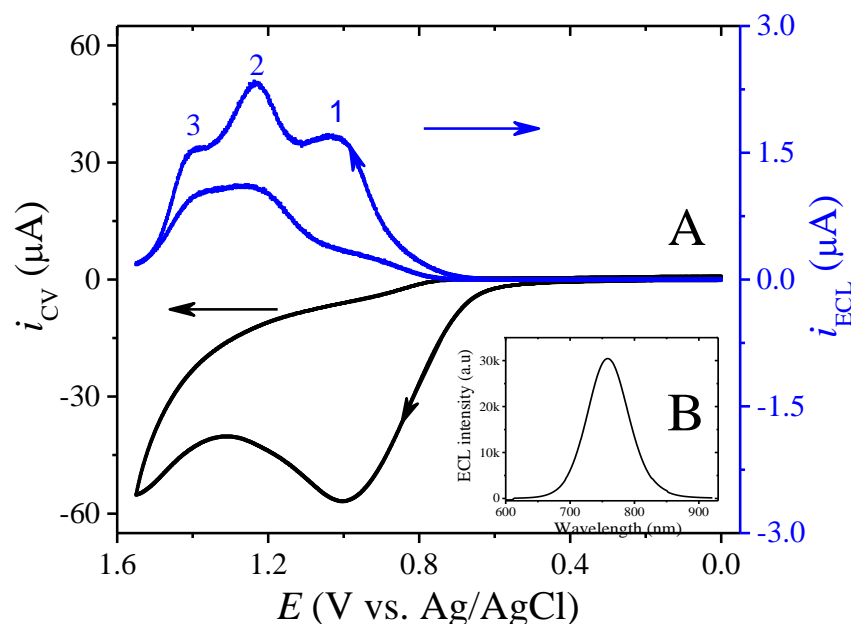
Figure 2.4 . (A) ECL (blue curve), CV (black curve) and (B) ECL spectra of the CdTe QDs/TPrA system.

Note: ECL, CV and ECL spectrum signals were generated from 140.0 nM CdTe QDs with 7.0 mM TPrA in 0.10 M PB (pH 8.5) by cyclic potential scanning at 50 mV/s between 0 V and 1.55 V for one cycle on GCE. In Figure 2.5A, response from the second cycle of the four overall potential scanning cycles was displayed.

Interestingly, three ECL peaks, at ~1.05 V, 1.21 V, 1.40 V, respectively, are obtained from the CdTe QDs/TPrA system when a high concentration of CdTe QDs (140.0 nM) and a low concentration of TPrA (7.0 mM) were used (Figure 2.4A). ECL spectra from CdTe QDs (Figure 2.4B) which were collected under the same experimental conditions as in Figure 2.4A show a single ECL emission peak at ~760 nm. These results indicate that all three ECL waves of the CdTe QDs/TPrA system are generated from the same excited state CdTe QDs[*]. which were produced through three different ECL pathways. This ECL profile is different from the generally accepted two-wave ECL signal from the Ru(bpy)$_3^{2+}$/TPrA system on GCE surface in the same potential range.[2,9]

The oxidation potential value of CdTe QDs and TPrA are the necessary information for unfolding the ECL mechanism of the CdTe QDs/TPrA system.[9,29] As shown in Figure 2.4A_black curve, oxidation of TPrA starts from ~0.6 V and peaks at ~1.0 V. However, unlike TPrA, the oxidation potential of CdTe QDs is unable to be directly measured by CV due to the low concentration of CdTe QDs stoke solution and relatively high detection limit of the CV technique.[30] Therefore, oxidation potential of CdTe QDs was estimated using an annihilation ECL experiment, mechanism of which is demonstrated in Equations 2.1-2.4.[1] In annihilation ECL, electrochemically reduced (CdTe QDs$^{\bullet-}$, Equation 2.2) and oxidized (CdTe QDs$^{\bullet+}$, Equation 2.1) CdTe QDs could produce their excited state (CdTe QDs*) through an electron transfer process (Equation 2.3). Based on this mechanism, while enough amounts of CdTe QDs$^{\bullet-}$ are available in the solution, once CdTe QDs$^{\bullet+}$ are formed, CdTe QDs* could be produced by the electron transfer reaction between CdTe QDs$^{\bullet-}$ and CdTe QDs$^{\bullet+}$ (Equation 2.3). This set of annihilation ECL experiments were conducted by applying potential on 100.0 nM CdTe QDs in 0.10 M PB (pH 8.5) as shown in Figure 2.5 (insert). When the potential pulsed with 0.1 s pulse width between -2.0 V, a potential negative enough to reduce CdTe QDs, and a positive potential, the lowest positive potential at which the ECL started to be produced can be estimated as the oxidation potential of CdTe QDs. The results of this set experiments are shown in Figure 2.5. A detectable ECL signal starts to generate when the potential is pulsed between -2.00 and $+1.20$ V, which indicates that CdTe QDs start to be oxidized at around 1.20 V.

$$\text{CdTe QDs} - e^- \rightarrow \text{CdTe QDs}^{\bullet+} \tag{2.1}$$

$$\text{CdTe QDs} + e^- \rightarrow \text{CdTe QDs}^{\bullet -} \tag{2.2}$$

$$\text{CdTe QDs}^{\bullet +} + \text{CdTe QDs}^{\bullet -} \rightarrow \text{CdTe QDs} + \text{CdTe QDs}^* \tag{2.3}$$

$$\text{CdTe QDs}^* \rightarrow \text{CdTe QDs} + hv \tag{2.4}$$

Note that the first ECL peak (~0.70 V) in Figure 2.4A starts immediately after the oxidation of TPrA (~0.6 V) yet well before CdTe QDs oxidation (1.2 V). This suggests that while oxidation of TPrA is necessary, formation of CdTe QDs$^{\bullet +}$ is not required for generation of the first ECL peak of the CdTe QDs/TPrA system. Hence, the "direct TPrA oxidation" mechanism (Scheme 2.1) can be a reasonable explanation for the first ECL wave from the CdTe QDs/TPrA system.[9] In this mechanism, after direct electrochemical oxidation of TPrA, a relatively long-lived TPrA$^{\bullet +}$ is formed which then produces free TPrA$^{\bullet}$ radical after deprotonation. CdTe QDs are then reduced by the strong reducing agent TPrA$^{\bullet}$ to CdTe QDs$^{\bullet -}$ which is oxidized to CdTe QDs* by TPrA$^{\bullet +}$ at the following step. This mechanism explains the generation of the first ECL wave from the CdTe QDs/TPrA system without the involvement of the direct electrochemical oxidation of CdTe QDs on the electrode surface.
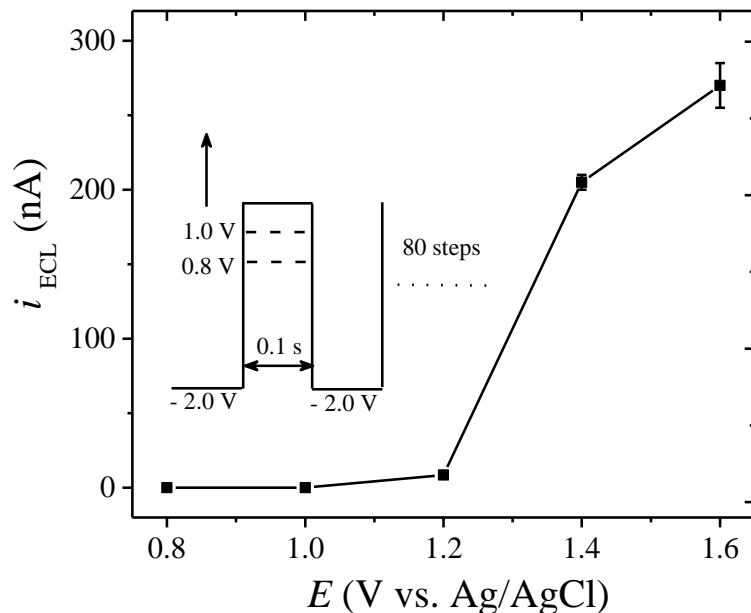
Figure 2.5 Effect of anodic potential on annihilation ECL intensity of CdTe QDs.

Note: ECL intensity of 100.0 nM CdTe QD in 0.1 M PB (pH 8.5) when pulsed between -2.0 V and different positive potentials with 0.10 s pulse width for 80 steps. The highest ECL intensity among the 80 steps was taken from each potential point.
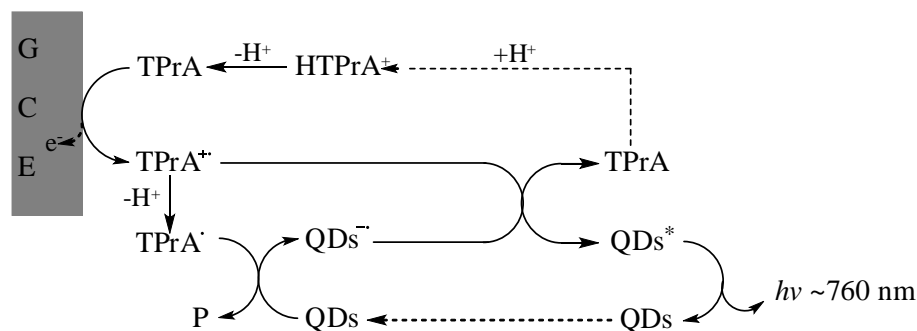
Scheme 2.1 "Direct oxidation of TPrA" mechanism.

Note: TPrA$^{\bullet+}$ = $(CH_3CH_2CH_2)_3N^{\bullet+}$, HTPrA$^+$ =Pr$_3$NH$^+$, TPrA$^{\bullet}$ = Pr$_2$N$^{\bullet}$CHCH$_2$CH$_3$, P = Pr$_2$N$^+$C=HCH$_2$CH$_3$. (Modified based on ref 9.)

   Dipropylamine (DPrA) and propylamine (PrA) can be generated after electrochemical oxidation of TPrA by successive dealkylation process (Equations 2.5-2.10).[31-33] Fujima et al reported that these DPrA and PrA could act as coreactants to generate ECL signal from TPrA coreactant systems at relatively high

45

anodic potentials.[34] The possibility of DPrA and PrA being the coreactants for generation

of the second and the third ECL waves from CdTe QDs in Figure 2.4A was examined by

the comparisons between ECL and CV responses of the CdTe QDs/DPrA,

CdTe QDs/PrA, and CdTe QDs/TPrA systems.

$$TPrA - e^- \rightarrow TPrA^{\bullet+} \tag{2.5}$$

$$TPrA^{\bullet+} \rightarrow TPrA^{\bullet} + H^+ \tag{2.6}$$

$$TPrA^{\bullet} - e^- + H_2O \rightarrow DPrA + EtCHO + H^+ \tag{2.7}$$

$$DPrA - e^- \rightarrow DPrA^{\bullet+} \tag{2.8}$$

$$DPrA^{\bullet+} \rightarrow DPrA^{\bullet} + H^+ \tag{2.9}$$

$$DPrA^{\bullet} - e^- + H_2O \rightarrow PrA + EtCHO + H^+ \tag{2.10}$$
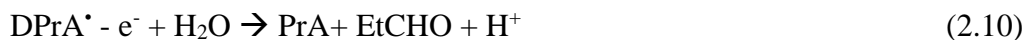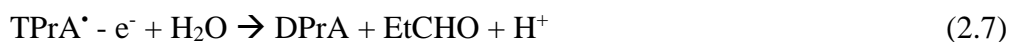
Note: $DPrA^+ = Pr_2NH_2^+$, $DPrA^{\bullet} = PrNHC^{\bullet}HCH_2CH_3$, $PrA^+ = PrNH_3^+$, $PrA^{\bullet} = NH_2C^{\bullet}HCH_2CH_3$,

CV and ECL signals of 140.0 nM CdTe QDs with 7.0 mM DPrA in 0.10 M PB

(pH 8.5) on a GCE are illustrated in Figure 2.6A. Two ECL peaks at ~1.20 V and ~1.35V

(Figure 2.6A-blue curve) and one DPrA oxidation current peak at ~1.20 V (Figure 2.6B-

black curve) are detected from the CdTe QDs/DPrA system in the anodic potential range

between 0 V and 1.55 V. Both ECL peaks of the CdTe QDs/DPrA system are generated

from CdTe QDs[*] as any one single-peak ECL spectra at ~760 nm is obtained

(Figure 2.6B). The first ECL peak of the CdTe QDs/DPrA system

(Figure 2.6_blue curve) starts to form almost spontaneously with the oxidation of DPrA

(Figure 2.6_black curve) at ~0.90 V and reaches the maximum value at ~1.16 V. This

indicates that direct oxidation of DPrA is required for the production of the first ECL wave from the CdTe QDs/DPrA system. A closer inspection reveals that the second ECL peak from the CdTe QDs/TPrA system (Figure 2.4A, ~1.21 V) is appeared at almost the same potential as first ECL peak from the CdTe/DPrA system (Figure 2.6A_blue curve, 1.16 V). Therefore, the second ECL wave from the CdTe QDs/TPrA system is likely to be generated from direct oxidation of DPrA that is produced immediately after TPrA oxidation as previously discussed. Because DPrA is produced from dealkylation of electrochemically oxidized TPrA, the concentration of DPrA in the CdTe QDs/TPrA system is much lower than the concentration of deliberately added DPrA in the CdTe QDs/DPrA system. This may explain the slightly higher positive peak potential of the second ECL peak of the CdTe QDs/TPrA system than that of the first ECL peak from the CdTe QDs/DPrA system (1.21 V vs. 1.16 V).

An ECL peak at the oxidation potential of PrA (~1.35 V, Figure 2.7A) and a single peak ECL spectra at ~760 nm wavelength (Figure 2.7B) are observed from 140.0 nM CdTe QDs with 14.0 mM PrA in 0.10 M PB (pH 8.5) on a GCE. The third ECL peak of the CdTe QDs/TPrA system (Figure 2.5A_blue curve, 1.40 V) and the second ECL peak of the CdTe QDs/DPrA (Figure 2.6A_blue curve, 1.35 V) system are at the similar potential as the single ECL wave of the CdTe QDs/PrA (Figure 2.7A_blue curve, 1.34 V) system. These results suggest that the third ECL wave of the CdTe QDs/TPrA system and the second ECL wave of the CdTe QDs/DPrA system are triggered by the direct oxidation of PrA which was produced after DPrA oxidation. The possible ECL mechanisms of the second and the third ECL waves from the CdTe QDs/TPrA system discussed above are summarized in Equations 2.11-2.18. According to

this mechanism, while the direct oxidation of TPrA was the reason for generation of the first ECL wave of CdTe QDs/TPrA system (Scheme 2.1), the second and the third ECL waves were produced from direct oxidation of DPrA and PrA, respectively. These DPrA and PrA were the products of successive dealkylation of TPrA immediately after its electrochemical oxidation. A similar mechanism was reported by Fujishima for a TPrA based anodic coreactant system when boron-doped diamond electrode was used as working electrode.[34]
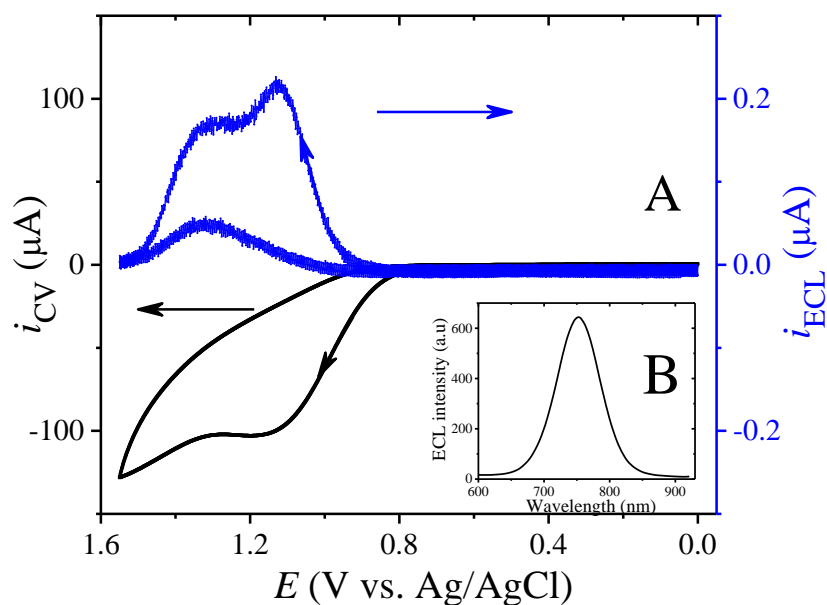
Figure 2.6 (A) ECL (blue curve), CV (black curve) and (B) ECL spectra of the CdTe QDs/DPrA system.

Note: ECL, CV and ECL spectrum signals were generated from 140.0 nM CdTe QDs with 7.0 mM DPrA in 0.10 M PB (pH 8.5) by cyclic potential scanning at 50 mV/s between 0 V and 1.55 V for one cycle on GCE.
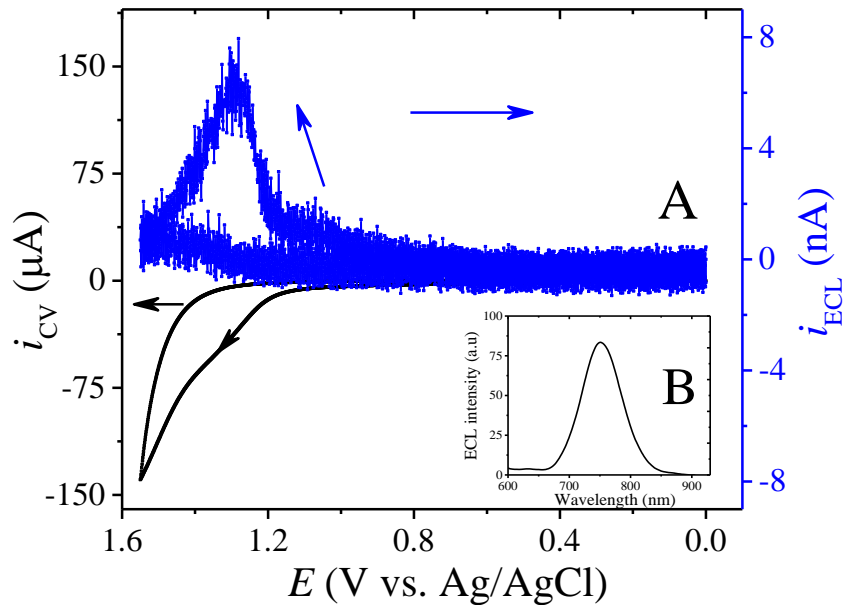
Figure 2.7 (A) ECL (blue curve), CV (black curve), and (B) ECL spectra of the CdTe QDs/PrA system.

Note: ECL, CV and ECL spectrum signals were generated from 140.0 nM CdTe QDs with 14.0 mM PrA in 0.10 M PB (pH 8.5) by

cyclic potential scanning at 50 mV/s between 0 V and 1.55 V for one cycle on GCE.

$$DPrA - e^- \rightarrow DPrA^{\bullet+} \tag{2.11}$$

$$PrA - e^- \rightarrow PrA^{\bullet+} \tag{2.12}$$

$$DPrA^{\bullet+} \rightarrow DPrA^{\bullet} + H^+ \tag{2.13}$$

$$PrA^{\bullet+} \rightarrow PrA^{\bullet} + H^+ \tag{2.14}$$

$$DPrA^{\bullet} + CdTe\ QDs \rightarrow CdTe\ QD^{\bullet-} + P_1 \tag{2.15}$$

$$PrA^{\bullet} + CdTe\ QDs \rightarrow CdTe\ QD^{\bullet-} + P_2 \tag{2.16}$$

$$DPrA^{\bullet+} + CdTe\ QD^{\bullet-} \rightarrow CdTe\ QD^* + DPrA \tag{2.17}$$

$$PrA^{\bullet+} + CdTe\ QD^{\bullet-} \rightarrow CdTe\ QD^{*} + PrA \qquad\qquad (2.18)$$
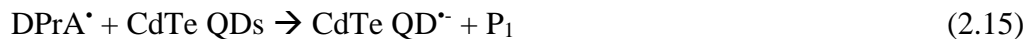
Note: $P_1 = PrHN^+{=}CHCH_2CH_3$, $P_2 = H_2N^+{=}CHCH_2CH_3$

Because the potential range of second and the third ECL waves in the CdTe

QDs/TPrA system is positive enough to oxidize CdTe QDs, contributions of the classic

"oxidative reduction" pathway to these two ECL waves cannot be excluded

(Scheme 2.2).[2] In this mechanism, electrochemically oxidized CdTe QDs (CdTe QDs$^{\bullet+}$)

is reduced by the TPrA$^{\bullet}$ to generate CdTe QDs*. Moreover, CdTe QDs* can also be

produced via Equation 2.3, where CdTe QDs$^{\bullet-}$ is generated from CdTe QDs after its

chemical reduction with TPrA$^{\bullet}$, DPrA$^{\bullet}$, or PrA$^{\bullet}$.
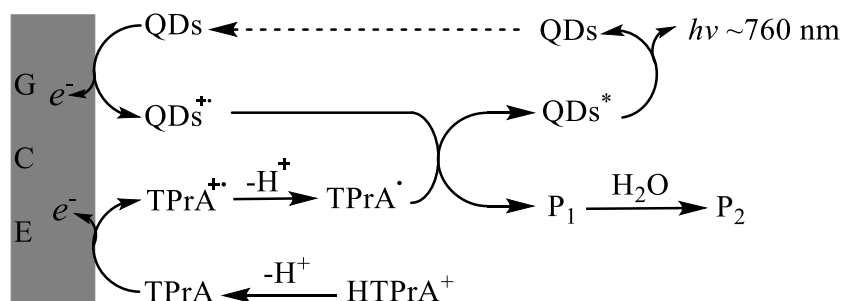
Scheme 2.2 Possible mechanism of the second ECL peak from the CdTe QDs/TPrA system.

Note: $P_1 = Pr_2N^+C{=}HCH_2CH_3$, $P_2 = Pr_2NH + CH_3CH_2CHO$

2.3.4 Effect of CdSe QDs on ECL Intensity of CdTe QDs

The effect of CdSe QDs on ECL intensity from CdTe QDs/TPrA system is shown in

Figure 2.8. When the potential pulses between 0 V and 0.80 V with a pulse width of 2.0 s

for 160 steps, an ECL emission peak at ~760 nm wavelength is observed from 4.6 nM

CdTe QDs with 70.0 mM TPrA in 0.10 M PB (pH 8.5) on a GCE (Figure 2.8a). More

than 15 times enhanced ECL signal (Figure 2.8b) at the same emission wavelength is

obtained with an addition of 150.0 nM CdSe QDs to the same test solution under the

same experimental conditions of Figure 2.8a. Because, CdSe QDs emits light at

~550.0 nm, the result in Figure 2.8 indicates that addition of CdSe QDs significantly

enhances the ECL signal of the CdTe QDs/TPrA system on GCE. In other words,

addition of CdSe QDs to the CdTe QDs/TPrA system drastically increases the amount of

CdTe QDs* formed during the ECL generation process.
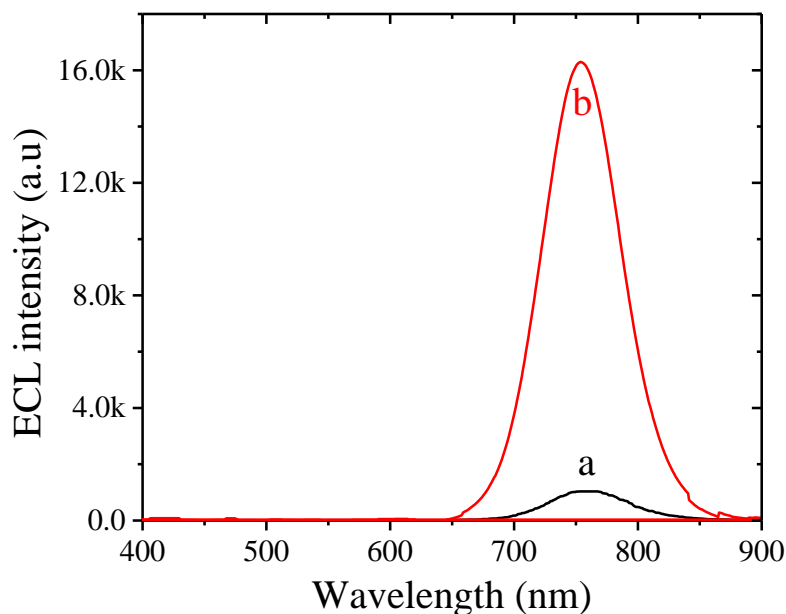
Figure 2.8 ECL spectra of the CdTe QD/TPrA system in the (a) absence and (b) presence of CdSe QDs.

Note: ECL spectrums were generated from 4.6 nM CdTe QDs with 70 mM TPrA in 0.10 M PB (pH 8.5) by potential pulsing between

0 and 0.8 V with 2 s pulse width for 160 steps on GCE (a) without and (b) with150.0 nM CdSe QDs.

CdTe QDs* can be generated through the ECL mechanism of the CdTe QDs/TPrA

system as-discussed in the last section. Extra amount of CdTe QDs* could be obtained

from CdTe QDs * after accepting energy from CdSe QDs* if CdSe QDs* are present in

CdTe QDs/TPrA system.[26] Therefore, energy transfer from CdSe QDs* to CdTe QDs

could be one of the possible reasons for the significant ECL signal enhancement.[26] For

the last statement to be valid, the following two requirements have to be fulfilled. First, CdTe QDs must be able to accept the energy from CdSe/ZnS QDs[*] to produce CdTe QDs[*] when these two QDs are placed in the same solution. Second, if the energy transfer between these two QDs could happen, enough amount of CdSe QDs[*] must be generated under the experimental conditions described in Figure 2.8.

The capability of CdTe QDs accepting energy from CdSe QDs[*] was examined using FL titration experiment (Figure 2.9). With addition of of CdSe QDs (0.0 nM to 60.0 nM), up to 1.6 times FL signal enhancement from a constant amount of CdTe QDs is detected (Figure 2.9A). On the other hand, up to ~79% quenching of FL intensity from a constant amount of CdSe QDs with an addition of CdTe QDs (0.0 mM to 10.0 mM) is observed (Figure 2.9B). These FL experimental results indicate, in the presence of CdSe QDs[*], emission intensity from CdTe QDs can be effectively enhanced by accepting energy from CdSe QDs[*] in the same solution.
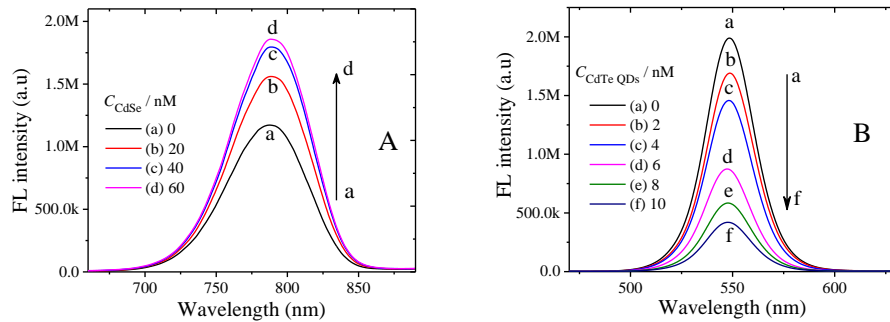
Figure 2.9 Photo-induced interaction between CdTe QDs and CdSe QDs.

Note: (A) FL signal from 20.0 nM CdTe QDs aqueous solution with (a) 0.0 (b) 20.0 (c) 40.0 (d) 60.0 nM CdSe QDs. (B) FL signal from 20.0 nM CdSe QDs aqueous solution with (a) 0.0 (b) 2.0 (c) 4.0 (d) 6.0 (e) 8.0 (f) 10.0 nM CdTe QDs.
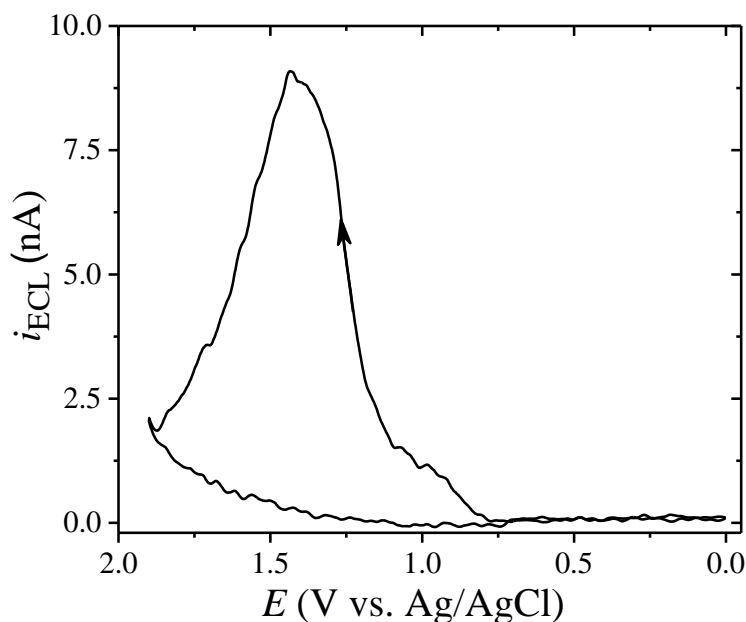
Figure 2.10 ECL response of the CdSe QDs/TPrA system.

Ability of CdSe QDs to generate CdSe QDs[*] under the ECL conditions was examined as shown in Figure 2.10. When the cyclic anodic potential is applied to 375.0 nM CdSe QDs with 70.0 mM TPrA in 0.10 M PB (pH 8.5) between a range of 0 V and 2.0 V, almost no ECL signal is generated before ~0.8 V and only a weak ECL signal with a peak at ~1.48 V is detected on a GCE (Figure 2.10). This suggests that almost no CdSe QDs[*] is formed when the ECL signal of the CdTe QDs/TPrA system is significantly enhanced by CdSe QDs in Figure 2.8. Absence of ECL emission peak at the emission wavelength of CdSe QDs (~550 nm) in Figure 2.8 further proves the lack of CdSe QDs[*] formation during the ECL signal enhancement process. Therefore, energy transfer between CdSe QDs[*] and

CdTe QDs is not the reason for the ECL enhancement of the CdTe QDs/TPrA system in Figure 2.8.

Interference of CdSe QDs on ECL generation mechanism of the CdTe QDs/TPrA system through electron transfer process could be another possible explanation for ECL signal enhancement of CdTe QDs. Because the strong ECL enhancement phenomenon is observed at 0.8 V, which is within the potential range of the first ECL wave from the CdTe QDs/TPrA system (0.70 V – 1.05 V), possible interference of CdSe QDs on the ECL mechanism of the first wave is proposed as follow.

$$\text{TPrA} - e^- \rightarrow \text{TPrA}^{\bullet+} \tag{2.20}$$

$$\text{TPrA}^{\bullet+} \rightarrow \text{TPrA}^{\bullet} + \text{H}^+ \tag{2.21}$$

$$\text{TPrA}^{\bullet} + \text{CdTe QDs} \rightarrow \text{CdTe QD}^{\bullet-} + \text{P}_1 \tag{2.22}$$

$$\text{TPrA}^{\bullet} + \text{CdSe QDs} \rightarrow \text{CdSe QD}^{\bullet-} + \text{P}_1 \tag{2.23}$$

$$\text{CdSe QD}^{\bullet-} + \text{CdTe QDs} \rightarrow \text{CdTe QD}^{\bullet-} + \text{CdSe QD} \tag{2.24}$$

$$\text{TPrA}^{\bullet+} + \text{CdTe QD}^{\bullet-} \rightarrow \text{CdTe QD}^{*} + \text{TPrA} \tag{2.25}$$
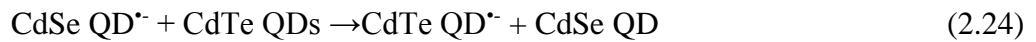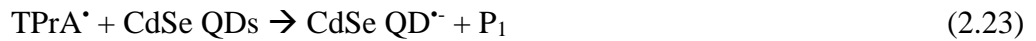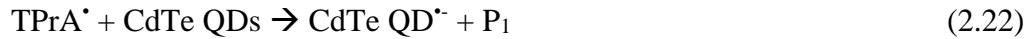
According to this mechanism, addition of CdSe QDs brings in two extra steps (Equations 2.23 and 2.24) to the first ECL wave mechanism of the CdTe QDs/TPrA system (Scheme 2.1). These two additional steps could increase the amount of CdTe QD$^{\bullet-}$ that is one of the reactants to generate CdTe QD* at the final step (Equation 2.25). Hence, generation of increasing amount of CdTe QD$^{\bullet-}$ could effectively elevate the

amount of CdTe QDs[*]. The thermodynamic favorability of the reactions in

Equations 2.23-2.24 are examined based on the Equations 2.26-2.27.

$$\Delta G = -nE_{cell}F \qquad (2.26)$$

$$E_{cell} = E_{reductiot} - E_{oxidation} \qquad (2.27)$$

In these two equations, ΔG is the Gipps free energy change of the system, n in the

number of electron transferred during the reaction, F is the Faradic constant, E_{cell} is the

overall cell potential while $E_{reduction}$ and $E_{oxidation}$ are the half-cell potential of the

reduction reaction and the oxidation reaction, respectively.

A positive E_{cell} is required from both steps in Equations 2.23-2.24 to be

thermodynamically favorable ($\Delta G < 0$). Therefore, redox potential of CdSe QDs needs to

be less negative than that of TPrA$^{\bullet}$ (-1.77 V) and more negative than that of CdTe QDs to

have positive E_{cell} for both steps according to Equation 2.27. As for the reasons described

in the previous section, redox potential of QDs are difficult to directly obtain using CV

experiment. Hence, ECL peak potentials of the QDs/$S_2O_8^{2-}$ system in aqueous condition

are estimated to be their redox potentials (Figure 2.12). According to the mechanism of

the $S_2O_8^{2-}$ coreactant system (Equations 2.28-2.31), reduction of QDs is required to

generate ECL from this system.[11] Therefore, the potential at which ECL is generated is

likely to be very close to the reduction potential of QDs, given the fact that S2O82- is

reduced at -0.46 V vs. Ag/AgCl.

$$S_2O_8^{2-} + e^- \rightarrow S_2O_8^{\bullet 3-} \qquad (2.28)$$

$$QDs + e^- \rightarrow QDs^{\bullet -} \qquad (2.29)$$

$$S_2O_8^{\bullet 3-} \rightarrow SO_4^{2-} + SO_4^{\bullet -} \tag{2.30}$$

$$QD^{\bullet -} + SO_4^{\bullet -} \rightarrow QDs^* + SO_4^{2-} \tag{2.31}$$
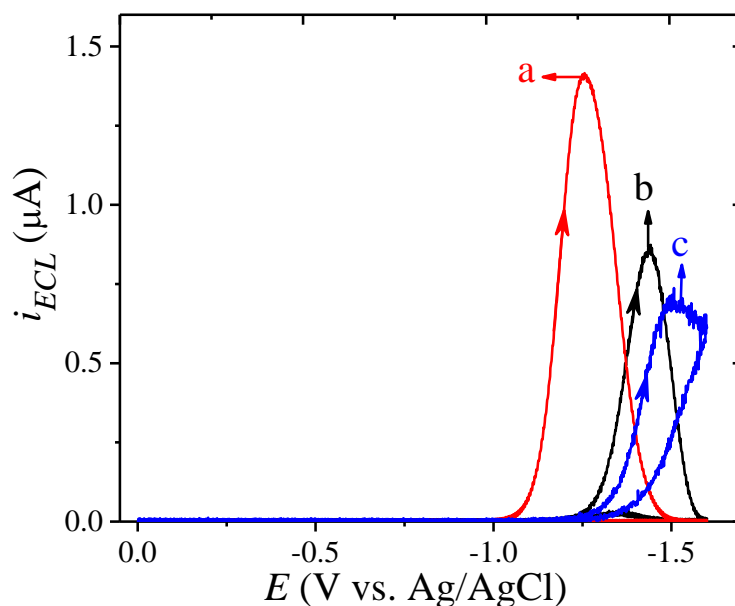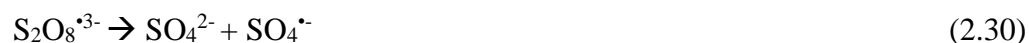
Figure 2.11 ECL responses of the CdTe QDs$_{(760\,nm)}$/S$_2$O$_8^{2-}$, CdTe QDs$_{(730\,nm)}$/S$_2$O$_8^{2-}$, and CdSe QDs/S$_2$O$_8^{2-}$ systems.

Note: ECL signals were generated from (a) 20 nM CdTe QDs$_{(760\,nm)}$, (b) 20 nM CdTe QDs$_{(730\,nm)}$, and (c) 400 nM CdSe QDs with 40.0 µM (N$_2$H$_4$)$_2$S$_2$O$_8$ in 0.10 M PB (pH 8.5) by cyclic potential scanning at 50 mV/s between 0. and -1.6 V for one cycle on GCE.

As shown in Figure 2.11, when the cathodic potential is scanned between 0 and −1.6 V, ECL peaks, located at -1.25 V, -1.50 V, respectively, are obtained from the CdTe QDs (Figure 2.11a) and CdSe QDs (Figure 2.11c) while (N$_2$H$_4$)$_2$S$_2$O$_8$ is used as coreactant on a GCE. When these ECL peak potentials are used as redox potentials of the two QDs, 0.17 V and 0.25 V of the E_{cell} values are obtained for the reactions in Equations 2.23 and 2.24, respectively. These data suggest that both steps in Equations 2.23-2.24 are thermodynamically favorable.
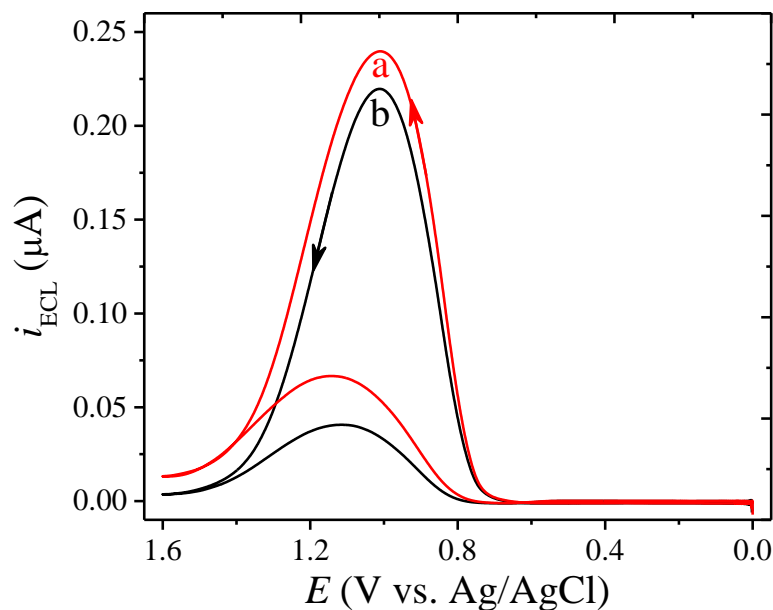
Figure 2.12 ECL response of the CdTe QDs$_{(730 nm)}$/TPrA system in the (a) presence and (b) absence of CdSe QDs.

Note: ECL signals were generated from 50 nM CdTe QDs$_{(730 nm)}$ with 70.0 mM TPrA in 0.10 M PB (pH 8.5) in the (a) presence and (b) absence of 50 nM CdSe QDs by cyclic potential scanning at 50 mV/s between 0.0 V and 1.6 V for one cycle.

A smaller size CdTe QDs with a more negative redox peak potential are used to test the essentiality of Equation 2.24 for ECL signal enhancement mechanism of the CdTe QDs/TPrA system by CdSe QDs. As illustrated in Figure 2.11b, redox potential of the smaller size CdTe QDs ($\lambda_{Emission}$ ~730 nm, -1.47 V) is more negative than that of CdTe QDs$_{(760 nm)}$ (-1.25 V). If CdSe QDs are added to the CdTe QDs$_{(730 nm)}$/TPrA ECL system, the E_{cell} value of the reaction in Equation 2.24 will be 0.03 V and ΔG value of this reaction will be much less negative than that of the same step in CdTe QDs$_{(770 nm)}$ based system. These data indicates that weak ECL signal enhancement will be generated from the CdTe QDs$_{(730 nm)}$/TPrA system when CdSe QDs are added. As expected, upon the addition of CdSe QDs to the CdTe QDs$_{(730 nm)}$/TPrA

57

system only ~9% of ECL enhancement is observed (Figure 2.12). This result further validates the proposed ECL mechanism (Equations 2.20 – 2.25),where Equation 2.24 is a crucial step for the ECL signal enhancement of the CdTe QDs/TPrA system with the addition of CdSe QDs.

2.4 Conclusion

In this chapter, ECL and FL behavior of CdTe QDs and their interaction with CdSe QDs were studied. When 7.0 mM TPrA was used as coreactant, CdTe QDs generated a three-peak ECL signal upon anodic potential scanin from 0 V to 1.55 V on GCE. A two-wave ECL signal at about the same potential of the second and the third ECL peak from the CdTe QDs/TPrA system and a single ECL peak at about the same potential of the third ECL peak of the CdTe QDs/TPrA system were obtained from CdTe QDs when DPrA and PrA were used as coreactant, respectively. These results were explained by generation of DPrA and PrA from successive dealkylation of TPrA under anodic potential scanning. CdTe QDs were proven to accept the energy transferred from CdSe QDs[*] under the FL titration experiment. However, this energy transfer mechanism was excluded from the ECL mechanism where significant ECL enhancement from the CdTe QDs/TPrA system was found upon addition of CdSe QDs. Because, almost no CdSe QDs[*] can be generated at potential less than 0.8 V. An electron-induced mechanism was proposed as the possible explanation for ECL signal enhancement from the CdTe QDs/TPrA system by CdSe QDs and validity of this mechanism was further proven by examining the essentiality of some crucial steps within this mechanism.

2.5 References

(1)   Bard, A. J.; Ed. *Electrogenerated Chemiluminescence*; Marcel Dekker, Inc.: New York, 2004.

(2)   Miao, W. *Chem. Rev.* **2008**, *108*, 2506.

(3)   Hercules, D. M. *Science* **1964**, *145*, 808.

(4)   Visco, R.; Chandross, E. *J. Am. Chem. Soc.* **1964**, *86*, 5350.

(5)   Santhanam, K. S. V.; Bard, A. J. *J. Am. Chem. Soc.* **1965**, *87*, 139.

(6)   Noffsinger, J. B.; Danielson., N. D, *Anal. Chem.* **1987**, *59*, 865.

(7)   Leland, J. K.; Powell., M. J. *J. Electrochem. Soc.* **1990**, *137*, 3127.

(8)   Zu, Y.; Bard, A. J. *Anal. Chem.* **2000**, *72*, 3223.

(9)   Miao, W.; Choi, J.-P.; Bard, A. J. *J. Am. Chem. Soc.* **2002**, *124*, 14478.

(10)   Rubinstein, I.; Bard, A. J. *J. Am. Chem. Soc.* **1981**, *103*, 512.

(11)   White, H. S.; Bard, A. J. *J. Am. Chem. Soc.* **1982**, *104*, 6891.

(12)   Deng, S.; Ju, H. *Analyst.* **2013**, *138*, 43.

(13)   Zhao, W.-W.; Wang, J.; Zhu, Y.-C.; Xu, J.-J.; Chen, H.-Y. *Anal. Chem.* **2015**, *87*, 9520.

(14)   Zhang, X.; Tan, X.; Zhang, B.; Miao, W.; Zou, G. *Anal. Chem.* **2016**, *88*, 6947.

(15)   Zhang, X.; Zhang, B.; Miao, W.; Zou, G. *Anal. Chem.* **2016**, *88*, 5482.

(16)   Ding, Z.; Quinn, B. M.; Haram, S. K.; Pell, L. E.; Korgel, B. A.; Bard, A. J. *Science.* **2002**, *296*, 1293.

(17)   Guo, Z.; Hao, T.; Du, S.; Chen, B.; Wang, Z.; Li, X.; Wang, S. *Biosens. Bioelectron.* **2013**, *44*, 101.

(18)   Lin, D.; Wu, J.; Yan, F.; Deng, S.; Ju, H. *Anal. Chem.* **2011**, *83*, 5214.

(19)   Zhang, Y.; Deng, S.; Lei, J.; Xu, Q.; Ju, H. *Talanta.* **2011**, *85*, 2154.

(20)   Hao, T.; Guo, Z.; Du, S.; Shi, L. *Sensor Actuat B-Chem* **2012**, *171-172*, 803.

(21)   Sun, L.; Chu, H.; Yan, J.; Tu, Y. *Electrochem. Commun.* **2012**, *17*, 88.

(22)   Wu, M. S.; Shi, H. W.; He, L. J.; Xu, J. J.; Chen, H.-Y. *Anal. Chem.* **2012**, *84*, 4207.

(23)   Rosado, D. J., Jr.; Miao, W.; Sun, Q.; Deng, Y. *J. Phys. Chem. B* **2006**, *110,* 15719.

(24)   Liang, G. D.; Shen, L. P.; Zhang, X. L.; Zou, G. Z. *Eur. J. Inorg. Chem.* **2011**, *25*, 3726.

(25)   Yu, W. W.; Qu, L.; Guo, W.; Peng, X. *Chem. Mater.* **2003**, *15*, 2854.

(26)   Lakowicz, J. R. *Principles of Fluorescence Spectroscopy*; Springer US, 2006.

(27)   Myung, N.; Bae, Y.; Bard, A. J. *Nano Lett.* **2003**, *3*, 1053.

(28)   Knight, A. W.; Greenway, G. M. *Analyst.* **1996**, *121*, 101R.

(29)   Kanoufi, F.; Zu, Y.; Bard, A. J. *J. Phys. Chem. B.* **2001**, *105*, 210.

(30)   Allen J. Bard, L. R. F. *Electrochemical Methods: Fundamentals and Applications*; 2nd ed.; Wiley: New York, 2000.

(31)   Mann, C. K. *Anal. Chem.* **1964**, *36*, 2424.

(32)   Masui, M.; Sayo, H.; Tsuda, Y. *J. Chem. Soc. B.* **1968**, 973.

(33)   Portis, L. C.; Bhat, V. V.; Mann, C. K. *J. Org. Chem.* **1970**, *35*, 2175.

(34)   Honda, K.; Yoshimura, M.; Rao, T. N.; Fujishima, A. *J. Phys. Chem. B.* **2003**, *107*, 1653.

CHAPTER III – ELECTROCHEMICAL INVESTIGATION OF AMIDE BOND

FORMATION ON ELECTRODE SURFACE

3.1 Introduction

Development of surface-confined electrochemical or electrogenerated

chemiluminesence (ECL) biosensors has made substantial progress over the past two

decades.[1-3] The ability of biosensors of detecting target molecules at low concentration

with high reliability has attracted the attention of many researchers in related fields.[4-9]

Like other detection techniques, stability and precision of electrochemical and ECL

biosensors, to a great extent, depend on the quality of immobilization of their various

components on an electrode surface. Different strategies have been used to chemically

immobilize biomolecules on an electrode surface for fabrication of electrochemical or

ECL based surface-confined biosensors. For instance, amine-amine crosslinking using

glutaraldhyde[10-12] as bridging ligand or amide bond formation between primary amines

and carboxylic acid groups in the presence of zero-length coupling agent 1-ethyl-3-(-3-

dimethylaminopropyl) carbodiimide hydrochloride (EDC) and

N-hydroxysulfosuccinimide (NHS), where NHS was used to improve coupling

efficiency.[13-16] Among these reactions, EDC/NHS coupling through amide bond

formation between carboxylic acid groups and primary amines is one of the most

frequently used strategies during electrochemical or ECL based biosensor fabrication.

Despite the mechanism of the EDC/NHS coupling has been well studied,[17-21]

experimental parameters of this reaction vary in a wide range in different studies when

used on electrode surfaces.[22-24] For example, concentrations of EDC and NHS were

spread from 1.0 mM to 200.0 mM, and the reaction time also varied from 0.5 to 24

hrs.[22-24] In addition, many of these kinds of biosensor studies used the signals generated from the final biosensors as an indirect proof of formation of amide bond through the EDC/NHS coupling, although the attachment could merely be a electrostatic interactions.

Cyclic voltammetery (CV) is the most popular electrochemical technique used in electrochemical studies. Besides the ability to provide a variety of information about a redox process rapidly, CV possesses high sensitivity towards surface properties of the working electrode.[25,26] Change of properties, such as surface charge or electro-impedance, on working electrode surface, can cause a detectable signal change from a selected redox system during a CV experiment.[26] According to the EDC coupling mechanism,[19,27] when the reaction is taking place on a working electrode surface, surface charge or electro-impedance will change after each reaction step. Therefore, CV could be an excellent technique to study this kind of reaction on an electrode surface, whereas other conventional analytical techniques, like IR or NMR, are practically difficult to be applied on traditional electrode surface.

In this chapter, reaction conditions of the EDC coupling on an electrode surface, such as reaction time, concentrations of reagents, and effect of NHS on coupling efficiency, were comprehensively investigated in two different situations involving one-step and two-step coupling strategies, using CV technique. The results in this chapter could provide useful guidelines towards immobilization of crucial components of the sensors on an electrode surface for biosensor studies.

3.2 Experimental Section

3.2.1 Chemical and Materials

1-Ethyl-3-(-3-dimethylaminopropyl) carbodiimide hydrochloride (EDC, 99%), *N*-hydroxysulfosuccinimide (NHS, 99%), and tris(hydroxymethyl)aminomethane (Tris, 99%) were purchased from Pierce Chemical (Dallas, TX). Ferroceneacetic acid (FcAA, 98%) and 1,7-diaminohaptane (98%) were purchased from Acros Organics (NJ, US). 4-Amino benzonicacid (4-ABA, 99%), potassium ferricyanide ($K_3Fe(CN)_3$, > 99%), lithium perchlorate ($LiClO_4$, > 95%), ethylenediamine (en, > 99.5%), 1-methylimidazole (> 99%), and 2-ethanesulfonic acid (MES, ≥ 99%) were obtained from Sigma-Aldrich (Saint Louis, MO). Sodium phosphate monobasic monohydrate ($NaH_2PO_4•H_2O$) and sodium bicarbonate ($NaHCO_3$) were received from J.T. Baker Chemicals Co. (Phillipsburg, NJ). Hexaammineruthenium(III) chloride ($[Ru(NH_3)_6]Cl_3$, 99%) was purchased from Strem Chemicals (Newburyport, MA). Potassium chloride (KCl, 99.1%) was received from Fisher Scientific (Hampton, NH), and tetrabutylammonium perchlorate (TBAP, 99+%, electrochemical grade) was purchased from Fluka (Milwaukee, WI). Unless stated otherwise, all chemicals were used as received. 50.0 mM of different buffer solutions (i.e., MES, Tris, 1-methylimmidazole, $NaHCO_3$, and phosphate) were prepared by adjusting the pH of the respective solutions with 50.0 mM of different buffer components to the target pH value using 6.0 M NaOH and 1.0 M HCl under a pH meter.

3.2.2 Cyclic Voltammetry Measurements

All CV measurements in this chapter were conducted with a model 660A electrochemical work station (CH instruments, Austin, TX) using a conventional three-

electrode system. The three electrodes were, a Ag/AgCl (3.0 M KCl) or Ag/Ag$^+$

(10.0 mM AgNO$_3$ in MeCN with 0.10 M tetrabutylammonium perchlorate (TBAP)) as

the reference electrode, a platinum mash as the counter electrode, a glassy carbon disk

electrode (GCE, 3.0 mm diameter) as the working electrode. Before each electrochemical

test, the GCE was polished on a polishing pad with 0.3 µm alumina powder slurry and

washed with large amounts of distilled water and ethanol, respectively, and wiped with

Kimwipes tissue to dry. In addition, the GCE and the counter electrode were sonicated in

strong acids, such as H$_2$SO$_4$ or HNO$_3$, followed up by sonication in water and ethanol

solution, respectively. The Vycor tip of the reference electrode was also regularly

replaced with a new one to prevent it from cross-contamination between different test

solutions. After cleaning with strong acids, the GCE was polished almost twice longer

time than that of polishing the electrode between each test to get rid of the oxidized film

formed on the surface of GCE.

3.2.3 Coupling Reaction on GCE Surface

Carboxylic acid groups on 4-ABA modified GCE surface were activated by

soaking the GCE in 50.0 mM MES buffer solution with EDC or EDC/NHS mixture for

certain period of time in room temperature. The above activated GCE was washed with

water and immediately socked in 50.0 mM MES buffer with en for a certain period of

time to couple en on 4-ABA modified GCE at room temperature.

FcAA was immobilized on 1,7-diaminohaptane modified GCE by socking the

electrode in 50.0 mM MES buffer solution containing FcAA and EDC at room

temperature under magnetic stirring.

After each reaction step, the GCE was rinsed with distilled water to get rid of any physically absorbed chemicals from the GCE surface.

3.3 Results and Discussion

3.3.1 Two-Step Coupling Strategy

Scheme 3.1 illustrates the mechanism of amide bond formation through EDC coupling between surface-confined carboxylic acid groups and primary amine groups in solution. At the first step of this mechanism, carboxylic acid groups on GCE surface react with EDC to form an intermediate, O-acylurea, which further reacts with NHS to generate a more stable intermediate, NHS-ester (Step One).[28] After activation of carboxylic groups on GCE with formation of the above two intermediates, primary amine groups can attack either one of the intermediates to form the final amide bonds at the second step of this reaction (Step Two). The optimum reaction conditions for these two steps were separately investigated on GCE surface and results of which will be discussed in the next few sections.
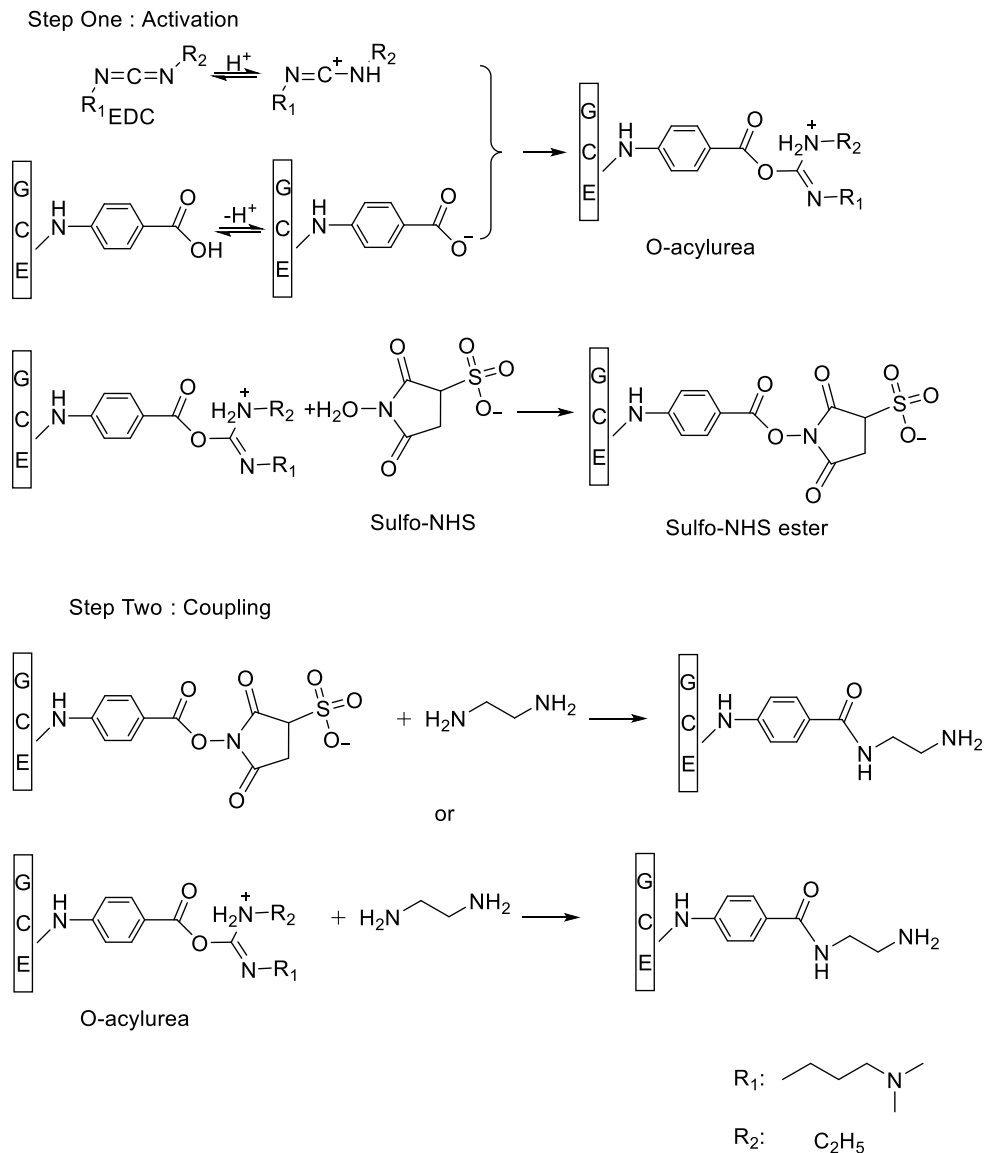
Scheme 3.1 EDC/NHS coupling mechanism on GCE surface.[19,27]

3.3.1.1 Introduction of Carboxylic Acid Groups on a GCE Surface

Carboxyl groups were introduced on GCE surface through electrochemical deposition of 4-ABA.[29-31] Through electrochemical oxidation, the primary amine groups can turn into amine free radicals which could covalently bond to the carbon of the GCE surface.[29] The electrochemical deposition of 4-ABA was conducted in 0.10 M PB (pH 6.5) with 1.0 mM of 4-ABA and 0.10 M KCl with cyclic potential scanning between 0.40

and 1.20 V at the scan rate of 10 mV/s for 6 cycles (Figure 3.1A). As shown in

Figure 3.1A, when the potential is scanned from 0.40 to 1.20 V, a single oxidation peak is

observed at ~0.80 V which matches the reported oxidation peak potential of the primary

amine groups in the similar conditions.[29] In addition, with increasing number of potential

cycles, a gradually suppressed oxidation current of the primary amine is detected

(Figure 3.1A). The oxidation current peak potential of the primary amine is also shifted

from ~0.80 V to ~0.93 V (Figure 3.1A). These changes in the oxidation current and the

peak potential of the primary amine is likely to be caused by the electro-impedance

enhancement and the decrease of "free spots" on GCE surface through attachment of the

4-ABA over each potential cycle.[26,29-31]
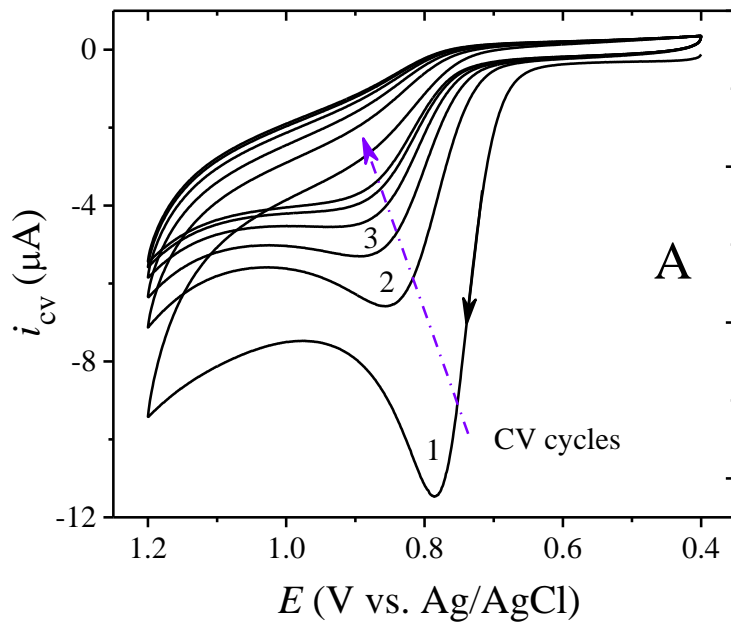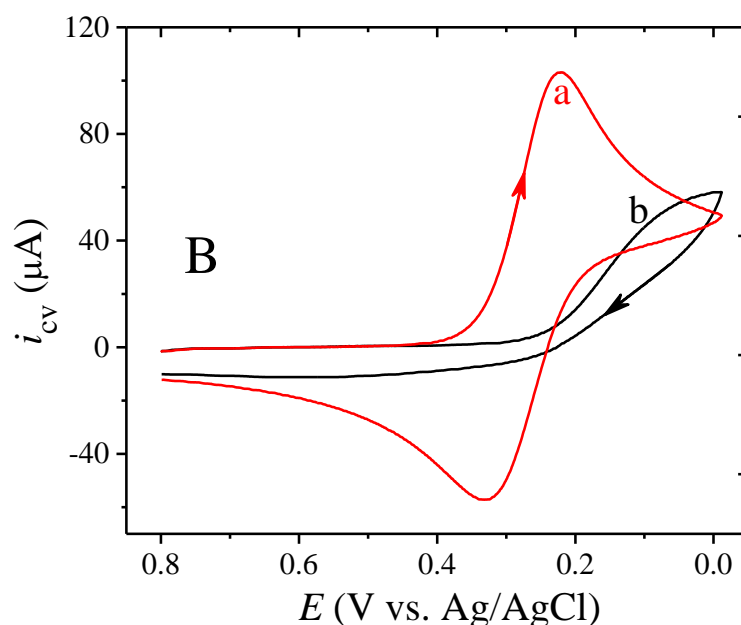
Figure 3.1 (A) Electrochemical deposition of 4-ABA on GCE, (B) CV responses of $K_3Fe(CN)_6$ on (a) bare GCE and (b) 4-ABA modified GCE (GCE/4-ABA).

Note: (A) 4-ABA electrochemically deposited on GCE surface by cyclic anodic potential scanning between 0.40 and 1.20 V on 1.0 mM 4-ABA in 0.10 M PB (pH 6.5) with 0.10 M KCl at a scan rate of 10 mV/s for six cycles on GCE. (B) CV signals were obtained from10.0 mM $K_3Fe(CN)_6$ in 50.0 mM MES buffer (pH 5.0) with 1.0 M KCl by cyclic potential scanning between 0.80 V and 0 V at 50 mV/s scan rate for one cycle on (a) bare GCE and (b) 4-ABA modified GCE (GCE/4-ABA).

To further prove the successful attachment of 4-ABA on GCE surface, CV signals of the $Fe(CN)_6^{3-}$/ $Fe(CN)_6^{4-}$ redox couple on GCE and those on GCE/4-ABA were compared. Due to a lower pK_a value of 4-ABA $(2.24)^{32}$ than the pH value of the test solution(5.0), more than 99% of the carboxylic acid groups on GCE/4-ABA surface were estimated to be negatively charged through deprotonation. When conducting CV experiment, this negatively charged GCE/4-ABA surface could effectively lower the concentration of $Fe(CN)_6^{3-}$ near the electrode surface through electrostatic repulsion. Alternatively, the electro-impedance change could affect the heterogeneous electro-transfer rate As a result, the CV signals from the $Fe(CN)_6^{3-}$/$Fe(CN)_6^{4-}$ redox couple on

68

GCE/4-ABA could be distorted as compared with those on a bare GCE.[26] Therefore, a much lower redox current (ΔI_p) and a larger redox peak potential separation (ΔE_p) from the $Fe(CN)_6^{3-}/Fe(CN)_6^{4-}$ redox couple on GCE/4-ABA than those on bare GCE are expected.[26]

Experimentally, a 99.2 µA reduction current at 0.22 V and a -48.7 µA oxidation current at 0.32 V are obtained from 10.0 mM $K_3Fe(CN)_6$ in 50.0 mM MES buffer (pH 5.0) with 1.0 M KCl in anodic potential range of 0.80 to 0 V on bare GCE (Figure 3.1B-a). A much lower reduction current (~50.0 µA) at 0.02 V and no oxidation current are observed from the same solution on GCE/4-ABA (Figure 3.1B-b). The significantly suppressed redox current (ΔI_p, 50.0 µA vs. 143.9 µA) and less positive reduction peak potential (0.02 V vs. 0.22 V) from the $Fe(CN)_6^{3-}/Fe(CN)_6^{4-}$ on GCE/4-ABA than those on bare GCE indicate that the successful electrochemical immobilization of 4-ABA on GCE.

3.3.1.2 Activation of Carboxylic Acid Groups with EDC

As mentioned in the previous section, a positively charged, unstable intermediate, O-acylurea, can form after activation of carboxylic acid group with EDC (Scheme 3.1).[19] Therefore, activation of GCE/4-ABA with EDC could effectively cause surface charge change on GCE/ABA from negative to positive (-COO$^-$ $\rightarrow$ O-acylurea$^+$). Response of CV signal from the $Ru(NH_3)_6^{3+}/Ru(NH_3)_6^{2+}$ redox couple towards this surface charge change was tested using CV experiment and the result of such experiment is illustrated in Figure 3.2. As shown in Figure 3.2, ΔI_p of the $Ru(NH_3)_6^{3+}/Ru(NH_3)_6^{2+}$ redox couple on GCE/4-ABA decreases by 22.6 µA and ΔE_p increases by 0.05 V after activation of GCE/4-ABA with 50.0 mM EDC. These CV signal changes from the $Ru(NH_3)_6^{3+}/Ru(NH_3)_6^{2+}$ redox

couple occur because, the initial electrostatic attraction between GCE/4-ABA and $Ru(NH_3)_6^{3+}$ is changed to the electrostatic repulsion with the formation of positively charged GCE/activated 4-ABA. The results in Figure 3.2 prove that the CV response of the $Ru(NH_3)_6^{3+}/Ru(NH_3)_6^{2+}$ redox couple can be used to prob the GCE/4-ABA surface property changes over its activation with EDC. The higher the EDC activation efficiencies are, the more carboxyl groups are activated on GCE/4-ABA, and the lower the redox current is generated from the $Ru(NH_3)_6^{3+}/Ru(NH_3)_6^{2+}$ redox couple on GCE/activated 4-ABA. Therefore, the redox current from the $Ru(NH_3)_6^{3+}/Ru(NH_3)_6^{2+}$ redox couple is an indirect indication of GCE/4-ABA activation efficiency with EDC.
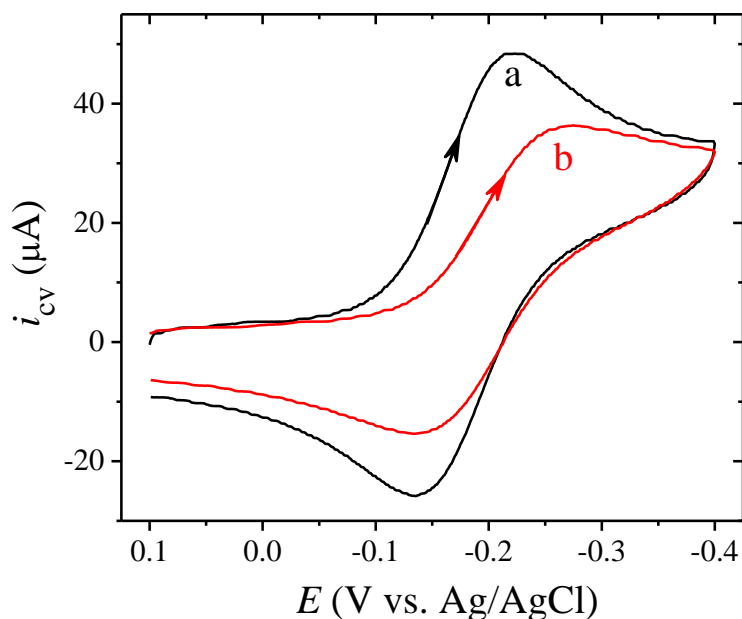
Figure 3.2 Response of redox signal from the $Ru(NH_3)_6^{3+}/Ru(NH_3)_6^{2+}$ redox couple towards the activation of carboxyl groups on GCE/4-ABA with EDC.

Note: CV signals were obtained from 4.0 mM [Ru(NH_3)_6]Cl_3 in 50.0 mM MES (pH 5.0) buffer with 1.0 M KCl by cyclic potential scanning between 0.10 V and -0.40 V at 50.0 mV/s scan rate on (a) GCE/4-ABA (b) GCE/activated 4-ABA. GCE/4-ABA was activated in 50.0 mM MES (pH 4.5) with 50.0 mM EDC at room temperature for 30 min.
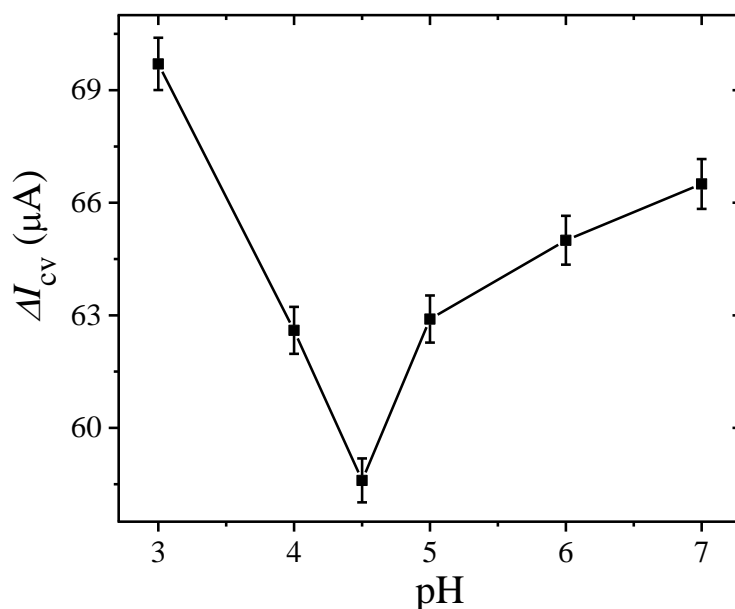
Figure 3.3 Effect of activation pH on redox current of the $Ru(NH_3)_6^{3+}/Ru(NH_3)_6^{2+}$ redox couple on GCE/activated 4-ABA.

Note: Redox currents (ΔI_p) were obtained from 4.0 mM [$Ru(NH_3)_6$]Cl_3 in 50.0 mM MES buffer (pH 5.0) with 1.0 M KCl by cyclic potential scanning between 0.10 V and -0.40 V at 50.0 mv/s scan rate on GCE/activated 4-ABA after activating GCE/4-ABA in 50.0 mM MES buffer at different pH with 50.0 mM EDC at room temperature for 30 min.

According to the mechanism in Scheme 3.1, deprotonation of the carboxylic groups on GCE/4-ABA and protonation of EDC are necessary for activation of GCE/4-ABA with EDC. This indicates that the pH value of the reaction media could play an important role during this carboxyl group activation step. Therefore, the effect of the pH on EDC activation efficiency was studied by conducting CV test with the $Ru(NH_3)_6^{3+}/Ru(NH_3)_6^{2+}$ redox couple on GCE/activated 4-ABA after activating the GCE/4-ABA with 50.0 mM EDC at different pH values. As shown in Figure 3.3, the redox current from the $Ru(NH_3)_6^{3+}/Ru(NH_3)_6^{2+}$ redox couple decreases with the increasing of pH values of the reaction media and reaches to a minimum value of 58.5

µA at pH 4.5. When the activation pH increases further from 4.50 the redox current intensity of the $Ru(NH_3)_6^{3+}/Ru(NH_3)_6^{2+}$ redox couple increases back to 66.5 µA.

The result in Figure 3.3 is obtained because, the optimum pH condition for deprotonation of the carboxyl groups and protonation of EDC overlaps in a narrow pH window from 4.50 to 4.75.[33-35] A pH value lower than 4.50 is not preferred for deprotonation of 4-ABA on GCE/4-ABA, while a higher pH (pH > 5) value was not favorable to protonation of EDC. Therefore, the maximum amounts of carboxylic acid groups are activated with EDC on GCE/4-ABA at pH 4.50, which result in the lowest redox current from the $Ru(NH_3)_6^{3+}/Ru(NH_3)_6^{2+}$ redox couple in Figure 3.3. In other words, pH 4.50 is the optimum pH for activation of carboxyl groups on electrode surface with EDC. This finding also matches with the optimum pH value for carboxyl group activation with EDC reported by Nakajima et al.[36]
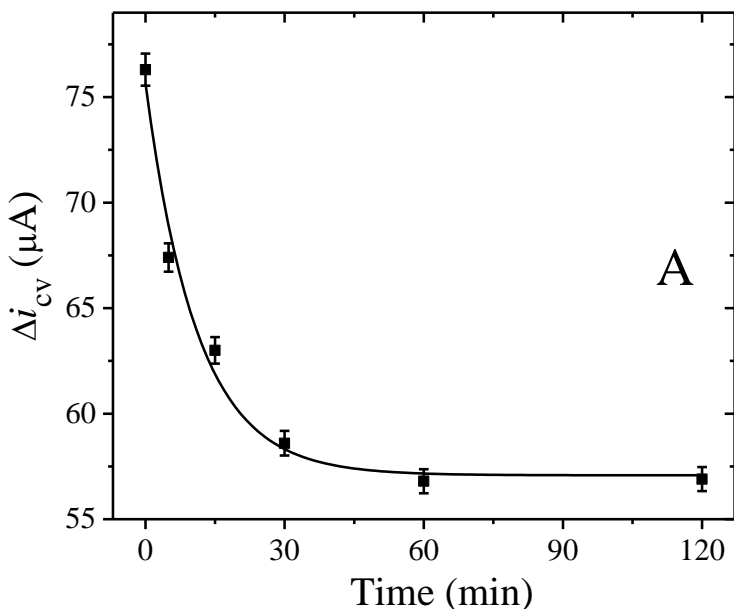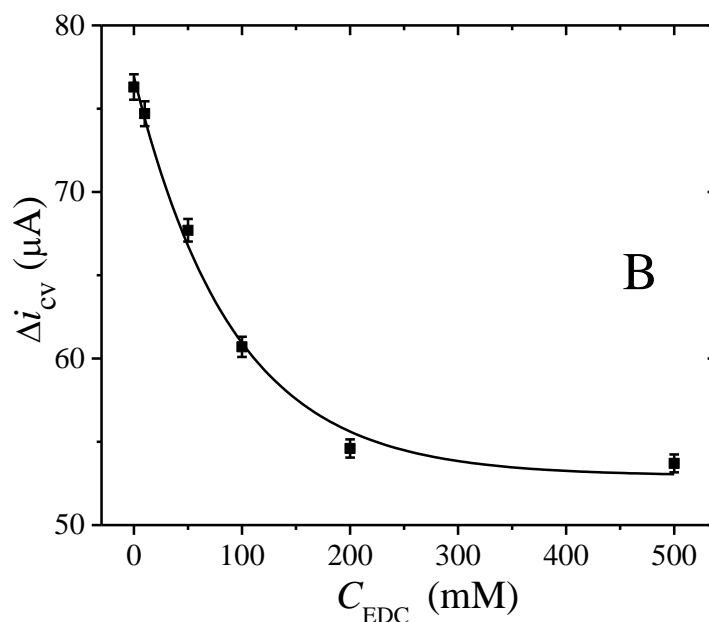
Figure 3.4 Effects of activation (A) reaction time and (B) concentration of EDC (C_{EDC}) on redox current of $Ru(NH_3)_6^{3+}/Ru(NH_3)_6^{2+}$ redox couple on GCE/activated 4-ABA.

Note: Redox currents (ΔI_p) were obtained from 4.0 mM [Ru(NH$_3$)$_6$]Cl$_3$ in 50.0 mM MES buffer (pH 5.0) with 1.0 M KCl by cyclic potential scanning between 0.10 V and -0.40 V at 50.0 mV/s scan rate on GCE/activated 4-ABA after activating GCE/4-ABA (A) in 50.0 mM MES buffer (pH 5) with 50.0 mM EDC at room temperature for a different amount of time and (B) in 50.0 mM MES buffer (pH 5) with different concentrations of EDC at room temperature for 30 min.

Effects of the reaction time and EDC concentration on the efficiency of

GCE/4-ABA activation with EDC were also studied in the similar way to the above pH

dependence study. The redox current of 4.0 mM $Ru(NH_3)_6^{3+}$ on GCE/activated 4-ABA is

plotted against the reaction time for which GCE/4-ABA was activated with 50.0 mM

EDC in 50.0 mM MES buffer (pH 5.0) (Figure 3.4A). The redox current of the

$Ru(NH_3)_6^{3+}/Ru(NH_3)_6^{2+}$ redox couple decreases rapidly during the first half hour of

GCE/4-ABA activation and levels off after 45 min.

This result suggests that activation of carboxyl acid groups on GCE/4-ABA

carried on in relatively fast reaction rate during the first half hour. and almost no carboxyl

73

group on GCE/4-ABA surface was activated after one hour. of activation with EDC. Therefore, half hour. to one hour. activation time of GCE/4-ABA with EDC at the above experimental condition is enough to activate the majority of carboxyl groups on GCE/4-ABA.

When GCE/4-ABA was activated for 30 min in 50.0 mM MES (pH 5.0) with increasing concentration of EDC, redox current of the $Ru(NH_3)_6^{3+}/Ru(NH_3)_6^{2+}$ redox couple on this GCE/activated 4-ABA decreases exponentially (Figure 3.4B). The redox current from the test solution barely changes when an EDC concentration higher than 200.0 mM EDC is used for activation of the GCE/4-ABA (Figure 3.4B). This result suggests that when 200.0 mM EDC is used, majority of the carboxylic acid groups on GCE/4-ABA are activated to positively charged O-acylurea. Therefore, 200.0 mM could be used as the optimum concentration of EDC while activating the carboxylic acid groups on an electrode surface.
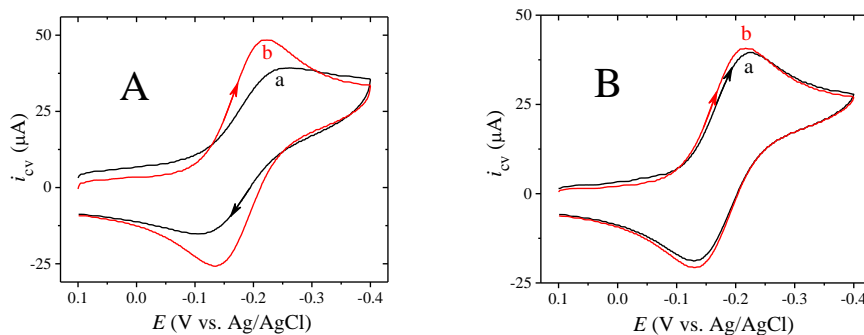
Figure 3.5 Effect of NHS on the stability of the redox current from the $Ru(NH_3)_6^{3+}/Ru(NH_3)_6^{2+}$ redox couple on GCE/activated 4-ABA.

Note: GCE/4-ABA was activated in 50.0 mM MES buffer (pH 5.0) with (A) 50.0 mM NHS and 50.0 mM EDC, and (B) 50.0 mM EDC for 30 min at room temperature. CV signals were obtained from 4.0 mM [Ru(NH$_3$)$_6$]Cl$_3$ in 50.0 mM MES buffer (pH 5.0) with 1.0 M KCl by cyclic potential scanning between 0.10 and -0.40 V at 50.0 mV/s scan rate on GCE/activated 4-ABA (a) immediately after activation, (b) after soaking GCE/activated 4-ABA in 50.0 mM MES buffer (pH 6.5) for 30 min at room temperature.

Since the amide bond formation yield is limited by instability of the intermediate formed after activation of carboxylic acid groups with EDC, NHS is usually used with EDC in this reaction to increase the product yield.[19,37] In the presence of NHS, unstable O-acylurea could further react with NHS to form a more stable intermediate, NHS-ester, which also could react with primary amine groups to generate the final amide bond (Scheme 3.1).[19,37] Therefore, addition of NHS gives activated carboxyl groups longer lifetime to react with primary amine groups. One of the major side reactions that affects the amid bond formation yield during EDC coupling reaction is hydrolyzation of active intermediate, O-acylurea, to regenerate carboxylic acid group.[38] Therefore, stability of the two different intermediates, O-acylurea and NHS-ester, against the hydrolization were examined by following experiments. Pre-prepared GCE/4-ABA was socked in 50.0 mM MES (pH 6.5) for 30 min after it was activated with EDC or EDC/NHS mixture for 30 min, respectively. CV signal of the $Ru(NH_3)_6^{3+}/Ru(NH_3)_6^{2+}$ redox couple on this electrode was recorded right after the activation reactions and after soaking the GCE/activated 4-ABA in the buffer solution, respectively. As illustrated in Figure 3.5A, when the GCE/4-ABA is activated only with EDC and kept in the buffer solution for 30 min, redox current of the $Ru(NH_3)_6^{3+}/Ru(NH_3)_6^{2+}$ redox couple on this electrode increases by 20.2 µA as compared with that on the same electrode immediately after the activation reaction (Figure 3.5A-a vs. Figure 3.5A-b). When GCE/4-ABA is activated with EDC/NHS mixture, on the other hand, redox current of the $Ru(NH_3)_6^{3+}/Ru(NH_3)_6^{2+}$ redox couple on this electrode increases only by 3.0 µA after socking the electrode in the buffer solution (Figure 3.5B-a vs. Figure 3.5B-b). The signal of the $Ru(NH_3)_6^{3+}/Ru(NH_3)_6^{2+}$ redox couple on only EDC activated GCE/4-ABA is increased as

75

much as 20.2 µA because, unstable O-acylurea reacted with water in the buffer solution to regenerate carboxyl groups on GCE surface. The GCE/4-ABA formed after this hydrolyzation can generate much higher redox current from the $Ru(NH_3)_6^{3+}/Ru(NH_3)_6^{2+}$ redox couple compared with GCE/activated 4-ABA as previously discussed. The NHS-esters obtained after GCE/4-ABA activation with EDC/NHS mixture is much more resistant towards hydrolyzation at the same condition, therefore only 3.0 µA signal enhancement was observed from the $Ru(NH_3)_6^{3+}/Ru(NH_3)_6^{2+}$ on this electrode. These results indicate that NHS could improve the stability of the active-intermediate against hydrolyzation by forming NHS-ester during EDC/NHS coupling reaction.

3.3.1.3 Coupling (Step Two)

After the activation of carboxylic acid groups, primary amine groups could react with the active intermediates to form the final amide bond (Scheme 3.1 step two).[19] The effects of the reaction conditions on efficiency of this reaction step were studied in current section. Ethylenediamine (en) was used in this section as the source of primary amine groups which could be attached onto the GCE/activated 4-ABA through amide bond formation to generate GCE/4-ABA-en as illustrated in Scheme 3.1-step two. Because both en and the O-acylurea on the electrode surface surface are positively charged at pH 5.0, the charge on the electrode surface will not change through the above coupling step. However, the electro-impedance of the electrode surface could decrease through this coupling reaction because of the replacement of relatively bulky molecules (O-acylurea) with much smaller sized en molecules. Response of the CV signal from the $Fe(CN)_6^{3-}/Fe(CN)_6^{4-}$ redox couple towards above electro-impedance change was examined. As shown in Figure 3.6A-a, the CV signal with 58.0 µA redox current is

obtained from 10.0 mM $K_3Fe(CN)_6$ in anodic potential range from 0.80 to 0 V on GCE/activated 4-ABA, which was obtained by activating GCE/4-ABA in 50.0 mM MES buffer (pH 4.5) for one hour. After this GCE/activated 4-ABA reacts with 1.0 M en in 50.0 mM MES buffer (pH 7.0) for one hour, 160.0 µA of redox current is obtained from the same $K_3Fe(CN)_6$ solution on this electrode. Even though there is electrostatic interaction between GCE/activated 4-ABA surface and the $Fe(CN)_6^{3-}$/ $Fe(CN)_6^{4-}$ redox couple, the high electro-impedance of O-acylurea has played the dominant role. When en replaces O-acylurea on the electrode surface after the coupling reaction, electrostatic interaction between electrode surface and the electro-active species remains while the electro-resistance on the electrode surface is decreased. Therefore, unlike GCE/activated 4-ABA, on GCE/4-ABA-en the electrostatic interaction between electrode surface and the $Fe(CN)_6^{3-}$/ $Fe(CN)_6^{4-}$ redox couple becomes the dominant factor on the CV signal generation. This leads to a much higher redox current from $Fe(CN)_6^{3-}$/ $Fe(CN)_6^{4-}$ redox couple on GCE/4-ABA-en as compared with that on GCE/activated 4-ABA (58.0 µA vs. 160 µA). Hence, the significant signal enhancement from the same $Fe(CN)_6^{3-}$/ $Fe(CN)_6^{4-}$ redox couple on GCE/activated 4- ABA before and after its reaction with en indicates successful formation of GCE/4-ABA-en. In addition, this redox current enhancement from the $Fe(CN)_6^{3-}$/ $Fe(CN)_6^{4-}$ redox couple after GCE/4-ABA-en formation could be used as an indication of en coupling efficiency with GCE/activated 4-ABA.

The effect of the concentration of en on its coupling efficiency with GCE/activated 4-ABA (EDC activated) was studied using the CV response of the $Fe(CN)_6^{3-}$/ $Fe(CN)_6^{4-}$ redox couple. In Figure 3.6B, redox current of 10.0 mM $K_3Fe(CN)_6$

on GCE/4-ABA-en is plotted against the concentration of en that was used in the coupling reaction between en and GCE/activated 4-ABA. The redox current of the $Fe(CN)_6^{3-}/Fe(CN)_6^{4-}$ redox couple on GCE/4-ABA-En increases logarithmically with increasing concentration of en used in the reaction to generate the GCE/4-ABA-en. This result suggests that, with increasing concentration of en in the reaction solution the efficiency of the coupling step between en and GCE/activated 4-ABA increases. Under the reaction conditions in Figure 3.6B, efficiency of this reaction barely increases when en concentration is higher than 1.0 M.
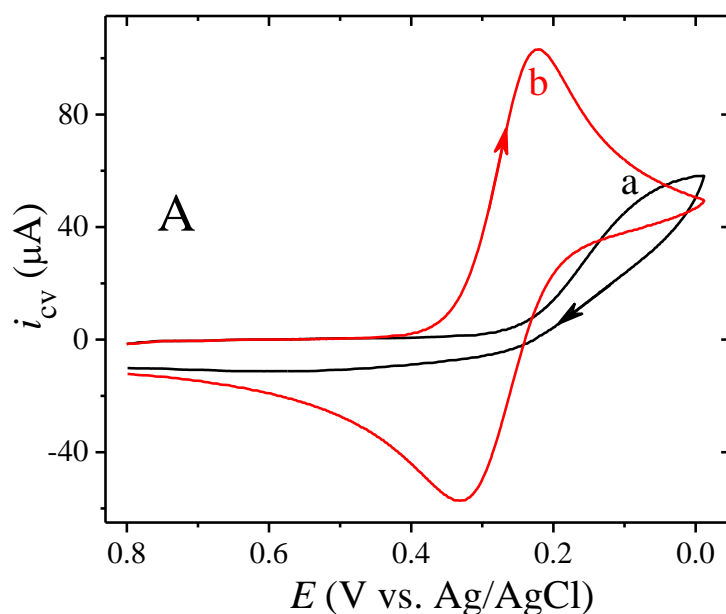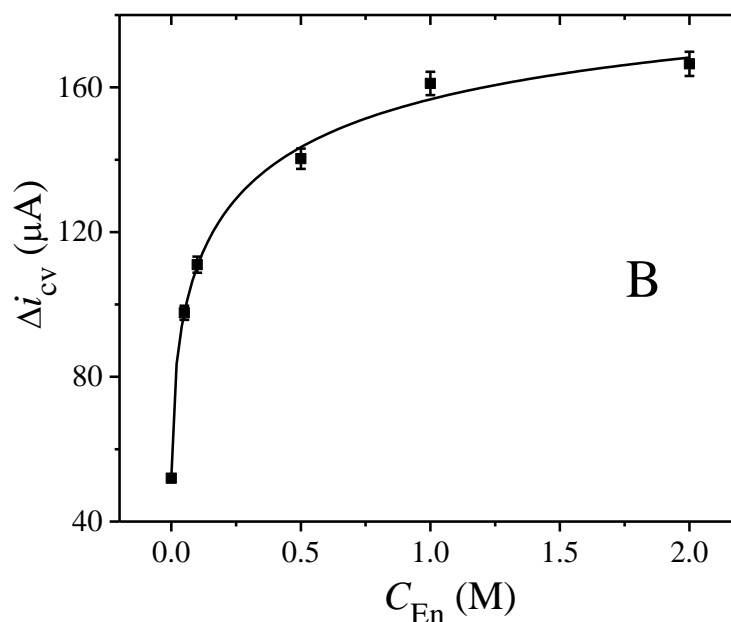
Figure 3.6 (A) Response of redox signal from the $Fe(CN)_6^{3-}/Fe(CN)_6^{4-}$ redox couple towards the attachment of en on GCE/activated 4-ABA by amide bond formation. (B) Effect of en concentration on redox current of the $Fe(CN)_6^{3-}/Fe(CN)_6^{4-}$ redox couple on GCE/4-ABA-en.

Note: CV signals were obtained from10.0 mM $K_3Fe(CN)_6$ in 50.0 mM MES buffer (pH 5.0) with 1.0 M KCl by cyclic

potential scanning between 0.80 V and 0.0 V at 50.0 mV/s scan rate for one cycle on (A-a) GCE/activated 4-ABA, (A-b, B)

GCE/4-ABA-en. GCE/4-ABA was activated in 50.0 mM MES buffer (pH 4.5) with 100.0 mM EDC for 1 hour. and coupled

with (A-b) 1.0 M (B) different amounts of en in 50.0 mM MES (pH 7.0) for 1 hour.

The effect of reaction time on the coupling efficiency between en and

GCE/activated 4-ABA was also examined by the similar way to the above study. As

displayed in Figure 3.7A, the redox current of the $Fe(CN)_6^{3-}/Fe(CN)_6^{4-}$ redox couple on

GCE/4-ABA-en increases with the reaction time of the coupling reaction. Additionally,

redox current of the $Fe(CN)_6^{3-}/Fe(CN)_6^{4-}$ redox couple is barely changed after one hour.

of reaction. This indicates that when a high concentration of en (~1.0 M) is used, majority

of the O-acylurea on GCE/activated 4-ABA surface are effectively replaced by en within

one hour of coupling reaction.

Coupling step between en and GCE/activated 4-ABA is more likely to favor

higher pH condition than the activation of GCE/4-ABA with EDC. This is because, the

coupling step only requires deprotonation of primary amine groups on en whereas the

activation step involves deprotonation and protonation two reactants as previously

discussed. In Figure 3.7B, the redox current of 10.0 mM $K_3Fe(CN)_6$ on GCE/4-ABA-en

is plotted against the pH value of the reaction media that was used in the coupling

reaction between en and GCE/activated 4-ABA to produce the GCE/4-ABA-en. Starting

from pH 6.0, the redox current from the $Fe(CN)_6^{3-}/ Fe(CN)_6^{4-}$ redox couple on

GCE/4-ABA-en increases linearly with the increasing pH value of the coupling reaction,

while other conditions remain constant. This indicates that the efficiency of the coupling

step increases with increasing pH value of the reaction media. Nevertheless, pH value

around 7.5 should be chosen for the coupling step in biological media to avoid denaturing

of the biological molecules by unfolding their structures.
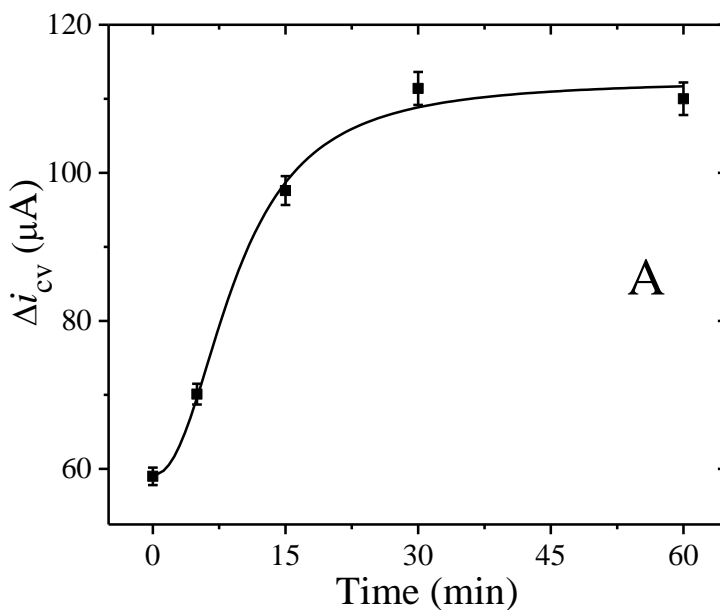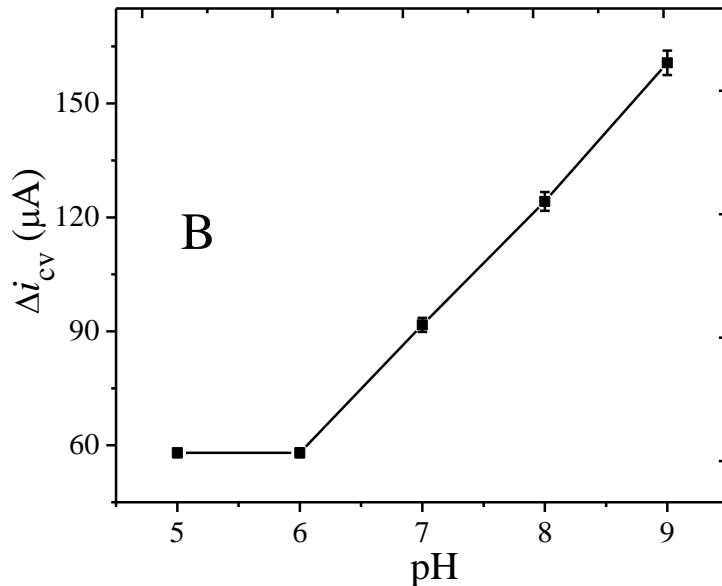
Figure 3.7 Effect of (A) reaction time and (B) pH on the redox current of the $Fe(CN)_6^{3-}/ Fe(CN)_6^{4-}$ redox couple on GCE/4-ABA-en.

Note: CV signals were obtained from10.0 mM $K_3Fe(CN)_6$ in 50.0 mM MES buffer (pH 5.0) with 1.0 M KCl by cyclic potential scanning between 0.80 V and 0.0 V at 50 mV/s scan rate for one cycle on GCE/4-ABA-en. GCE/4-ABA-En was obtained by activating GCE/4-ABA in 50.0 mM MES buffer (pH 4.5) with 100.0 mM EDC for 1 hour. and immediately reacting with (A) 0.10 M en in 50.0 mM MES buffer (pH 7.0) for different amount of time, (B) 0.10 M en in 50.0 mM MES buffer for 1 hour. at different pH.

3.3.2 One-Step Coupling Strategy

When molecules with carboxylic acid groups need to be attached on to the primary amine groups on an electrode surface through EDC coupling, the two-step strategy discussed in the previous sections will be practically difficult. Because, after the activation of the carboxyl groups the molecules with the activated intermediates will need to be separated from the reaction mixture before the coupling step. Therefore, a one-step strategy will be more feasible in such case. In the rest of this chapter, the effect of the

81

reaction conditions, such as reactant concentration, pH value of the reaction media, and reaction time on the efficiency of this one-step EDC coupling strategy will be discussed.

3.3.2.1 Introduction of Primary Amine Group on GCE Surface

According to Liu's report,[39] when 1,7-diaminohaptane was electrochemically deposited on GCE, ~75% of the 1,7-diaminohaptane molecules were attached on GCE with one primary amine group when keeping the primary amine group on the other side of the molecule intact. Hence, primary amine groups were introduced on GCE surface by electrochemical deposition of 1,7-diaminohaptane.[29] When the anodic potential is scanned between 0 and 1.30 V for one cycle, an oxidation potential of ~1.09 V (vs. Ag/Ag$^+$) is observed from 1.0 mM 1,7-diaminohaptane in ethanol with 0.10 LiClO$_4$ (Figure 3.8A). A higher oxidation peak potential of this primary amine (1.28 V vs. NHE) than that of the primary amine on 4-ABA (1.08 V, vs. NHE) could be resulted from a slower electron transfer rate in ethanol than in aqueous solution.[26]
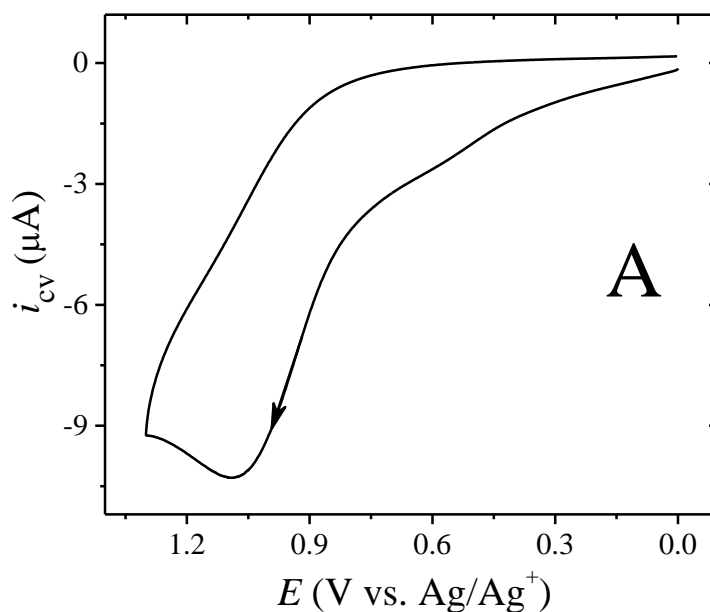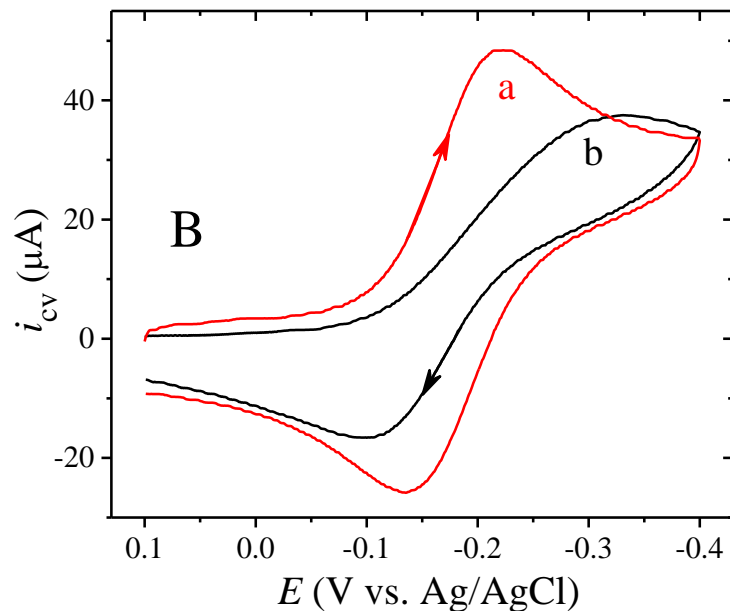
Figure 3.8 (A) Electrochemical deposition of 1,7-diaminohaptane on GCE surface, and (B) CV signals of the $Ru(NH_3)_6^{3+}/Ru(NH_3)_6^{2+}$ redox couple on (a) bare GCE (b) 1,7-diaminohaptane modified GCE (GCE/DAH).

Note: (A) 1,7-Diaminohaptane was electrochemically deposited on GCE surface by anodic cyclic potential scanning between 0 and 1.30 V on 1.0 mM 1,7-diaminohaptane in ethanol with 0.10 M $LiClO_4$ at a scan rate of 10.0 mV/s for one cycle on GCE. (B) CV signals were obtained from 4.0 mM $[Ru(NH_3)_6]Cl_3$ in 50.0 mM MES (pH 5.0) buffer with 1.0 M KCl by cyclic potential scanning between 0.10 V and -0.40 V at 50.0 mV/s scan rate on (a) bare GCE (b) GCE/DAH.

Successful deposition of 1,7-diaminohaptane on GCE surface was further examine by conducting CV experiment with the $Ru(NH_3)_6^{3+}/Ru(NH_3)_6^{2+}$ redox couple on GCE before and after electrochemical deposition of 1,7-diaminohaptane. As shown in Figure 3.8, compared with bare GCE (Figure 3.8B-a), two wider separated redox peaks (ΔE_p, 0.08 V vs. 0.23 V) with lower currents (ΔI_p, 54.2 µA vs. 74.5 µA) are observed at pH 5.0 on GCE with electrodeposited 1,7-diaminohaptane (Figure 3.8B-b). These signal changes are the indications of successful attachment of 1,7-diaminohaptane on GCE surface. At pH 5.0 primary amines on GCE/1,7-diaminohaptane (GCE/DAH) are

positively charged due to protonation. Therefore, compared with bare GCE, a CV signal with less redox current is generated on GCE/DAH from the $Ru(NH_3)_6^{3+}/Ru(NH_3)_6^{2+}$ redox couple due to the electrostatic repulsion between the electrode surface and the electro-active species in the test solution (Figure 3.8B).

3.3.2.2 One-Step Coupling Condition Study

In the two-step strategy, CV signals of external electro-active redox couples, the $Fe(CN)_6^{3-}/Fe(CN)_6^{4-}$ and the $Ru(NH_3)_6^{3+}/Ru(NH_3)_6^{2+}$, were used as an indirect indication of reaction efficiency. In the one-step strategy, however, an electro-active probe with carboxylic acid group was directly attached on the primary amine groups on GCE/DAH surface through amide bond formation (Scheme 3.2). Therefore, redox current from this electro-active probe modified GCE (GCE/DAH-FcAA) after EDC coupling reaction could serve as a direct evidence of amide bond formation and the indication of reaction efficiency. CV signals obtained from GCE/DAH-FcAA after GCE/DAH reacted with different concentrations of FcAA in 50.0 mM MES buffer (pH 7.0) with 50.0 mM EDC are shown in Figure 3.9. When the potential is scanned between -0.10 and 0.60 V in 0.10 M $LiClO_4$ aqueous solution, two well-defined redox peaks at ~0.32 and ~0.36 V, respectively, were observed on GCE/DAH-FcAA. The redox current from the GCE/DAH-FcAA increases with increasing concentration of FcAA in the coupling solution, as more of electro-active probes (FcAA) are attached on GCE/DAH through amid bond formation with the assistance of EDC. Therefore, the redox current from GCE/DAH-FcAA is used as a direct indication of one-step coupling efficiency with EDC for the following studies.

84
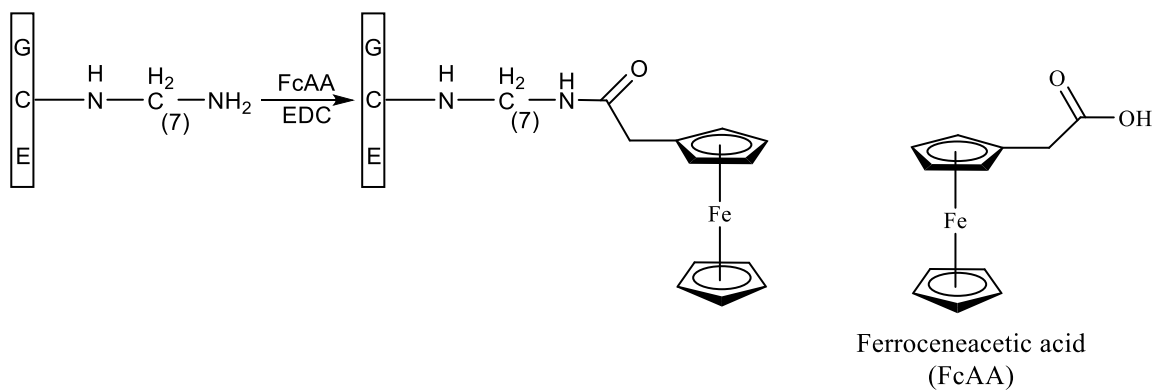
Scheme 3.2 One-step coupling of FcAA on GCE/DAH in the presence of EDC.
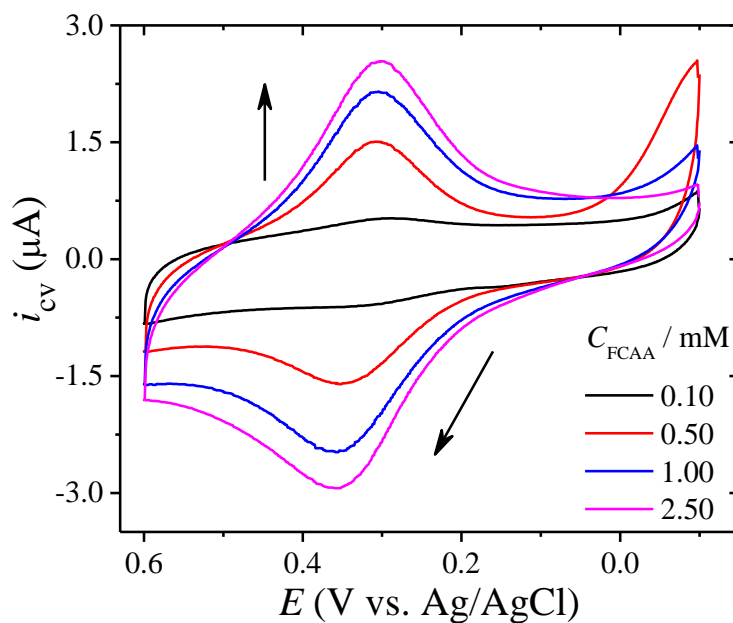
Figure 3.9 CV signals from GCE/DAH-FcAA.

Note: CV signals were obtained from GCE/DAH-FcAA in 0.10 M LiClO$_4$ aqueous solution by cyclic potential scanning between -0.10 V and 0.60 V at 100.0 mV/s scan rate after reacting GCE/DAH in 50.0 mM MES buffer (pH 7) with 50.0 mM EDC and different concentrations of FcAA at room temperature for 24 hours. The potential was scanned for 5 cycles for each concentration point, the responses from the second cycle from each CV set are displayed.
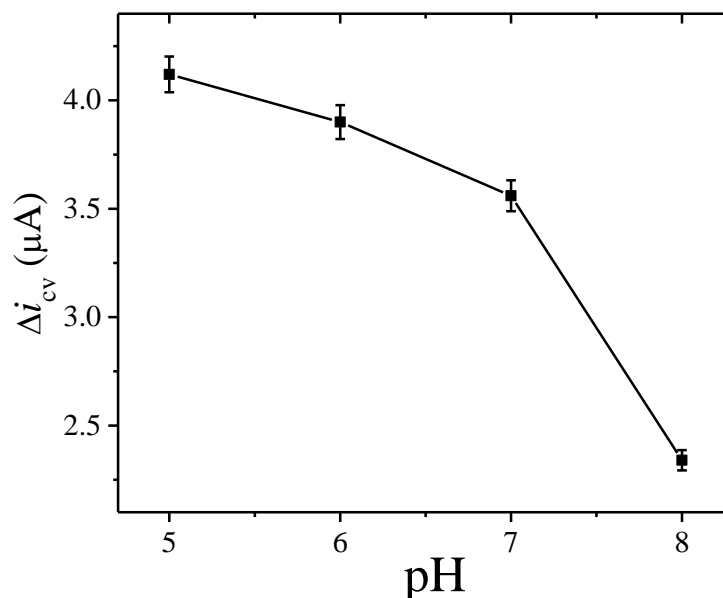
Figure 3.10 Effect of one-step reaction pH on redox current from GCE/DAH-FcAA.

As previously discussed, both activation and coupling steps of the overall EDC coupling reaction were sensitive to the pH value of the reaction media. pH 4.5 was proven to be the optimum pH condition for the activation of carboxyl groups by EDC in section 3.3.1.2. On the other hand, the efficiency of coupling step (step two in Scheme 3.1) was increased with increasing pH value of the reaction media as discussed in the same section. Therefore, when these two steps are carried out in the same reaction media during one-step strategy, the optimum pH value of the reaction media is expected to be higher than 4.5. In Figure 3.10, redox currents from GCE/DAH-FcAA are plotted against the pH value of the reaction media in which GCE/DAH-FcAA is formed, where

the redox has a maximum value at pH 5.0 and then decreases with the increasing pH value of the one-step coupling reaction media. When the one-step reaction was taking place in a reaction medium with pH value lower than 5.0, a redox current lower than the that at pH 5.0 in Figure 3.10 was expected from GCE/DAH-FcAA. However, due to the low solubility of FcAA in acidic media, those data points were failed to be obtained. Since coupling efficiency was not changed drastically from pH 5.0 to pH 7.0, so a pH value around 7.0 should guarantee a high coupling yield without damaging the activity of biological molecules.
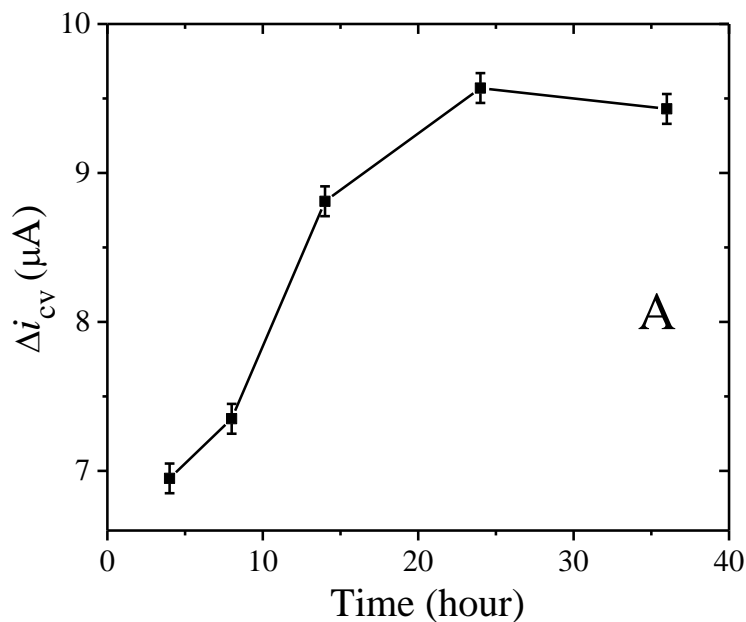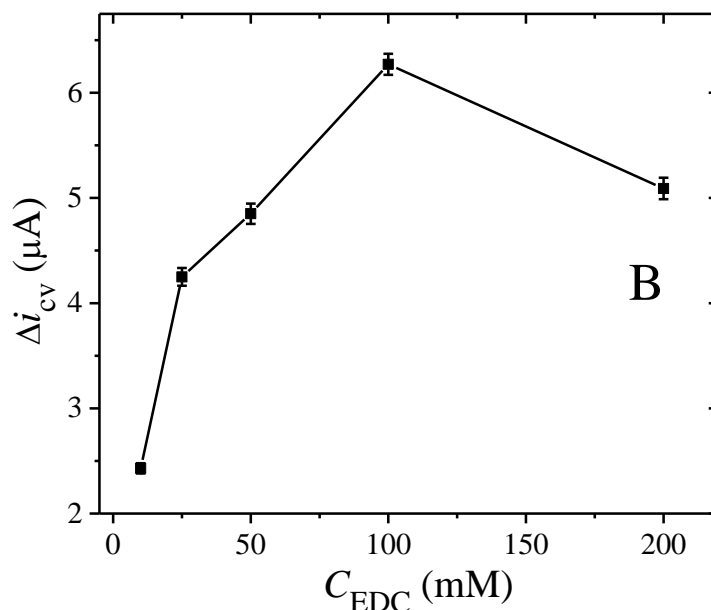
Figure 3.11 Effect of (A) reaction time and (B) concentration of EDC on redox current from GCE/DAH-FcAA.

Note: CV signals were obtained from GCE/DAH-FcAA in 0.10 M LiClO$_4$ aqueous solution by cyclic potential scanning between -0.10 V and 0.60 V for at 100.0 mV/s scan rate after reacting GCE/1,7-daminohaptane (A) in 50.0 mM MES buffer (pH 7.0) with 50.0 mM EDC and 5.0 mM FcAA at room temperature for different amount of time. (B) in 50.0 mM MES buffer (pH 7.0) with different concentration of EDC and 1.0 mM FcAA at room temperature for 4 hrs. The potential was scanned for 5 cycles for each data point, the redox current from the second cycles were taken.

Effects of other two reaction conditions, reaction time and concentration of EDC, on the efficiency of one-step EDC coupling strategy were also investigated. After obtaining GCE/DAH-FcAA by reacting GCE/DHA with 5.0 mM FcAA in the presence of EDC for different amount time, redox currents of GCE/DAH-FcAA were recorded. As shown in Figure 3.11A, the redox current from GCE/DAH-FcAA is increased with increasing of the reaction time and no signal enhancement was observed after 24 hrs. This result indicates no more FcAA was reacted with GCE/DHA in the presence of EDC after 24 hrs. of one-step reaction. Note that, this optimum time (24 hrs.) is much longer

than the total time that are required for the two-step strategy as discussed in section

3.3.1.2 (total of ~1.5 hrs.). This is because a much lower concentration of reactant

(1.0 mM FcAA) are used for one-step strategy than that for two-step strategy (1.0 M en),

therefore, the reaction efficiency of one step-strategy is much lower than that in two-step

strategy in these studies.

In Figure 3.11B, the effect of concentration of EDC on redox current from

GCE/DAH-FcAA is demonstrated. The redox current from GCE/DAH-FcAA is initially

increased with increasing concentration of EDC, and decreased back when a higher

concentration of EDC (>100.0 mM) is used for GCE/DAH-FcAA formation through one-

step coupling. Therefore, 100.0 mM EDC could be chosen as the optimum concentration

of EDC for one-step EDC coupling reaction on electrode surface. It has been reported

that excessive concentration of EDC is favorable to other side reactions during EDC

coupling which limit the final amid bond formation yield.[27] This explains the redox

current decrease from GCE/DAH-FcAA when more than 100.0 mM EDC was used for

GCE/DAH-FcAA formation during one-step coupling reaction.

Chemical compositions in the reaction buffer could also affect the EDC coupling

yield. The redox currents from GCE/DAH-FcAA when five different buffers are used for

the one-step coupling, respectively, are shown in Figure 3.12. Compared with MES and

NaHCO$_3$, when phosphate buffer, 1-methylimidazole, or Tris buffer are used as the

reaction buffer, much lower redox currents are obtained from GCE/DAH-FcAA. This is

because, Tris, 1-methylimidazole, and phosphate contain either amine groups or

phosphate groups which could react with activated carboxylic acid groups on FcAA to

prevent the formation of the final amide bond.[27] A slightly lower redox current from

GCE/DAH-FcAA is obtained when NaHCO$_3$ is used as reaction buffer, as compared with MES buffer. The decomposition of NaHCO$_3$ overtime could be a possible reason for this observation, even though NaHCO$_3$ does not interfere with EDC coupling reaction. This result suggests, among commonly used buffers, MES is the most suitable one to be used for EDC coupling reaction.
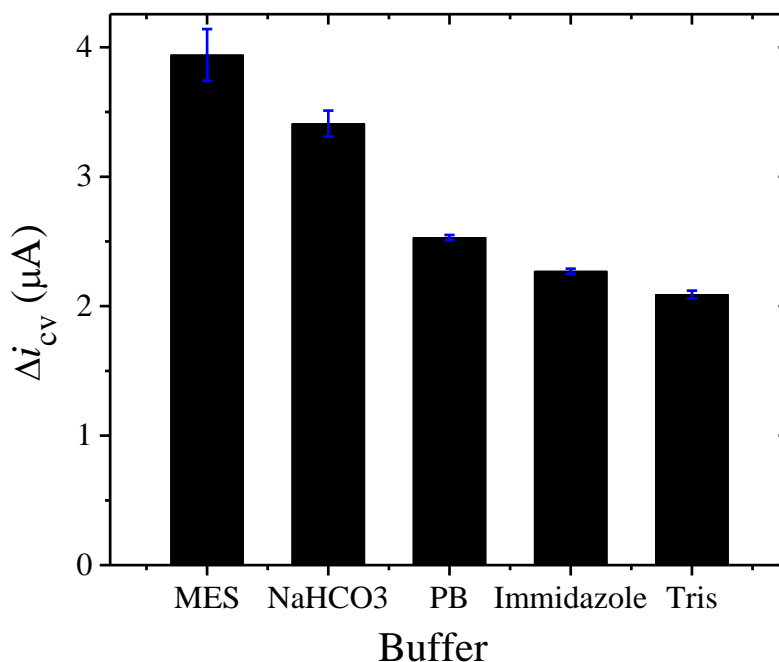
Figure 3.12 Effect of buffer composition on redox current from GCE/DAH-FcAA.

Note: CV signals were obtained from GCE/DAH-FcAA in 0.10 M LiClO$_4$ aqueous solution by cyclic potential scanning between -0.10 V and 0.60 V at 100.0 mV/s scan rate after reacting GCE/1,7-daminohaptane in 50.0 mM of different buffers (pH 7.0) with 100.0 mM EDC and 1.0 mM FcAA at room temperature for 2 hrs. The potential was scanned for 5 cycles for each data point, the redox current from the second cycles were taken.

3.4 Conclusion

In this chapter, coupling reaction of carboxylic groups and primary amine groups on an electrode surface when EDC was used as the zero-length coupling reagent was

studied with cyclic voltammetry. Effects of different experimental conditions, such as

pH, concentration of the reagents, reaction times, on the EDC coupling efficiency were

investigated systematically for both one-step and two-step coupling strategies. Reaction

media with pH 4.50 was proven to be the optimum pH condition for activation of

carboxylic groups on GCE surface and a ~ pH 7.5 value of the reaction media was

preferred to the coupling step of the reaction. Presence of NHS was proven to provide

stability to the activated intermediate against hydrolyzation during EDC/NHS coupling.

When the activation and the coupling step were taking place in the same reaction media,

maximum coupling efficiency was obtained at pH 5.0 and MES was proven to be the

most adequate buffer option for this reaction. The results in this chapter could provide

detailed guideline with respect to the electrochemical and ECL biosensor studies about

how to effectively immobilize the various components of the sensor on the electrode

surface through EDC coupling strategy.

3.5 References

(1)   Wang, J. *Anal. Chem.* **1999**, *71*, 328.

(2)   Miao, W. *Chem. Rev.* **2008**, *108*, 2506.

(3)   Kimmel, D. W.; LeBlanc, G.; Meschievitz, M. E.; Cliffel, D. E. *Anal. Chem.* **2012**, *84*, 685.

(4)   Wei, H.; Wang, E. *Trends Anal. Chem.; TrAC.* **2008**, *27*, 447.

(5)   Zhang, L.; Li, J.; Xu, Y.; Zhai, Y.; Li, Y.; Wang, E. *Talanta* **2009**, *79*, 454.

(6)   Sun, X.; Du, Y.; Zhang, L.; Dong, S.; Wang, E. *Anal. Chem.* **2007**, *79*, 2588.

(7)   Guo, Z.; Shen, Y.; Wang, M.; Zhao, F.; Dong, S. *Anal. Chem.* **2004**, *76*, 184.

(8)   Downey, T. M.; Nieman, T. A. *Anal. Chem.* **1992**, *64*, 261.

(9)   Choi, H. N.; Cho, S.-H.; Lee, W.-Y. *Anal. Chem.* **2003**, *75*, 4250.

(10)   Xu, S.; Liu, Y.; Wang, T.; Li, J. *Anal Chem* **2011**, *83*, 3817.

(11)   Jie, G.; Zhang, J.; Wang, D.; Cheng, C.; Chen, H.-Y.; Zhu, J.-J. *Anal. Chem.* **2008**, *80*, 4033.

(12)   Ji, J.; He, L.; Shen, Y.; Hu, P.; Li, X.; Jiang, L. P.; Zhang, J. R.; Li, L.; Zhu, J. J. *Anal. Chem.* **2014**, *86*, 3284.

(13)   Zhou, H.; Liu, J.; Xu, J.-J.; Chen, H.-Y. *Anal. Chem.* **2011**, *83*, 8320.

(14)   Wu, M.-S.; Shi, H.-W.; Xu, J.-J.; Chen, H.-Y. *Chem. Commun.* **2011**, *47*, 7752.

(15)   Shan, Y.; Xu, J.-J.; Chen, H.-Y. *Chem. Commun.* **2010**, *46*, 5079.

(16)   Shan, Y.; Xu, J.-J.; Chen, H.-Y. *Chem. Commun.* **2009**, 905.

(17)   Hoare, D. G.; Koshland, D. E. *J. Am. Chem. Soc.* **1966**, *88*, 2057.

(18)   Wang, C.; Yan, Q.; Liu, H. B.; Zhou, X. H.; Xiao, S. J. *Langmuir.* **2011**, *27*, 12058.

(19)   Sam, S.; Touahir, L.; Salvador Andresa, J.; Allongue, P.; Chazalviel, J. N.; Gouget-

Laemmel, A. C.; Henry de Villeneuve, C.; Moraillon, A.; Ozanam, F.; Gabouze, N.; Djebbar, S. *Langmuir.* **2010**, *26*, 809.

(20)   Palazon, F.; Montenegro Benavides, C.; Léonard, D.; Souteyrand, É.; Chevolot, Y.; Cloarec, J.-P. *Langmuir.* **2014**, *30*, 4545.

(21)   Bartczak, D.; Kanaras, A. G. *Langmuir.* **2011**, *27*, 10119.

(22)   Voicu, R.; Boukherroub, R.; Bartzoka, V.; Ward, T.; Wojtyk, J. T. C.; Wayner, D. D. M. *Langmuir.* **2004**, *20*, 11713.

(23)   Liang, G.; Liu, S.; Zou, G.; Zhang, X. *Anal Chem* **2012**, *84*, 10645.

(24)   Lahiri, J.; Isaacs, L.; Tien, J.; Whitesides, G. M. *Anal Chem.* **1999**, *71*, 777.

(25)   Nicholson, R. S.; Shain, I. *Anal Chem.* **1964**, *36*, 706.

(26)   Faulkner, L. R; Bard, A. J. *Electrochemical Methods–Fundamentals and Applications* 2nd ed.; John Wiley and Sons: New York, 2000.

(27)   Hermanson, G. T. *Bioconjugate techniques*; 2nd ed.; Academic Press: San Diego, 2008.

(28)   Staros, J. V.; Wright, R. W.; Swingle, D. M. *Anal. Biochem.* **1986**, *156*, 220.

(29)   Masui, M.; Sayo, H.; Tsuda, Y. *J. Chem. Soc. B.* **1968**, 973.

(30)   Downard, A. J. *Electroanalysis* **2000**, *12*, 1085.

(31)   Barbier, B.; Pinson, J.; Desarmot, G.; Sanchez, M. *J. Electrochem. Soc.* **1990**, *137*, 1757.

(32)   Kortum, G. E. A. *Dissociation Constants of Organic Acids in Aqueous Solution*; Butterworth: Lincolnshire, United Kingdom, 1961.

(33)   Kuo, J. W.; Swann, D. A.; Prestwich, G. D. *Bioconjugate Chem.* **1991**, *2*, 232.

(34)   Madison, S. A.; Carnali, J. O. *Ind. Eng. Chem. Res.* **2013**, *52*, 13547.

(35)   Souguir, Z.; Roudesli, S.; About-Jaudet, E.; Le Cerf, D.; Picton, L. *J. Colloid Interface Sci.* **2007**, *313*, 108.

(36)   Nakajima, N.; Ikada, Y. *Bioconjugate Chem.* **1995**, *6*, 123.

(37)   Staros, J. V. *Biochemistry* **1982**, *21*, 3950.

(38)   Grabarek, Z.; Gergely, J. *Anal. Biochem.* **1990**, *185*, 131.

(39)   Liu, J.; Dong, S. *Electrochem. Commun.* **2000**, *2*, 707.

CHAPTER IV – EFFECTS OF MULTI-WALLED CARBON NANOTUBE ON THE

ELECTROGENERATED CHEMILUMINESCENCE AND FLOURESCENCE OF

CdTe QUANTUM DOTS[*]

4.1 Introduction

Electrogenerated chemiluminescence (ECL) is a process of light generation from

luminophores after electrochemical redox reactions on an electrode surface with or

without the assistance of an ECL coreactant.[1] Because of its capability of detecting trace

amounts of target molecules, ECL has been widely used in the development of highly

sensitive chemical and biological sensors over the past two decades.[2,3] Initially, ECL

based chemical and biosensors were exclusively developed by using $Ru(bpy)_3^{2+}$

(bpy = 2,2'-bipyridine) as an ECL emitter.[4,5] However, quantum dots (QDs) have rapidly

caught the attention of the scientific community since successful ECL generation from

silicon and a few other nanoparticles.[2,6-11] This is because, QDs possess some distinct

advantages, such as size tunable optical properties, excellent biocompatibility, and high

quantum efficiency, over other ECL labels, which make QDs outstanding candidates for

ECL labels in chemical and bioanalysis studies.[12-15]

Many different materials have been applied on electrode surface to improve the

performance of ECL biosensors, and carbon nanotubes (CNTs) is one of the most

frequently chosen option for such purpose.[16-24] Properties, such as high conductivity,

mechanical strength, surface functional groups, and high aspect ratio, made CNTs to be

an excellent supporting material in fabricating electrochemical and ECL based biosensors.[2,25-27] It has been reported that use of CNTs significantly increased electrochemical and ECL signals from electro-active probes at lower potential due to the fast electron transfer rate and large surface area of CNTs.[28] However, conflict reports have been also seen in the literature, where ECL signals were found to be suppressed considerably after introducing CNTs into biosensors with either QDs[29] or Ru(bpy)$_3^{2+}$ [30] as the ECL probe, even though the electrochemical signals of the ECL systems were indeed remarkably enhanced.

With the increasing use of highly sensitive and selective QDs/coreactant type ECL based biosensors involving nano-carbon materials, it becomes clear that a systematic study on the effect of CNTs on the ECL of QDs with commonly used ECL coreactants is necessary. This type of study could provide a guideline for the community on how to use CNTs effectively in fabricating ECL based chemical and biochemical sensors for either enhancing or quenching ECL signals. In this chapter, multi-walled CNTs immobilized on glassy carbon electrode will be used to investigate the ECL responses of CdTe QDs in the presence of anodic coreactant TPrA and 2-(dibutylamino)ethanol (DBAE) as well as cathodic coreactant ammonium persulfate $(NH_4)_2S_2O_8$. Fluorescence will be employed to verify the quenching mechanism.

4.2 Materials and Methods

4.2.1 Chemicals

3-Mercaptopropionic acid (MPA, ≥ 99%), chitosan, tri-*n*-propylamine (TPrA, ≥ 99%), sodium tellurite (Na$_2$TiO$_3$, ≥ 99%), 2-(dibutylamino)ethanol (DBAE, 99%), and ammonium persulfate ($(NH_4)_2S_2O_8$, ≥ 99%) were purchased from Sigma-Aldrich (Saint

Louis, MO). Multi-walled carbon nanotubes (CNTs, $\geq$ 95%, outer diameter 30-50 nm) were purchased from Cheap Tubes Inc. (Cambridgeport, VT). Hydrazine hydride ($N_2H_4 \cdot H_2O$, 100%) and phosphoric acid (H_3PO_4, 85%) were purchased from Fishier Scientific (Pittsburgh, PA). Sodium phosphate monobasic monohydrate ($NaH_2PO_4 \cdot H_2O$) was received from J.T. Baker Chemicals Co., (Phillipsburg, NJ). Cadmium chloride ($CdCl_2 \cdot 2.5H_2O$) was obtained from Mallinckrodt Chemical Works (Saint Louis, MO). High purity nitrogen was supplied by Airgas (Hattiesburg, MS) and acetic acid (HAc, 99.8%) was received from Matheson Coleman & Bell (OH). 0.10 M NaH_2PO_4 solution was used to prepare 0.10 M phosphate buffer (PB) solution (pH 8.5) with addition of pH adjusting reagents, NaOH or H_3PO_4, under the monitoring of a pH meter.

4.2.2 Apparatus

A homemade ECL instrument which contains a CHI 660A electrochemical workstation (CH Instrument, TX) and a photomultiplier tube (PMT, Hamamatsu R928, Japan) placed in a light-tight box was used to conduct cyclic voltammetry (CV) and ECL measurements in this chapter.[3,31] The PMT was supplied with -700 V of voltage by a high voltage power supply (Model 472A Brandenburg PMT power supply, England). A conventional three-electrode electrochemical cell system, namely, a glassy carbon electrode (GCE, 3 mm in diameter) or modified GCE as the working electrode, a Ag/AgCl (3.0 M KCl) as the reference electrode, and a platinum mesh as the counter electrode, was used for CV and ECL measurements. Before each measurement or modification, the GCE was polished with 0.3-0.05 µm alumina slurry, washed with water and dried with the Kimwipes facial tissue.

ECL spectra were collected with a Princeton Instruments spectrum system, which consisted of a Spec-10:400B/LN-eXcelon digital charge-coupled device (CCD) camera, a ST-133B controller, and an ActonSP-2156 imaging spectrograph monochromator, equipped with a Model 173 potentiostat coupled with a Model 175 universal programmer (Princeton Applied Research). In order to reduce the signal background, liquid nitrogen was used to cool the CCD camera to -120 °C. Light from the bottom of the ECL cell was directed to the monochromator through a 1.5 mm slit using a 1-m long fiber optic bundle.

Fluorescence experiments were conducted with a PTI QuantaMaster^{TM} 40 intensity based spectrofluorometer (Photon Technology International, Inc., NJ) with a slit width of 1.0 mm, excitation wavelength at 650 nm, and an emission wavelength range from 660 to 950 nm. An Evolution 300 UV-vis spectrometer (Thermo Fishier Scientific, MA) was used to collect UV-vis absorption spectra with a 1.00 cm quartz curvet.

Deionized (DI) water was generated with an Elix Advantage Water Purification System (EMD Millipore, Darmstadt, Germany).

4.2.3 Modification of GCE

2.0 mg/mL (or 0.2% wt%) of chitosan modified CNTs suspension was prepared by ultrasonicating suitable amount of CNTs in 0.1% (wt%) chitosan-0.1% (wt%) HAc solution for 1.5 hr. The obtained suspension was stable for weeks at 4 ºC. 15.0 µL of the above solution was dropped on pre-cleaned GCE surface and air dried for 1.5 hr to obtain chitosan mixed CNTs modified GCE. The solid film covering the entire glassy carbon surface (i.e., 3 mm) formed from the last step could be removed by polishing the as-prepared GCE with 0.3-0.05 µm alumina slurry.

To modify the GCE with CNTs alone (i.e., no chitosan), a freshly prepared 2.0 mg/mL (or 0.25% wt%) CNTs-ethanol suspension, which was obtained by ultrasonification of the mixture for 1.0 hr, was casted on a pre-cleaned GCE surface and air dried for 20 min. Caution was taken when placing such an electrode into the electrolyte solution as the CNTs film could be detached from the electrode surface.

4.2.4 Synthesis of CdTe QDs

3-MPA capped water soluble CdTe QDs were synthesized with procedures modified from the one-pot strategy reported by Zou et al.[32] Briefly, 3.20 mL of 0.20 M $CdCl_2$ was added to 200.0 mL DI water containing three-necked flask under constant stirring. After adding 336.0 μL of MPA to the above solution, the reaction media was adjusted to ~pH 8.0 with NaOH (6.0 M) and 20.6 mg of $NaTiO_3$ was added to the solution immediately. After refluxing the reaction media for 10 min, 7.68 mL of $N_2H_4 \cdot H_2O$ was added and the new mixture was further refluxed for 24 hr. The resultant CdTe QDs were washed with 1:1 water/acetone (v/v) once and 1:10 water/acetone (v/v) 1-2 times after separated with centrifugation at 12, 000 rpm. The final precipitates were re-dispersed in either DI water for FL and UV-vis measurements or 0.10 M PB solution (pH 8.5) for ECL studies. All solutions were kept in dark at 4 °C prior to use. The concentrations of the CdTe QDs stock solutions were estimated with the empirical equations reported by Yu et al on the basis of the UV-vis absorption spectra.[33] Because QDs are generally well-capped with capping agents, no notable toxicity towards DNA or other biomolecules has been reported under the time scale of ECL sensor analysis.

Unless stated otherwise, all experiments in this chapter were conducted at the room temperature of 20 ± 1 °C without degassing the test solutions with high purity nitrogen.

4.3 Results and Discussion

4.3.1 Characterization of MPA Capped CdTe QDs

FL emission spectrum, UV-vis absorption spectrum, and ECL spectrum of as-prepared CdTe QDs are shown in Figure 4.1. Nearly mono-dispersed size of the QDs was indicated by a single symmetrical FL emission peak at 770 nm (Figure 4.1A-a) and a single absorption peak at ~710 nm (Figure 4.1B).[34] The diameter of the QDs was estimated to be 6.43 nm based on its UV-vis absorption spectrum and an empirical equation.[33] ECL spectrum of as-prepared CdTe QDs (Figure 4.1A-b), which is almost overlapped with its FL spectrum except for a slightly broader tail beyond 800 nm, was obtained from CdTe QDs/TPrA anodic system. These data suggest that the 3-MPA capping agent successfully passivated the surface state of as-prepared CdTe QDs.[9]
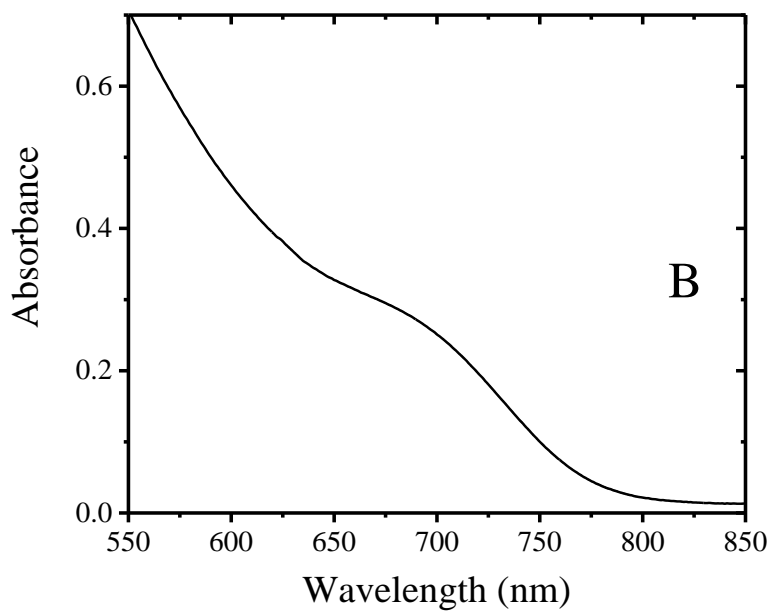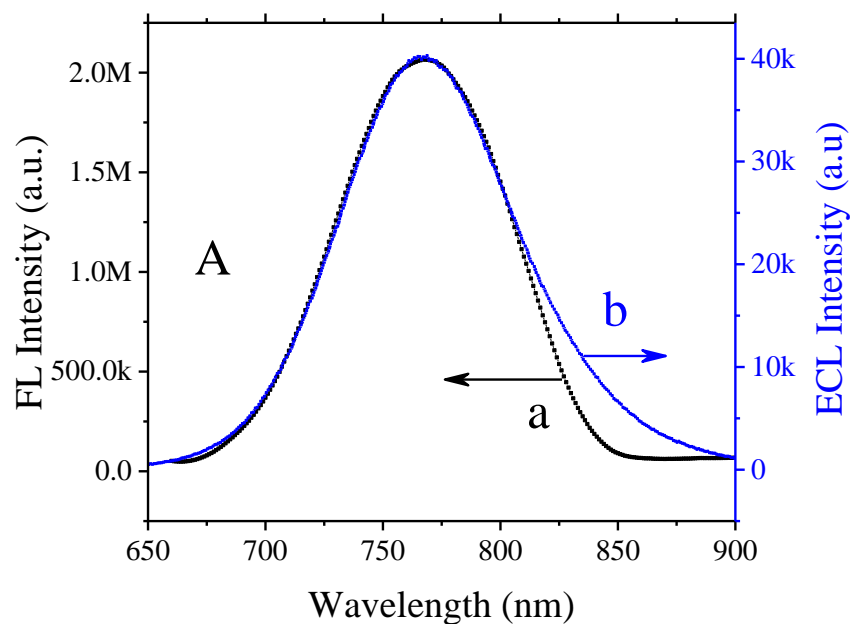
Figure 4.1 (A) (a) Fluorescence, (b) ECL, and (B) UV-vis absorption spectra of CdTe QDs.

Note: The fluorescence and absorption spectra were obtained from 2.5 nM and 500 nM CdTe QDs, respectively, using a 1.00 cm curvet. The ECL spectrum was generated at a GCE with 250 nM CdTe QDs with 35 mM TPrA in 0.10 M PB (pH 8.5) solution using cyclic potential scan between 0.0 and 2.0 V vs Ag/AgCl for one cycle at a scan rate of 100 mV/s.

4.3.2 Quenching Effect of CNTs on the ECL Behavior of the CdTe QDs/TPrA System

Because TPrA is one of the most commonly used anodic ECL coreactant in fundamental ECL studies and chemical/biosensor related applications,[1,3,35] the effect of CNTs on ECL was first tested with the CdTe QDs/TPrA anodic system. Cyclic voltammagrams obtained from 125.0 nM CdTe QDs in 0.10 M PB (pH 8.5) with 52.5 mM TPrA using three different working electrodes are shown in Figure 4.2A. At bare GCE, the oxidation of TPrA started at ~0 .6 V and reached a 0.35 mA peak current at around 1.15 V (Figure 4.2A-a). In contrast, a nearly 7-fold increased oxidation peak current (i.e., 2.34 vs 0.35 mA) and a less positive oxidation potential (i.e., ~0.45 vs 0.60 V) of TPrA were observed at CNTs modified GCE (Figure 4.2A-b). This finding is consisted with the electrocatalytic property and large surface area of CNTs.[36,37] On the basis of well-studied anodic coreactant ECL mechanisms,[3,11,38,39] one would expect significantly higher ECL responses to be produced at the CNTs modified GCE, because the larger the oxidation current is, the more intermediates (e.g., TPrA$^{+\bullet}$, TPrA$^{\bullet}$, CdTe QDs$^{+\bullet}$, Equations. 4.1-4.7) needed for ECL generation are produced, resulting in the higher in ECL intensity.

$$\text{TPrA} - \text{e} \rightarrow \text{TPrA}^{+\bullet} \tag{4.1}$$

$$\text{TPrA}^{+\bullet} - \text{H}^+ \rightarrow \text{TPrA}^{\bullet} \tag{4.2}$$

$$\text{TPrA}^{\bullet} + \text{CdTe QDs} \rightarrow \text{CdTe QDs}^{-\bullet} \tag{4.3}$$

$$\text{TPrA}^{+\bullet} + \text{CdTe QDs}^{-\bullet} \rightarrow \text{CdTe QDs}^{*} \tag{4.4}$$

$$CdTe\ QDs - e \rightarrow CdTe\ QDs^{+\bullet} \tag{4.5}$$

$$CdTe\ QDs^{+\bullet} + CdTe\ QDs^{-\bullet} \rightarrow CdTe^{*} \tag{4.6}$$

$$CdTe\ QDs^{*} \rightarrow CdTe\ QDs + h\nu \tag{4.7}$$
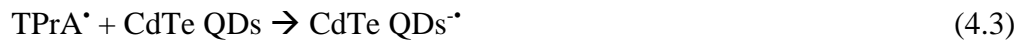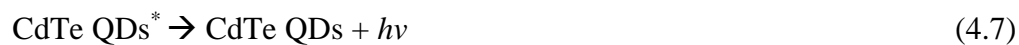
Experimentally, however, extremely weak ECL responses are observed at the CNTs modified GCE (Figure 4.2B-b) as compared with those obtained from the bare GCE (Figure 4.2 B-a). Close inspection reveals that the forward ECL current is changed from 2.2 μA at the bare GCE to 0.06 μA at the CNTs modified GCE. Clearly, such a 37-fold ECL current decrease is directly related to the quenching effect of the surface-confined CNTs towards the ECL generation of the CdTe QDs/TPrA system.
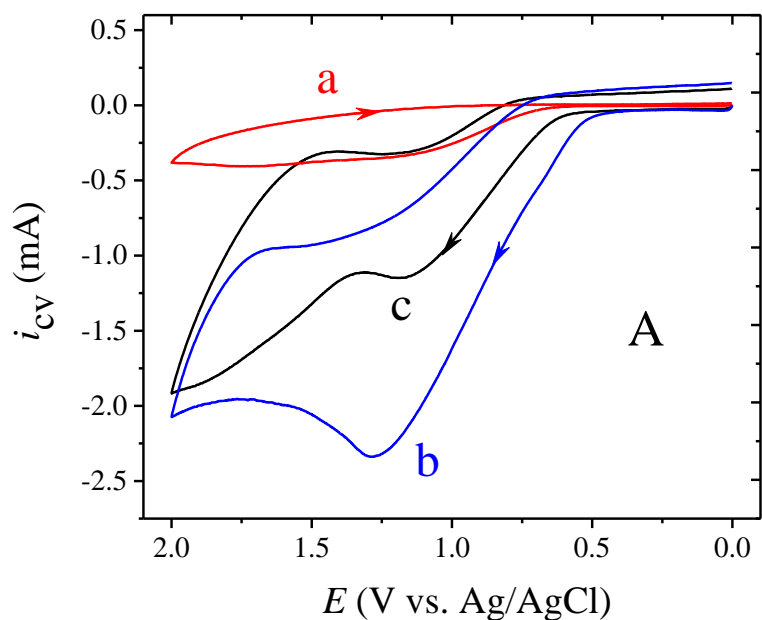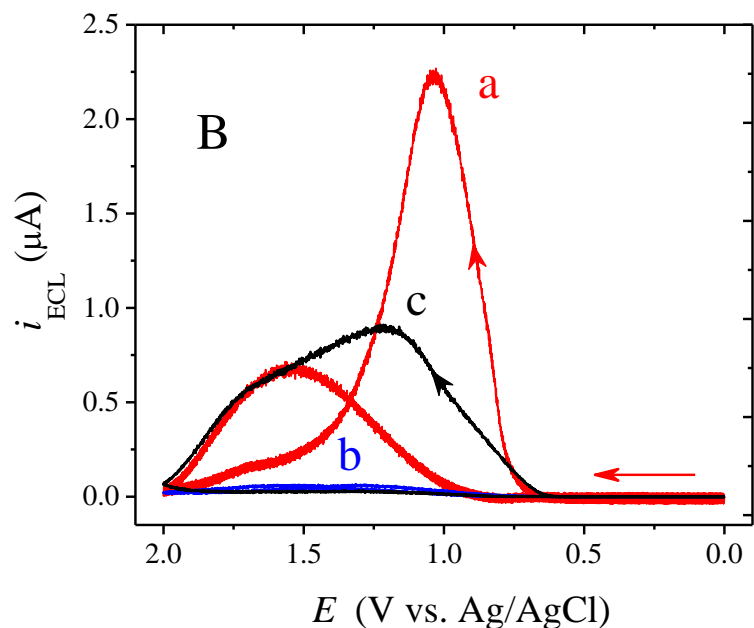
Figure 4.2 (A) CV and (B) ECL responses of the CdTe QDs/TPrA system.

Note: Signals were obtained from 125.0 nM CdTe QDs in 0.10 M PB (pH 8.5) with 52.5 mM of TPrA at a scan rate of 100 mV/s at (a) bare GCE, (b) CNTs modified GCE, and (c) GCE casted with chitosan modified CNTs containing 30 μg of CNTs mixed with 15 μg of chitosan.

To understand the CNTs quenching behavior, a set of FL titration experiments were conducted. As shown in Figure 4.3A, with the addition of 0 to 0.22 mg/mL CNTs to a 2.5 nM constant concentration of CdTe QDs, the FL intensity decreases gradually by 71.5%. Figure 3B displays the Stern-Volmer plot of FL quenching by CNTs, where F_0 is the FL intensity in the absence of CNTs and F is the FL intensity in the presence of added CNTs. The Stern-Volmer constant (K_{SV}, Equation. 4.8a),[40-42] which is the slope of Figure 4.3B, is calculated to be 11.7 L/g.
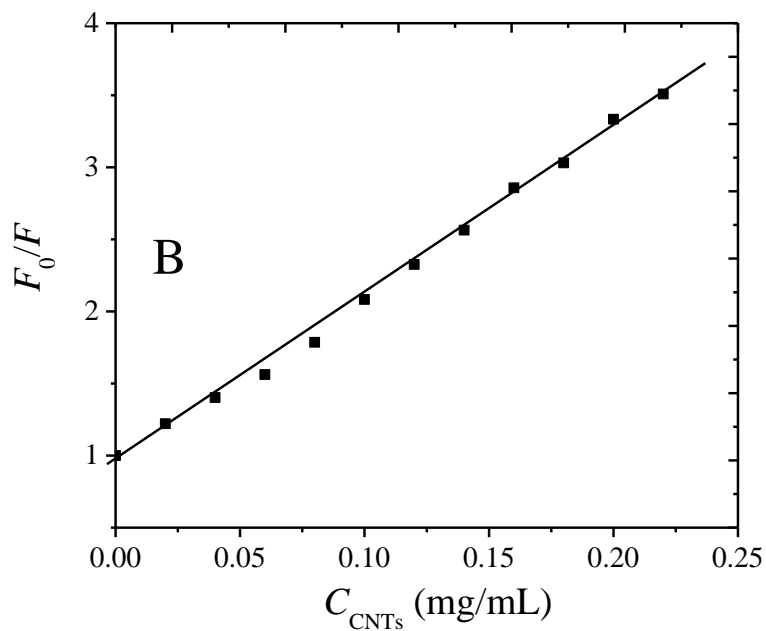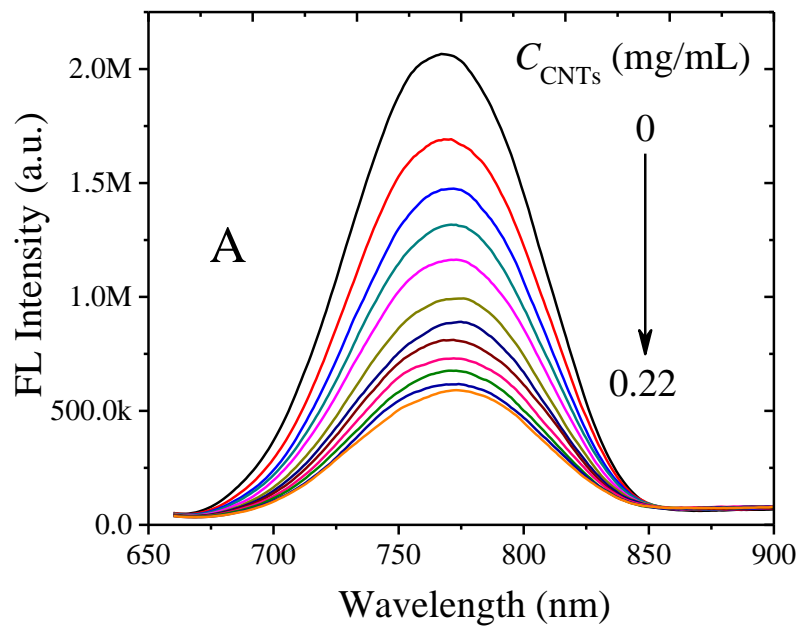
Figure 4.3 Effect of CNTs on FL of CdTe QDs.

Note: (A) FL spectra changes of 2.5 nM CdTe QDs in the presence of added CNTs and (B) Stern-Volmer plot of FL quenching shown in (A) by CNTs.

$$\frac{F_0}{F} = 1 + K_{SV}[CNTs] \qquad\qquad\qquad (4.8a)$$

The quenching constant (K_q) of CNTs can be estimated with Eq. 4.8b:

$$K_q = K_{SV}(K_f + K_{nr}) \qquad\qquad\qquad (4.8b)$$

where K_f is the rate constants of FL and K_{nr} is the non-radiative decay of the excited state CdTe QDs[*]. The reciprocal of ($K_f + K_{nr}$) gives the FL lifetime of the excited state CdTe QDs[*] species τ :

$$\tau = \frac{1}{K_f + K_{nr}} \qquad\qquad\qquad (4.8c)$$

A variety of lifetime values from ~2 to 22 ns for CdTe QDs[*] have been reported.[43-48] If an average lifetime value of 10 ns is used for the present study, then a quenching constant of 1.2×10^9 L/g•s is obtained.

The FL quenching of CdTe QDs[*] by CNTs is probably due to dynamic (i.e., collisional) rather than static quenching.[49] This is because, according to the manufacturer, the as-received CNTs essentially have no surface functional groups that could bind to CdTe QDs. The commonly existing -COOH group on CNTs does not result in the formation of CdTe QDs/CNTs aggregates due to the electrostatic repulsion, as both the surfaces of CNTs and MPA capped CdTe QDs are negatively charged in pH 8.5 PB solution. The above discussion is consistent with our experimental data shown in Figure 4.4, where neither absorption peak shift in UV-vis absorption spectroscopy nor new emission peak in FL was observed for CdTe QDs-CNTs mixture suspensions.
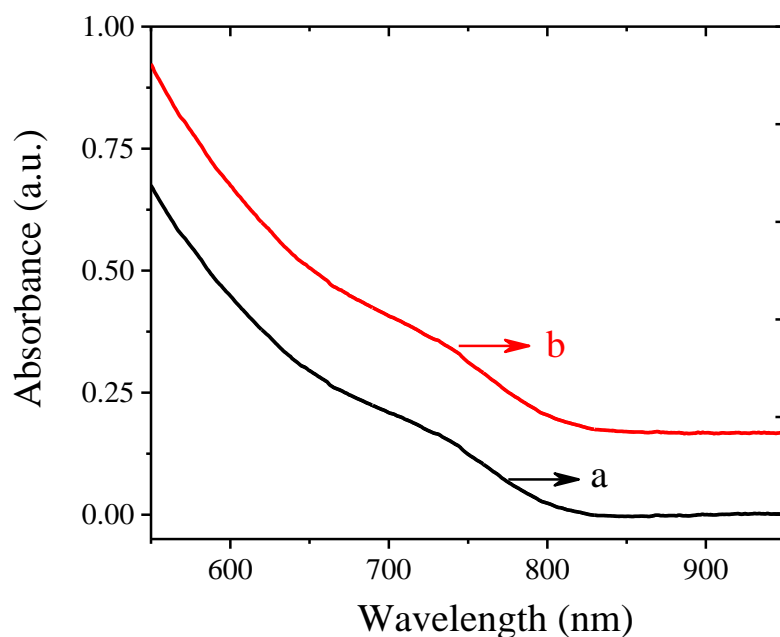
Figure 4.4 UV-vis absorption spectra of 0.50 mM of CdTe QDs in the(a) absence and (b) presence of 0.2 mg/mL CNTs.

Because CNTs are chemically and electrochemically inert under the ECL experimental conditions, no interference between CNTs and the chemical species associated with ECL generation (i.e., $TPrA^{+\bullet}$, $TPrA^{\bullet}$, CdTe $QDs^{+\bullet}$) is expected. As a result, redox reaction based ECL quenching[42] is unlikely to occur. In other words, ECL quenching of the CdTe QDs/TPrA system by CNTs should also follow the dynamic quenching mechanism as described earlier in FL. If this is true, then physical separation of CNTs from CdTe QDs[*] should significantly decrease the quenching effect. Figures 4.2A-c and 4.2B-c show the results of such an experiment, where the GCE is casted with a layer of chitosan modified rather than bare CNTs. Not surprisingly, the ECL signal on chitosan modified CNTs (Figure 4.2B-c) is ~14 times larger than that obtained from bare CNTs modified GCE (Figure 4.1B-b), even though the former electrode produces only an

half of the oxidation current as the latter does (Figure 4.2A-c vs. 4.2A-b). Data shown in Figure 4.2 suggest that CNTs are partially covered with a layer of chitosan, which prevents the direct physical contact of QDs from bare CNTs and decreases the effective surface area of the electrode to a certain extent. Consequently, comparing with the bare GCE, the GCE with chitosan modified CNTs shows a much larger CV current (Figure 4.2A-c vs. 4.2A-a) but a relatively small ECL response (Figure 4.2B-c vs. 4.2B-a).

Modification of CNTs with chitosan has led to the decrease in ECL quenching; however, this modification could also decrease the effective area and increase the resistance of the electrode, resulting in lowering the ECL generation, which is undesirable especially when constructing surface-confined biosensors for quantifying of biomolecules. Therefore, the effect of chitosan concentration in modifying CNTs on ECL production was studied. As shown in Figure 4.5, the ECL intensity, which is displayed as the area of the ECL current on forward potential scan, maximizes at 0.1% (wt%) of chitosan for a total amount of 30 μg CNTs on each electrode. This optimal concentration was used throughout the entire study unless otherwise stated.

The effect of CNTs on the cathodic coreactant ECL of the CdTe QDs/$(NH_4)_2S_2O_8$ system in 0.10 M PB (pH 8.5) solution was also repeatedly studied; however, no consistent and reproducible data was ever found regardless of degassing. This could be ascribed to the instability of $(NH_4)_2S_2O_8$ and its products after electrochemical reduction under the present ECL experimental conditions.
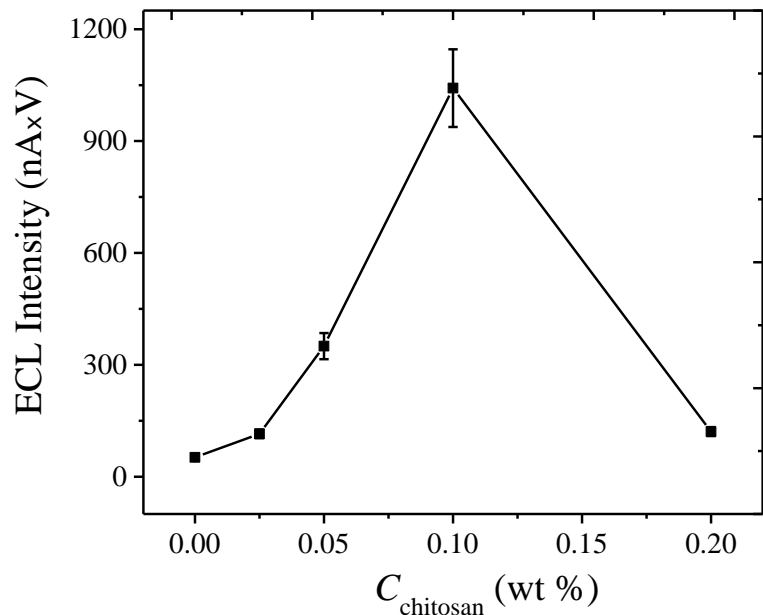
Figure 4.5 Effect of different amounts of chitosan on the ECL intensity of CdTe QDs.

Note: Effect of GCE with different amounts of chitosan modified CNTs on the ECL intensity of 125.0 nM CdTe QDs-52.5 mM TPrA in 0.10 M PB (pH 8.5) at a scan rate of 100 mV/s. Each GCE contained 30 μg of CNTs.

4.3.3 Quenching vs Enhancement

As discussed in the previous section, CNTs play two distinctive roles during the anodic coreactant ECL production. On one hand, CNTs increase the amount of electrochemically generated intermediates that could potentially increase the ECL intensity of the system. On the other hand, CNTs dynamically quench the excited state of the ECL luminophore (i.e., CdTe QDs[*]) leading to the decrease in ECL intensity. Therefore, by manipulating the experimental conditions such as solution concentrations of coreactant and CdTe QDs, the ECL intensity of the system on CNTs modified electrode could be tuned to become either enhanced or quenched with respect to the bare electrode.

4.3.3.1 CdTe QDs Concentration Effect

As shown in Figure 4.6, in this set of experiments, the ratio of the ECL intensity from GCE coated with chitosan modified CNTs [$i_{ECL (CNTs)}$] over that from bare GCE [$i_{ECL (Bare GCE)}$] is plotted against the concentration of CdTe QDs, where a constant ECL coreactant concentration and the integrated area of ECL current on the forward cyclic potential scanning are used. With the increase of C_{QDs}, the $i_{ECL (CNTs)}/i_{ECL (Bare GCE)}$ decreases exponentially for TPrA (Figure 4.6A) as well as for DBAE (Figure 4.6B) coreactant ECL system.
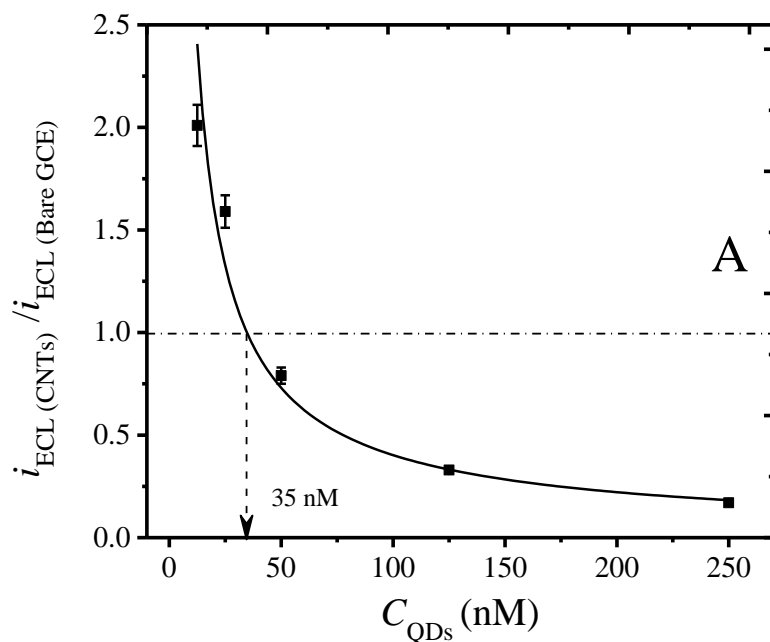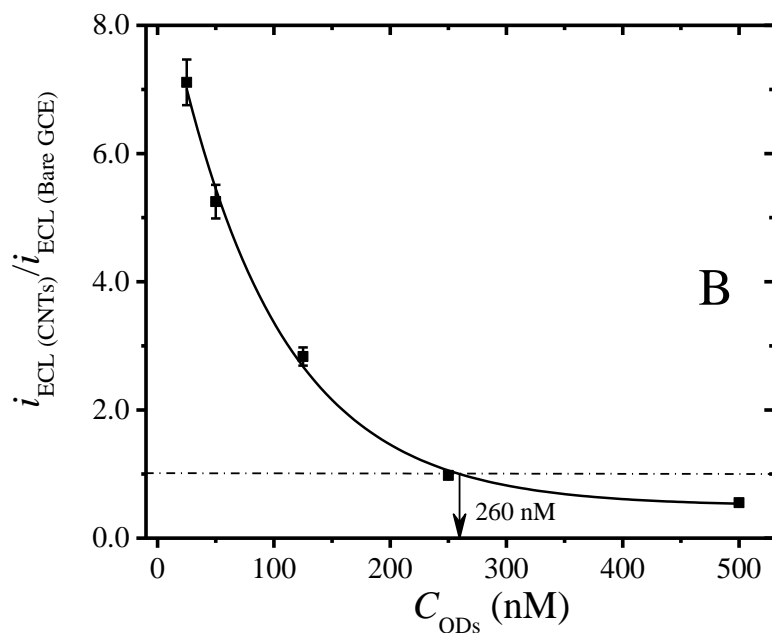
Figure 4.6 Effect of CdTe QDs concentration on the ECL intensity ratio of GCE coated with chitosan modified CNTs over bare GCE.

When relatively low concentrations of QDs are used, i.e., < 35 and < 260 nM CdTe QDs for the TPrA and DBAE system, respectively, ECL enhancement with CNTs modified electrode is observed. This enhancement becomes significant at very low concentrations of CdTe QDs. For example, at 15 nM (Figure 4.6A) and 25 nM (Figure 4.6B) of QDs, about 2 and 7-fold of ECL enhancement is evident for the TPrA and DBAE system, respectively. On the other hand, ECL at the CNTs modified electrode could be quenched by up to ~80% as compared with that at the bare GCE if high concentrations of CdTe QDs are present in the solution.
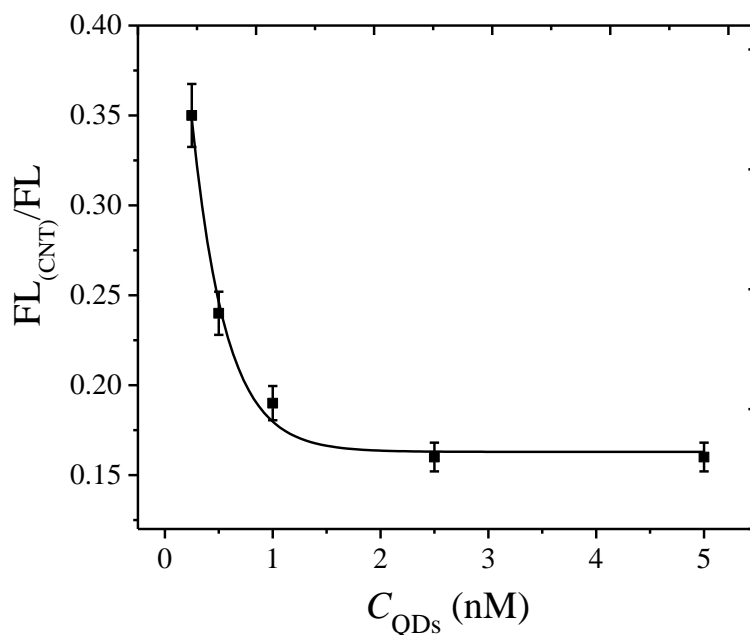
Figure 4.7 Effect of CdTe QDs concentration on the ratio of FL intensity of CdTe QDs with CNTs-chitosan mixture over that of CdTe QDs without added CNTs.

Note: The measurements were conducted in water containing 20 µg/mL CNTs-10 µg/mL chitosan mixture under constant stirring.

This quenching behavior is consistent with the dynamic quenching mechanism described earlier. Given the fact that the coreactant concentration used in this study is sufficiently large, the collision frequency of the excited state CdTe QDs[*] at the CNTs modified electrode increases with the increase of the concentration of CdTe QDs in solution, which results in the increase of the dynamic quenching efficiency and thus the decrease in ECL intensity. To validate the above argument, a set of FL experiments studying the relationship between FL intensity and CdTe QDs concentration were conducted. As shown in Figure 4.7, where the effect of CdTe QDs concentration on the ratio of FL intensity of CdTe QDs with CNTs/chitosan mixture [$I_{FL\,(CNTs)}$] over that of CdTe QDs without added CNTs (I_{FL}) is demonstrated, with the increase of the

112

concentration of CdTe QDs, the ratio of $I_{FL (CNTs)}/I_{FL}$ decreases exponentially. These results confirm that both ECL and FL hold the same dynamic quenching mechanism.

4.3.3.2 Coreactant Concentration Effect

Figure 4.8 shows the effect of coreactant concentration of TPrA (Figure 4.8A) and DBAE (Figure 4.8B) on the ECL intensity ratio of GCE coated with chitosan modified CNTs [$i_{ECL (CNTs)}$] over bare GCE [$i_{ECL (Bare GCE)}$] obtained from 50 nM CdTe QDs in 0.10 M of PB (pH 8.5) solution. In both cases, a minimum $i_{ECL (CNTs)}/i_{ECL (Bare GCE)}$ ratio at 10 mM for TPrA and 5 mM for DBAE is observed, respectively. Again, this could be explained by using the two opposing factors simultaneously applied at the electrode. On one hand, CNTs modified electrode can increase the oxidation current of coreactant and QDs, which is favorable to ECL generation. On the other hand, CNTs can quench ECL. When the coreactant concentration is lower than the critical concentration of 10 mM for the CdTe QDs/TPrA system (Figure 4.8A) or 5 mM for the CdTe QDs/DBAE system, the ECL intensity increase with the increase of coreactant concentration at the CNTs modified GCE is less than that at the bare GCE, causing the decrease in $i_{ECL (CNTs)}/i_{ECL (Bare GCE)}$ ratio. Beyond the critical concentration of the coreactant, electrochemical oxidation of the coreactant becomes a dominant role for ECL production over the ECL quenching by CNTs. As such, the $i_{ECL (CNTs)}/i_{ECL (Bare GCE)}$ ratio increases with the increase of coreactant concentration.

Notably, under the experimental conditions given in Figure 4.8, for the CdTe QDs/TPrA system, ECL signals generated at CNTs modified GCE electrode are always weaker than that at bare GCE (i.e., $i_{ECL (CNTs)}/i_{ECL (Bare GCE)} < 1.0$, Figure 4.8A). On contrast, for the CdTe QDs/DBAE system, much higher ECL responses are obtained at

113

CNTs vs bare GCE over an entire coreactant concentration range of 1.0 to 50 mM DBAE

(Figure 4.8B). For example, at C_{DBAE} = 50 nM, ECL intensity is enhanced by ~30 times

on CNTs modified GCE vs bare GCE. This is because like $S_2O_8^{2-}$, DBAE coreactant

plays double role, ECL coreactant and ECL quencher, on conventional working

electrodes. [11,50,51] For example, the ECL intensity of the CdSe QDs/DBAE system

showed a peak value at C_{DBAE} ≈ 30, 40, and 53 mM at Pt, Au, and GCE, respectively.

Beyond the above critical concentrations, ECL was gradually quenched.[11] Data shown in

Figure 4.8B is another example of illustrating the electrode material dependence of ECL

quenching by DBAE (or its derivatives), where in contrast to bare GCE, CNTs-modified

GCE seems to be unfavorable towards DBAE-related quenching although quenching of

CdTe QDs[*] by CNTs still remains.
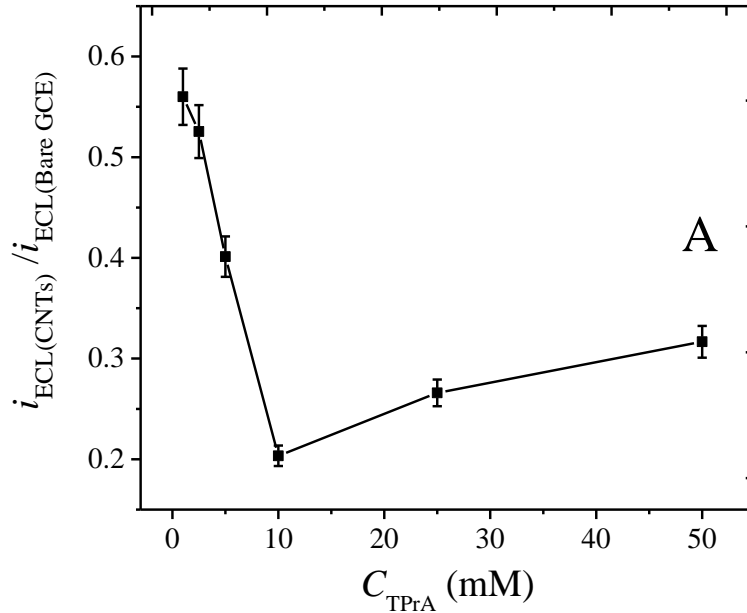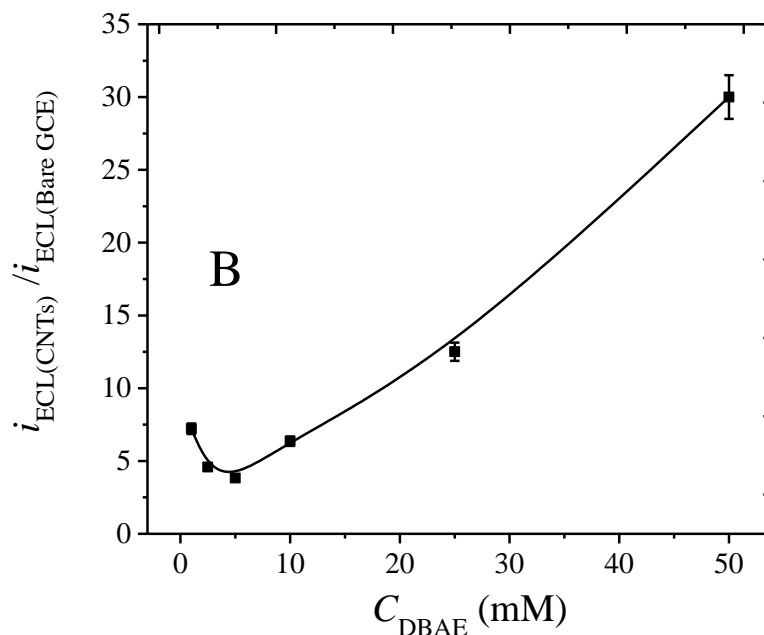
Figure 4.8 Effect of coreactant concentration on the ECL intensity ratio of GCE coated with chitosan modified CNTs over bare GCE.

Note: Effect of coreactant concentration of (A) TPrA and (B) DBAE on the ECL intensity ratio of GCE coated with chitosan modified CNTs over bare GCE obtained from 50 nM CdTe QDs in 0.10 M of PB (pH 8.5) at a scan rate of 100 mV/s. Each GCE contained 30 μg of CNTs mixed with 15 μg of chitosan.

4.4 Conclusion

Effects of CNTs on the ECL behavior of CdTe QDs using TPrA and DBAE as the anodic coreactant were investigated. Depending on the concentration of coreactant as well as CdTe QDs, use of surface-confined CNTs could either quench or enhance the ECL intensity. For a given coreactant concentration, lowering the amount of CdTe QDs in solution was found to be beneficial for enhancing ECL. This was because CNTs-modified electrode increased the oxidation current of the system, which was favorable to ECL generation. Additionally, ECL quenching by CNTs became dominant at high concentrations of CdTe QDs, as expected from the dynamic quenching mechanism. FL data, which were consistent with the dynamic quenching mechanism, revealed that the

excited state CdTe QDs* was quenched by CNTs in solution with a Stern-Volmer and an estimated quenching constant of 11.7 g/L and 1.2×10^9 L/g•s, respectively. Finally, the ECL performance at CNTs was also affected by the type of the coreactant used, in which significant enhancement in ECL was observed from the CdTe QDs/DBAE system under the given experimental conditions.

4.5 References

(1)   Bard, A. J. *Electrogenerated Chemiluminescence*; Marcel Dekker: New York, 2004.

(2)   Deng, S.; Ju, H. *Analyst* **2013**, *138*, 43.

(3)   Miao, W. *Chem. Rev.* **2008**, *108*, 2506.

(4)   Gatto-Menking, D. L.; Yu, H.; Bruno, J. G.; Goode, M. T.; Miller, M.; Zulich, A. W. *Biosens. Bioelectron.* **1995**, *10*, 501.

(5)   Juris, A.; Balzani, V.; Barigelletti, F.; Campagna, S.; Belser, P.; von Zelewsky, A. *Coord. Chem. Rev.* **1988**, *84*, 85.

(6)   Ding, Z.; Quinn, B.; Haram, S.; Pell, L.; Korgel, B.; Bard, A. J. *Science* **2002**, *296*, 1293.

(7)   Myung, N.; Ding, Z.; Bard, A. J. *Nano Lett.* **2002**, *2*, 1315.

(8)   Myung, N.; Bae, Y.; Bard, A. J. *Nano Lett.* **2003**, *3*, 1053.

(9)   Bae, Y.; Myung, N.; Bard, A. J. *Nano Lett.* **2004**, *4*, 1153.

(10)   Myung, N.; Lu, X.; Johnston, K. P.; Bard, A. J. *Nano Lett.* **2004**, *4*, 183.

(11)   Wang, S.; Harris, E.; Shi, J.; Chen, A.; Parajuli, S.; Jing, X.; Miao, W. *PCCP* **2010**, *12*, 10073.

(12)   Lisdat, F.; Schäfer, D.; Kapp, A. *Anal. Bioanal. Chem.* **2013**, *405*, 3739.

(13)   Muzyka, K. *Biosens. Bioelectron.* **2014**, *54*, 393.

(14)   Osman, K.; Shou-Nian, D.; Qi-Le, L. *Curr Anal Chem* **2014**, *10*, 622.

(15)   Zhou, H.; Liu, J.; Zhang, S. *TrAC, Trends Anal. Chem.* **2015**, *67*, 56.

(16)   Kim, D.-J.; Lyu, Y.-K.; Choi, H. N.; Min, I.-H.; Lee, W.-Y. *Chem. Commun.* **2005**, 2966.

(17)   Sun, X.; Du, Y.; Dong, S.; Wang, E. *Anal. Chem.* **2005**, *77*, 8166.

(18) Chang, Z.; Zhou, J.; Zhao, K.; Zhu, N.; He, P.; Fang, Y. *Electrochim. Acta.* **2006**, *52*, 575.

(19) Choi, H. N.; Lee, J.-Y.; Lyu, Y.-K.; Lee, W.-Y. *Anal. Chim. Acta.* **2006**, *565*, 48.

(20) Du, Y.; Qi, B.; Yang, X.; Wang, E. *J. Phys. Chem. B.* **2006**, *110*, 21662.

(21) Zhang, L.; Guo, Z.; Xu, Z.; Dong, S. *J. Electroanal. Chem.* **2006**, *592*, 63.

(22) Li, J.; Xu, Y.; Wei, H.; Huo, T.; Wang, E. *Anal. Chem.* **2007**, *79*, 5439.

(23) Zhang, L.; Xu, Z.; Sun, X.; Dong, S. *Biosens. Bioelectron.* **2007**, *22*, 1097.

(24) Wang, K.; Liu, Q.; Wu, X.-Y.; Guan, Q.-M.; Li, H.-N. *Talanta.* **2010**, *82*, 372.

(25) Zhao, Q.; Gan, Z.; Zhuang, Q. *Electroanalysis.* **2002**, *14*, 1609.

(26) Luo, X.-L.; Xu, J.-J.; Wang, J.-L.; Chen, H.-Y. *Chem. Commun.* **2005**, 2169.

(27) Dai, H.; Xu, G.; Zhang, S.; Gong, L.; Li, X.; Yang, C.; Lin, Y.; Chen, J.; Chen, G. *Biosens. Bioelectron.* **2014**, *61*, 575.

(28) Guo, L.; Liu, X.; Hu, Z.; Deng, S.; Ju, H. *Electroanalysis.* **2009**, *21*, 2495.

(29) Lin, D.; Wu, J.; Yan, F.; Deng, S.; Ju, H. *Anal. Chem.* **2011**, *83*, 5214.

(30) Tang, X.; Zhao, D.; He, J.; Li, F.; Peng, J.; Zhang, M. *Anal. Chem.* **2013**, *85*, 1711.

(31) Rosado, D. J., Jr.; Miao, W.; Sun, Q.; Deng, Y. *J. Phys. Chem. B.* **2006**, *110*, 15719.

(32) Liang, G.-d.; Shen, L.-p.; Zhang, X.-l.; Zou, G.-z. *Eur. J. Inorg. Chem.* **2011**, n/a.

(33) Yu, W. W.; Qu, L.; Guo, W.; Peng, X. *Chem. Mater.* **2003**, *15*, 2854.

(34) Peng, Z. A.; Peng, X. *J. Am. Chem. Soc.* **2002**, *124*, 3343.

(35) Miao, W. In *Handbook of Electrochemistry*; Zoski, C. G., Ed.; Elsevier: HR Amsterdam, 2007, p 541.

(36) Sherigara, B. S.; Kutner, W.; D'Souza, F. *Electroanalysis.* **2003**, *15*, 753.

(37) Punbusayakul, N. *Procedia Eng.* **2012**, *32*, 683.

(38) Miao, W.; Choi, J.-P.; Bard, A. J. *J. Am. Chem. Soc.* **2002**, *124*, 14478.

(39) Miao, W.; Choi, J.-P. In *Electrogenerated Chemiluminescence*; Bard, A. J., Ed. 2004, p 213.

(40) Legenza, M. W.; Marzzacco, C. J. *J. Chem. Educ.* **1977**, *54*, 183.

(41) Cheng, P. P. H.; Silvester, D.; Wang, G.; Kalyuzhny, G.; Douglas, A.; Murray, R. W. *J. Phys. Chem. B.* **2006**, *110*, 4637.

(42) Parajuli, S.; Jing, X.; Miao, W. *Electrochim. Acta.* **2015**, *180*, 196.

(43) Wuister, S. F.; van Driel, F.; Meijerink, A. *J. Lumin.* **2003**, *102–103*, 327.

(44) Alphandéry, E.; Walsh, L. M.; Rakovich, Y.; Bradley, A. L.; Donegan, J. F.; Gaponik, N. *Chem. Phys. Lett.* **2004**, *388*, 100.

(45) Ray, K.; Badugu, R.; Lakowicz, J. R. *J. Am. Chem. Soc.* **2006**, *128*, 8998.

(46) Zhang, J.; Badugu, R.; Lakowicz, J. R. *Plasmonics.* **2007**, *3*, 3.

(47) Yoshiyuki, N.; Takuya, N.; Makiko, S.; Tsuyoshi, K. *Jpn. J. Appl. Phys.* **2008**, *47*, 1385.

(48) Omogo, B.; Aldana, J. F.; Heyes, C. D. *J. Phys. Chem. C.* **2013**, *117*, 2317.

(49) Lakowicz, J. R. *Principles of Fluorescence Spectroscopy*; Springer US, 2006.

(50) White, H. S.; Bard, A. J. *J. Am. Chem. Soc.* **1982**, *104*, 6891.

(51) Liu, X.; Shi, L.; Niu, W.; Li, H.; Xu, G. *Angew. Chem. Int. Ed.* **2007**, *46*, 421.

CHAPTER V – TOWARDS SENSITIVE DETECTION OF AMYLOID $\beta_{1\text{-}42}$ USING

QUANTUM DOTS BASED ELECTROGENERATED CHEMILUMINESCENCE

5.1 Introduction

Electrogenerated chemiluminescene (ECL) has been widely used as a high

sensitivity bioanalytical technique over the past few decades.[1-3] Because of its capability

of sensitive light generation with minimum background interruption, many chemical and

biological sensors have been successfully fabricated based on the ECL technique.[4-8]

Finding of quantum dots as ECL emitters in early 2000's[9-12] catalyzed the development

of the ECL based bioanalytical techniques.[13-18]

A large number of performance enhancement strategies have been reported for

ECL based techniques and the biomarkers of various diseases have been successfully

detected at low concentration levels.[13,14,19-21] Loading of polystyrene miro-beads (PSBs)

with ECL emitters is one of the most effective strategies to improve sensitivity of an ECL

biosensor.[19-21] For example, instead of using individual rubrene molecule, if rubrene

loaded PSBs are used as the antibody labels in an ECL immunoassay, the number of ECL

emitters attached to each antibody could be significantly increased.[19] As a result, the ECL

signal correlated to each target antigen could also be enhanced considerably. The

ultrasensitive detection of Zika virus in clinical samples using ruberen loaded PSBs as the

ECL label has been recently reported.[19-21]

One drawback of previously reported ECL emitters-loaded PSBs method is that

the ECL emitters loaded in PSBs were limited to water insoluble compounds. The ECL

emitters were captured in PSBs through hydrophobic interaction between the ECL

emitters and the inner phase of PSB.[19-21] As a result, the water soluble QDs with high

120

ECL efficiency are difficult to be loaded in PSBs for ECL bioanalysis. Water soluble CdTe QDs loaded PSBs have been successfully used in photoluminescence imaging.[22] However, their applications in ECL studies are yet to be explored.

Early and accurate diagnosis is crucial for effective therapeutic treatment of the Alzheimer's Diseases (AD) patients.[23] However, due to the lack of early onset symptoms, many AD patients are late diagnosed or misclassified.[24] Sensitive and selective detection of biomarkers of AD is one of the critical factors to accurately diagnose the patients at the early stage of the disease.[23] Although, tremendous efforts and progresses have been made, development of high performance bioanalytical techniques for detection AD biomarkers such as $A\beta_{1-42}$ is still a challenge.[23,25-28]

In this chapter, fabrication of a potentially highly sensitive ECL immunoassay towards detection of $A\beta_{1-42}$ using water soluble CdTe QDs loaded PSBs as ECL labels was proposed with preliminary results.

5.2 Experimental Section

5.2.1 Chemicals and Materials

Carboxylate polystyrene beads (PSBs, diameter = 10.3 µm, 2.6% (w/w) aqueous suspension with approximately 6.5×10^7 beads mL^{-1}) were purchased from PolySciences Inc. (Warrington, PA). Poly(allyamine hydrochloride) (referred as PE) was obtained from Aldrich (St. Louis, MO). Unless otherwise stated other chemicals used in this chapter were the same as those described in previous chapters.

5.2.2 Apparatus

Details of the ECL work station, three-electrode ECL cells, and FL spectrometer could be found in Chapter IV.

5.2.3 Synthesize of Water Soluble CdTe QDs

Water soluble CdTe QDs were synthesized based on the one-spot synthetic strategy developed by Zou et al with some modifications.[29] Detail procedures of this synthesis strategy was elaborated in Chapter IV.

5.2.4 Preparation of CdTe QDs-PSB Conjugates

Water soluble CdTe QDs cannot be trapped in hydrophobic inner phase of PSBs as the way other organic soluble ECL emitters captured.[19-21] However, because of the much larger surface area of PSBs (diameter = ~10.3 µm) as compared with that of CdTe QDs (diameter = ~6.4 nm), CdTe QDs could be loaded on the surface of the PSBs. Caruso et al reported the successful loading of water soluble CdTe QDs on the PSBs surface through electrostatic interaction with the assistance of polyelectrolyte multilayers.[22] In this chapter, the MPA capped CdTe QDs were loaded on the surface of the PSBs by using the strategy reported by Caruso et al after minor modification (Scheme 5.1).[22] Briefly, 200.0 µL of PSBs suspension was added in to a 1.50 mL centrifuge tube and cleaned with distilled water with centrifugation at 5000 rpm for at least 3 times. 1.0 mg/mL poly(allylamine hydrochloride) (PE) solution was prepared in 0.50 M NaCl. 1.0 mL of the above solution was added to the clean PSBs in the centrifuge tube and the mixture was shaken for 30 min at room temperature with a Dynal sample mixer at 30 rpm. Due to opposite electro-charges of PE (+) and PSBs (-), a layer of PE will be attached on the surface of PSBs. The above suspension was cleaned with distilled water with centrifugation at 5000 rpm for 5 mins at least three times. 500.0 µL of 0.5 µM CdTe QDs stock solution was added to the above PE coated PBS and this suspension was gently shaken for 60 min at RT. In this way, negatively charged CdTe QDs was attached

onto the positively charged PE coated PSBs. After the cleaning of the CdTe QDs/PE/PSB

conjugate at 2000 rpm centrifuge speed, two more layers of PE and QDs were coated on

the CdTe QDs/PE/PSB with the same procedure of formation of the first layer. Finally,

one last layer of PE was coated on the (PE/CdTe QDs)$_3$/PSB to stabilize the overall

conjugate and to introduce free amine groups on the overall conjugate surface for further

modification with biomolecules (Scheme 5.1). The final conjugates were re-suspended in

200.0 µL of distilled water and kept in 4 °C for further use. The final conjugates were

stable for weeks under this storage condition. For the rest of this chapter the above

prepared PSBs with four layers of PE and three layers of CdTe QDs will be referred as

CdTe QDs-PSBs conjugate.

The color of the CdTe QDs-PSBs conjugates became darker and darker (red-

brown) with increasing number of CdTe QDs layers. Theoretically, the number of

CdTe QDs layer could be more than three. However, for demonstration of their

characteristics, CdTe QDs-PSBs conjugates with three layer of QDs were prepared. For

bioanalytical application, more layers of CdTe QDs could be loaded on PSBs surface to

increase the number of QDs on each PSBs.
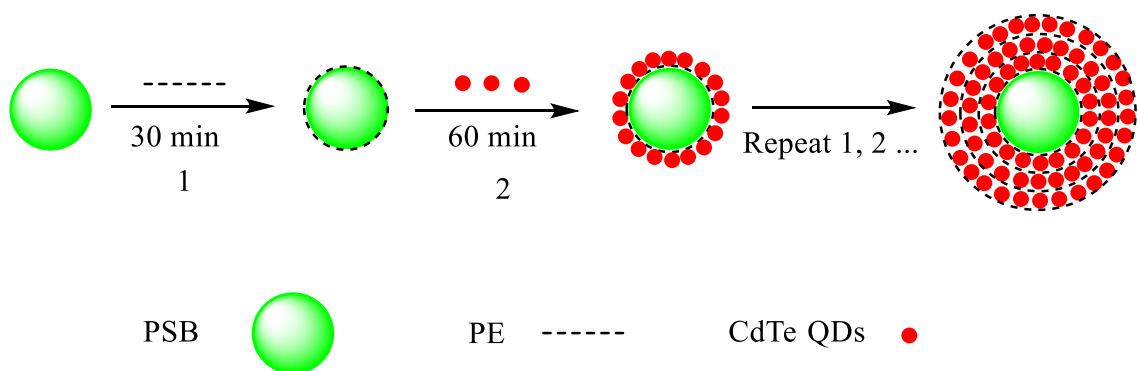
Scheme 5.1 Layer-by-layer loading of CdTe QDs on PSBs surface.

5.2.5 Modification of GCE with CdTe QDs-PSBs Conjugates

The GCE was polished with 0.3 µm aluminum powder slurry and rinsed with large amounts of distilled water. After the washed GCE was dried with Kimwipes facial tissue, 15.0 µL of the CdTe QDs-PSBs conjugates stock solution was drop-casted on the GCE and air dried for 1.5 hrs. Then, the GCE surface was carefully rinsed with distilled water before the ECL experiment.

5.3 Results and Discussions

5.3.1 Characterization of CdTe QDs-PSBs Conjugates

5.3.1.1 FL

FL signal obtained from 6.5×10^6 as-prepared CdTe QDs-PSBs conjugates in 2.0 mL water was shown in Figure 5.1. A strong FL emission peak at ~766 nm is generated from the CdTe QDs-PSBs. This peak emission peak wavelength overlaps with the emission peak wavelength of as-prepared CdTe QDs, which indicates that the FL signal in Figure 5.1 is generated from CdTe QDs loaded on the surface of PSBs. The amount of CdTe QDs loaded on each PSBs was estimated to be $\sim 4.6 \times 10^5$ based on the similar FL intensity of 6.5×10^6 CdTe QDs-PSBs conjugates and that of 2.50 nM CdTe QDs water solution at the same experiment condition.
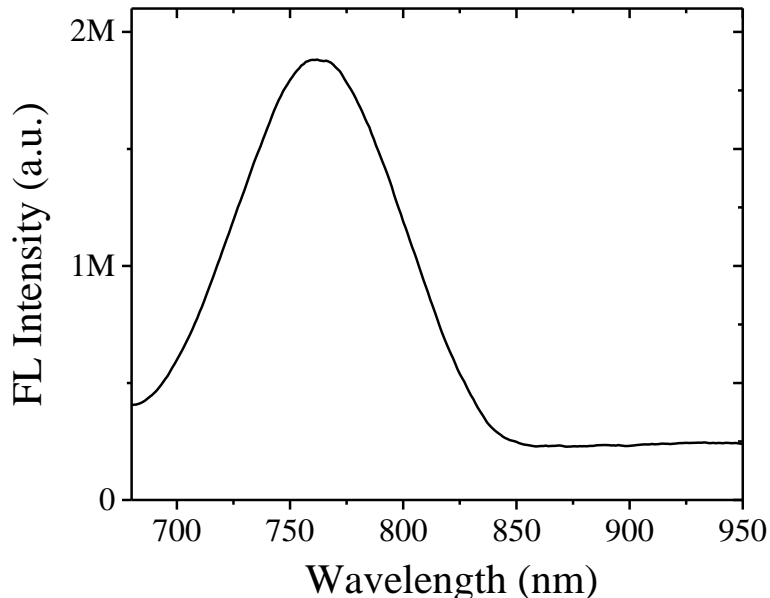
Figure 5.1 FL spectra of CdTe QDs-PSBs conjugates.

Note: CdTe QDs-PSBs conjugates were excited at 650.0 nm wavelength.

5.3.1.2 ECL

ECL signal generated from the CdTe QDs-PSB conjugate modified GCE in TPrA coreactant system is shown in Figure 5.2. When TPrA is used as anodic ECL coreactant, upon potential scanning from 0.0 V to 2.0 V, an ECL current starts to form at ~0.78 V and reaches to a maximum current of 2.08 µA at ~1.26 V. One main concern with casting the CdTe QDs-PSBs conjugates on GCE surface was the electrode surface impedance enhancement, which could be introduced by relatively poor conductivity of PSBs. However, the generation of as strong as 2.08 µA ECL current from the CdTe QDs-PSBs conjugate-modified GCE suggests that the relatively poor conductivity of PSBs did not have a major impact on the ECL signal generation from the system.

Figure 5.2 ECL signals from surface-confined CdTe QDs-PSBs conjugates when TPrA is used as coreactant.
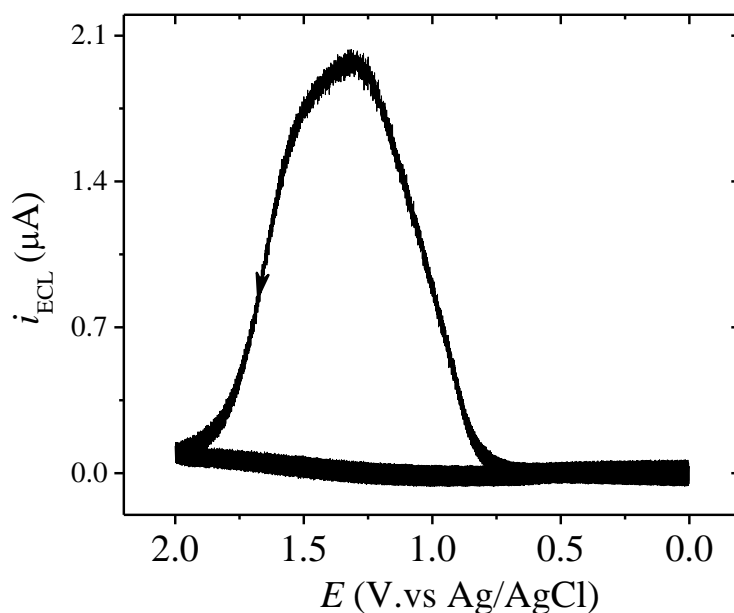
Note: ECL Signal was obtained from CdTe QDs-PSBs conjugates modified GCE in 0.10 M PB (pH 8.5) with 70.0 mM at a scan rate of 100 mV/s.

5.4 Future Work

The sketch of potentially highly sensitive ECL immunoassay towards Aβ-42 is shown in Scheme 5.2. According to this design, Aβ$_{1-42}$ will be captured by the anti-Aβ-42 which is modified on CdTe QDs-PSBs surface. Aβ$_{1-42}$ specified anti- Aβ$_{1-42}$ modified magnetic bead (MB) will also be captured on the above Aβ$_{1-42}$ -anti- Aβ$_{1-42}$ -CdTe QDs-PSB conjugates through sandwich type immunoassay formation. The final sandwich type immunoassay conjugates will be separated from reaction media magnetically and will be suspended in 50.0 mM of PBS (pH 7.4) after centrifugation cleaning for multiple times. 15.0 µL the final suspension will be drop casted on a GCE surface and air dried at RT. The immunoassay casted GCE will be used to conduct ECL test in 0.10 M PBS (pH 8.5)

with 70.0 mM TPrA and 150.0 nM CdSe QDs. The ECL signal generated from above

GCE will be correlate to the concentration of $A\beta_{1-42}$ in the sample.

Anti-AB$_{1-42}$ AB$_{1-42}$ CdTe QDs/PE/PSB   MB
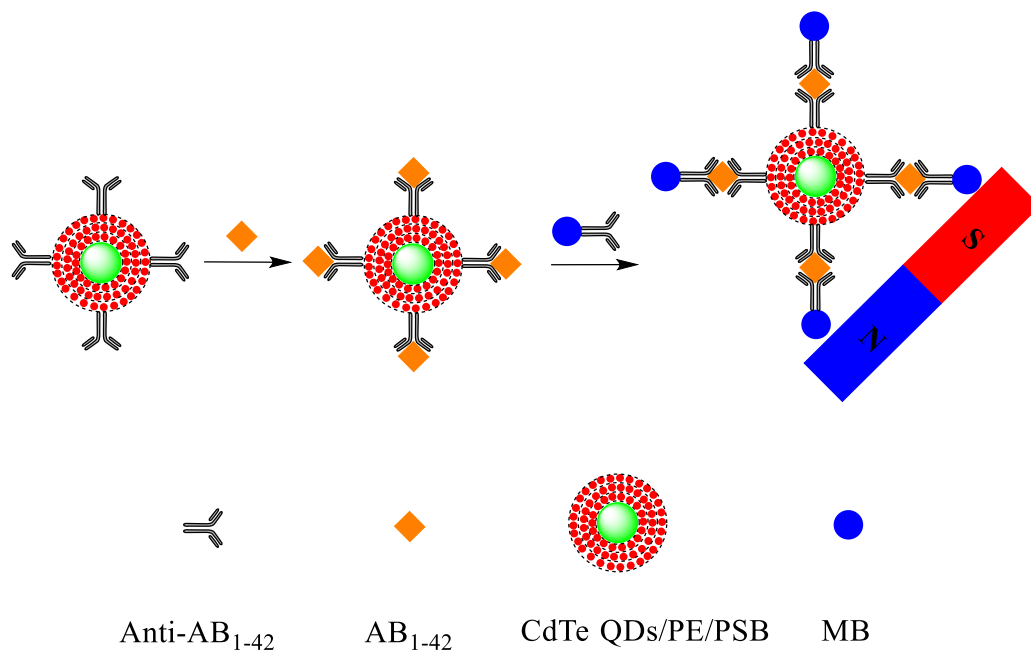
Scheme 5.2 ECL immunoassay illustration of $A\beta_{1-42}$ detection.

Loading of PSBs with ECL emitters reportedly could amplifies the ECL signal

intensity of the ECL immunoassays by several orders of magnitude.[20,21,30] As-proposed

ECL immunoassay could improve the quality of currently existed ECL immunoassays by

applying water soluble QDs loaded PSBs as ECL labels rather than organic soluble

molecular based ECL emitters. In addition, CdSe QDs could enhance the ECL signal

from CdTe QDs up to ~20 times (Chapter II), therefore it could be used as an additional

signal enhancement agent in this ECL immunoassay to further increase the intensity of

the ECL signal. Finally, unlike many QDs based cathodic ECL immunoassays, the ECL

signal from this system will be generated at anodic potential. This will effectively prevent

the interference of the oxygen, which could potentially quench the cathodic ECL

intensity.

5.5 Conclusion

Water soluble CdTe QDs were successfully loaded on the surface of PSBs through electrostatic interaction with the assistance of poly(allylamine hydrochloride). The final CdTe QDs-PSBs conjugates showed promising ECL properties as a potential ECL labels in bioanalysis studies. Using FL experimental results of CdTe QDs-PSBs conjugates, ~4.6×10^5 CdTe QDs were estimated to be loaded on the surface of each PSBs. This large amount of CdTe QDs on PSBs could amplify the ECL signal generation when CdTe QDs-PSBs conjugates are used as ECL labels in ECL immunoassays. Based on these preliminary results and the strong interaction between CdSe QDs and CdTe QDs that was discussed in Chapter II, a potentially highly sensitive ECL immunoassay to detect $A\beta_{1\text{-}42}$ was proposed.

5.6 References

(1)   Miao, W. *Chem. Rev.* **2008**, *108*, 2506.

(2)   Deng, S.; Ju, H. *The Analyst.* **2013**, *138*, 43.

(3)   Wu, P.; Hou, X.; Xu, J.-J.; Chen, H.-Y. *Chem. Rev.* **2014**, *114*, 11027.

(4)   Zhang, X.; Ding, S.-N. *ACS Sensors.* **2016**, *1*, 358.

(5)   Graybill, R. M.; Bailey, R. C. *Anal. Chem.* **2016**, *88*, 431.

(6)   Feng, Q.-M.; Shen, Y.-Z.; Li, M.-X.; Zhang, Z.-L.; Zhao, W.; Xu, J.-J.; Chen, H.-Y. *Anal. Chem.* **2016**, *88*, 937.

(7)   Bist, I.; Song, B.; Mosa, I. M.; Keyes, T. E.; Martin, A.; Forster, R. J.; Rusling, J. F. *ACS Sensors.* **2016**, *1*, 272.

(8)   Ji, J.; He, L.; Shen, Y.; Hu, P.; Li, X.; Jiang, L.-P.; Zhang, J.-R.; Li, L.; Zhu, J.-J. *Anal. Chem.* **2014**, *86*, 3284.

(9)   Ding, Z.; Quinn, B.; Haram, S.; Pell, L.; Korgel, B.; Bard, A. J. *Science.* **2002**, *296*, 1293.

(10)   Myung, N.; Ding, Z.; Bard, A. J. *Nano Lett.* **2002**, *2*, 1315.

(11)   Myung, N.; Bae, Y.; Bard, A. J. *Nano Lett.* **2003**, *3*, 1053.

(12)   Bae, Y.; Myung, N.; Bard, A. J. *Nano Lett.* **2004**, *4*, 1153.

(13)   Zhang, Y.; Deng, S.; Lei, J.; Xu, Q.; Ju, H. *Talanta.* **2011**, *85*, 2154.

(14)   Shen, W.; Tian, D.; Cui, H.; Yang, D.; Bian, Z. *Biosens. Bioelectron.* **2011**, *27*, 18.

(15)   Guo, Y.; Jia, X.; Zhang, S. *Chem. Commun.* **2011**, *47*, 725.

(16)   Algar, W. R.; Susumu, K.; Delehanty, J. B.; Medintz, I. L. *Anal. Chem.* **2011**, *83*, 8826.

(17)   Wang, K.; Liu, Q.; Wu, X.-Y.; Guan, Q.-M.; Li, H.-N. *Talanta.* **2010**, *82*, 372.

(18)   Jie, G.; Li, L.; Chen, C.; Xuan, J.; Zhu, J.-J. *Biosens. Bioelectron.* **2009**, *24*, 3352.

(19)   Acharya, D.; Bastola, P.; Le, L.; Paul, A. M.; Fernandez, E.; Diamond, M. S.; Miao, W.; Bai, F. *Sci. Rep.* **2016**, *6*, 32227.

(20)   Miao, W.; Bard, A. J. *Anal. Chem.* **2004**, *76*, 7109.

(21)   Miao, W.; Bard, A. J. *Anal. Chem.* **2004**, *76*, 5379.

(22)   Wang, D.; Rogach, A. L.; Caruso, F. *Nano Lett.* **2002**, *2*, 857.

(23)   Scarano, S.; Lisi, S.; Ravelet, C.; Peyrin, E.; Minunni, M. *Anal. Chim. Acta.* **2016**, 940, 21.

(24)   Humpel, C. *Trends Biotechnol.* **2011**, *29*, 26.

(25)   Pi, J.; Long, Y.; Huang, N.; Cheng, Y.; Zheng, H. *Talanta.* **2016**, *146*, 10.

(26)   Wang, C.; Liu, D.; Wang, Z. *Chem. Commun.* **2012**, *48*, 8392.

(27)   Lien, T. T. N.; Takamura, Y.; Tamiya, E.; Vestergaard, M. d. C. *Anal. Chim. Acta* **2015**, *892*, 69.

(28)   Oh, J.; Yoo, G.; Chang, Y. W.; Kim, H. J.; Jose, J.; Kim, E.; Pyun, J.-C.; Yoo, K.-H. *Biosens. Bioelectron.* **2013**, *50*, 345.

(29)   Liang, G.-d.; Shen, L.-p.; Zhang, X.-l.; Zou, G.-z. *Eur. J. Inorg. Chem.* **2011**, n/a.

(30)   Pittman, T. L.; Thomson, B.; Miao, W. *Anal. Chim. Acta.* **2009**, *632*, 197.

CHAPTER VI – CONCLUDING REMARKS

ECL has been developed as a promising analytical technique over the past few decades owning to its ability to sensitively detect various target species. Quantum dots (QDs) provided ECL based analytical technique with a superior alternative of conventional ECL labels, e.g., $Ru(bpy)_3^{2+}$. Due to the unique optical and electronic properties of QDs, a large number of high performance ECL based sensors have been developed using QDs as ECL labels. Although their potential in analytical field is increasingly explored, less attention has been given to the fundamental aspects of QDs based ECL systems. Understanding of the fundamental ECL characteristics of QDs could be very useful for fabrication of more efficient and specific ECL sensors.

In Chapter II of this dissertation, mechanisms of ECL current generation from the CdTe QDs/TPrA system with three distinctive peaks (vs. potential) were unfolded. A strong ECL interaction along with a FL energy transfer interaction between CdTe QDs with an emission at 760 nm and CdSe QDs with an emission at 550 nm were also demonstrated and an electron transfer mechanism was proposed to explain this strong ECL interaction. Effects of reaction conditions on EDC coupling efficiency on an electrode surface were illustrated in Chapter III. Conditions such as pH, solution concentrations of the reagents, addition of NHS, and compositions of buffer were systematically studied for both one-step and two-step EDC coupling strategies. Based on the results of this study, optimum reaction conditions for EDC coupling through different strategies were suggested as a guideline to the scientific community. In Chapter IV, first, a significant quenching effect of CNTs on ECL signal from the CdTe QDs/TPrA system was shown. Then, a significant ECL enhancement of ECL signal from the CdTe

QDs/TPrA system by CNTs on electrode surface was also explored. The completely opposite effects of CNTs on ECL intensity of CdTe QDs were proven to be depend on factors such as concentration of ECL reagents and types of coreactant. Successful loading of polystyrene micro-beads (PSBs) with a large number of water soluble CdTe QDs was achieved in Chapter V. Initial studies suggested that these CdTe QDs loaded PSBs could be an excellent ECL label candidate for bioanalysis studies. Based on the information from Chapter II to Chapter V, a potentially highly sensitive ECL immunoassay to detect Amyloid β-42 was proposed at the end of Chapter V.

The studies presented in this dissertation could be used for many different purposes by the scientific community. For instance, based on the strong interaction between the CdSe QDs and the CdTe QDs, the sensitivity of ECL sensor with the same CdTe QDs as ECL label could be significantly increased with the addition of the CdSe QDs. In addition, based on the CdSe QDs and CdTe QDs ECL interaction mechanism, new QDs pairs could be developed with similar or even stronger ECL interactions. The optimum conditions of EDC coupling reaction on an electrode surface, could potentially serve as a useful guideline for effective immobilization of biomolecules or other chemical components of the surface-confined electrochemical or ECL biosensors. The results in Chapter IV provides a clear protocol on how and when to use CNTs in surface-confined ECL sensors for performance enhancement purposes. Additionally, superior supporting materials for ECL studies could be developed based on the effect of CNTs on ECL properties of CdTe QDs. Finally, the proposed ECL immunoassay strategy at the end of Chapter V could potentially be used to sensitively detect any target antigen with a specific antibody.

132